Synchronization and Channel Estimation in OFDM Systems

Jan-Jaap van de Beek

Luleå University of Technology
Division of Signal Processing
Luleå, Sweden

September 1998

Supervisor

Professor Per Ola Börjesson, Luleå University of Technology.

ISSN: 1402 – 1544
ISRN: LTU - DT - - 98/32 - - SE

Published 1998
Reproduced by Universitetstryckeriet, Luleå.

Abstract

This thesis consists of a prologue and six parts that address two aspects of *orthogonal frequency-division multiplexing* (OFDM) communication systems: synchronization and channel estimation. For the synchronization aspect, focus is on estimators of time and frequency offsets that exploit the cyclic prefix. For the channel estimation aspect, a concept is presented and analyzed that exploits the frequency correlation of the channel and combines low complexity with high performance.

Synchronization errors in OFDM can cause intersymbol and intercarrier interference. One way to suppress these interferences in OFDM systems is to track the carrier frequency of the received signal and the proper start of the OFDM symbols. The joint maximum likelihood estimator of symbol time and carrier frequency offsets for OFDM systems using a cyclic prefix is presented. The maximum likelihood estimator, derived for an additive white Gaussian noise channel, exploits the redundancy introduced by the prefix and is independent of how the subcarriers are modulated. Therefore, it does not require extra pilot information.

Some properties of practical OFDM systems change the premises of this estimator. In particular, in systems with pulse shaping, channel dispersion, or slowly changing synchronization errors, estimator performance can gain from more suitably chosen signal models. Three extended signal models, the associated maximum likelihood estimators, and structures for their implementation are presented.

Furthermore, tracking synchronization of a multiuser OFDM system, which often has been questioned, is feasible using a scheme incorporating the above estimator concept. Simulations show that the symbol error rate in the uplink of a multiuser OFDM system is not noticeably affected in a system with coherently demodulated subcarriers and only little in a differentially demodulated system.

Channel estimation is usually needed in coherent OFDM receivers in order to compensate for a frequency-selective channel. For this purpose, a channel equalizer needs to be fed estimates of the subcarrier attenuations. This thesis presents low-rank approximations of the linear minimum mean-squared error channel estimator. These exploit the fact that the subcarrier attenuations are correlated. The approximation is based on a suitable transformation of the channel attenuations.

Channel estimators based on the discrete Fourier transform are analyzed. The symbol error rate of systems employing these channel estimators may experience an irreducible error floor if the channel is not sample-spaced. This thesis also presents and analyzes low-rank channel estimators using a transform based on singular-value decomposition of the channel attenuations. These channel estimators are proposed to be designed generically, *i.e.*, for particular fixed, assumed channel correlations and signal-to-noise ratio. The resulting channel estimators, with suitably chosen fixed design parameters, combine low-complexity and high performance.

Contents[1]

[1] Citations in this table of contents refer to the reference list on page 14.

The work resulting in the above six parts [1–6] has also, in parallel, served the European standardization of the UMTS within ETSI. The technical documents [7–11] are standardization contributions to ETSI's working group SMG2, where standards for the radio interface of terrestrial UMTS are being developed.

Preface

One important skill for a flute player, in the words of my music teacher years ago, is "*being performer and audience, simultaneously*". Listening to and judging your own performance, she taught, makes a good musician. I have realized that this skill also helps making a good researcher. Countless times of re-reading my own draft manuscripts, trying to imagine how they would be read by others, weighing, discussing, and rewriting them have resulted in this thesis.

Background

In the beginning of the nineties I visited Luleå University of Technology a number of short periods. I worked with the processing of ultrasonic signals, results of which were later part of my licentiate thesis. These visits turned out to be the prelude of a longer stay in Luleå starting in the fall of 1993 when I became a graduate student. As any such new start, this move came with new experiences and challenges. There were, for example, the light and beautiful summers but also the area's peripheral geographical location, noticeable in many aspects of everyday life. Some of the new opportunities and chances have influenced my work and the writing of this thesis so much that I like to mention them here.

Among the new opportunities was the challenging one of learning a new language. I still don't comprehend that I think, dream, and count in a language that appeared indecipherable only a couple of years ago. Thinking in another language puts ideas in new and sometimes unexpected perspectives. This sentence, not to mention the rest of this thesis, would have been different if Dutch had been the mother tongue of every Swede.

Furthermore, during my years as a graduate student I've had the opportunity to teach various undergraduate courses. I've liked this teaching very much. Not only did I learn a lot, I'm sure it has also improved the way I documented and presented the ideas in this thesis.

Finally, I've been working *together* with a lot of people. During two and a half years, for instance, I had my office at Telia Research AB in Luleå and I worked in a team of Telia's employees. We contributed to the European standardization of the third generation personal communication systems, the UMTS, within ETSI. During the last two years I also worked together with people from Ecole Nationale Supérieure des Télécommunications (ENST) in Toulouse, France. The mutual support of both cooperations has at times crucially accelerated this thesis' development. I feel privileged having been part of these cooperations and, having worked with my fellow students and colleagues.

Acknowledgements

I owe many of the above opportunities to my advisor, Per Ola Börjesson. Therefore, I first wish to thank him for all his efforts to create prerequisites and chances. I'm also very grateful for his scientific guidance and enthusiastic support.

But there are more people who have in one way or another supported the writing of this thesis. I want to thank Sarah Kate Wilson and Per Ödling for encouraging and inspiring me, and for all their help; Ove Edfors and Magnus Sandell, for their help and their committed interest and enthusiasm (also for many things that have little to do with our joint papers); Daniel Landström, Julia Martinez Arenas, and Mattias Wahlqvist for working together, for their help and good spirits; Christer Östberg and the other people at Telia Research for the cooperative, open athmosphere; and Marie-Laure Boucheret for the scientific support during my visits in Toulouse. I also want to mention all my other (former and present) colleagues at the Division of Signal Processing in Luleå, including Petra Deutgen, Krister Engberg, Håkan Ericsson, Anders Grennberg, Rickard Nilsson, Lennart Olsson, Ulla Persson, Paul Petersen (who helped me editing parts of this thesis), Frank Sjöberg, and Nils Sundström because they have created a stimulating and pleasant environment.

The work presented in this thesis was to a large extent carried out within CDT (the Centre for Distance-Spanning Technology), within the telecommunications framework program of NUTEK (the Swedish National Board for Industrial and Technical Development), and with support from Telia Research AB. I want to acknowledge CDT, NUTEK, and Telia Research for their efforts and support.

In my licentiate thesis I wrote that being a PhD student involves some clear choices of priority in exchange for an enjoyable and enriching time. I can only add that the above people and many more have made my time in Luleå an enrichment and much fun. I'm grateful to write that it's been relatively easy to invest all the efforts, because of the comprehension, love, and support of my parents and my Mia.

The composition of this thesis

This thesis is composed of a prologue and six self-contained parts which my coauthors and I wrote with the intention to publish as a book chapter and journal papers. The six parts contain the original and identical contents of their published versions; only typesetting is different to suit the format of this thesis. Because of this composition, the thesis in places repeats some introductory ideas. The relation between the six parts is made clear in the preceding prologue, which introduces, summarizes, and comments on each of them.

Prologue

This thesis comprises the original contents of six of my publications: [1–6]. Four of these have been or will be published as a book chapter [1] and as journal papers [2, 5, 6]. Two are published as research reports [3, 4] and are currently being reviewed for possible publication as journal papers (an earlier version of [3] is being reviewed).

The work resulting in [1–6] has also, in parallel, served the European standardization of the UMTS within ETSI. The technical documents [7–11] are standardization contributions to ETSI's working group SMG2, where standards for the radio interface of terrestrial UMTS are being developed.

Finally, results were also presented at conferences, symposia, meetings of the European COST 259 action, or published as research reports, see [12–26]. My licentiate thesis [27] in 1996 included three of the above publications, along with the research report [28].

1 Introduction

In digital radio communication systems information symbols are transmitted by means of suitably chosen waveforms that modulate a carrier signal with a suitably chosen frequency. In most systems variable factors imposed by the radio environment and hardware imperfections generate fluctuations in how these waveforms actually are received. For example, channel dispersion and alterations in the symbol rate and the carrier frequency affect the transmitted signal [29].

Because of these fluctuations, the receiver's *knowledge* of the transmitter's symbol rate, carrier frequency, and waveform constellation is not always sufficient to assure reliable detection. In order to detect the information symbols reliably, the receiver may need to counteract the channel uncertainties. *Synchronization* with the remote transmitter and *equalization* of the channel are often necessary [30, 31].

The requirements on the synchronization and equalization depend, among other factors, on the type of modulation. For example, differential demodulation usually reduces the need for channel estimation and equalization at the receiver. This thesis is concerned with how channel uncertainties are estimated in *orthogonal frequency-division multiplexing* (OFDM) transmission systems [32]. It addresses the estimation of symbol time offsets, carrier frequency offsets, and channel dispersion. With the aid of these estimates a receiver can reduce the negative effects that synchronization errors and channel dispersion have on system performance.

Synchronization and channel estimation in OFDM are each associated with particular challenges and difficulties. For OFDM-synchronization the main challenge is the high sensitivity to frequency offsets as compared to single carrier systems [33]. Although timing requirements for OFDM may not be so tight as for single carrier systems, OFDM prompts for symbol synchronizers which do not resemble traditional synchronization schemes for single carrier systems by their structure [34]. For OFDM channel estimators the main challenge is to find high performance yet implementable estimator structures [35].

The core of the thesis investigates two estimation concepts, one for synchronization errors and one for channel dispersion. The synchronization concept exploits a redundancy

that is present in most OFDM signals and known as the *cyclic prefix*. This redundancy facilitates the estimation of symbol time and carrier frequency offsets. In addition to publications associated with this thesis, important recent contributions on this estimation concept are [36–40].

The channel estimation concept exploits the frequency correlation of the channel. In many OFDM systems this concept can improve channel estimation significantly, even if the channel statistics are not exactly known at a receiver. In addition to publications associated with this thesis, other recent OFDM channel estimation contributions are found in [35, 42–48].

For a number of wireless applications OFDM has been or is currently being investigated. Recently, the *European Telecommunications Standards Institute* (ETSI) has based some European broadcast standards on OFDM. First, the *digital audio broadcasting* (DAB) [49] standard, filed in 1995, and the terrestrial *digital video broadcasting* (DVB) standard [50], filed in 1997, use OFDM. Differential demodulation reduces the need for a channel estimator and a channel equalizer in DAB receivers. For the coherently demodulated DVB signals channel equalization is necessary. Both audio and video receivers need to synchronize their oscillators and clocks to the transmitter's. DAB signals facilitate synchronization by regularly inserted null symbols while the DVB standard defines a pilot pattern consisting of pilot tones and scattered, boosted pilot symbols.

Currently, two more European standardization procedures, where OFDM plays or has played a role, progress within ETSI. First, in the standardization of the radio interface of the *universal mobile telecommunications system* (UMTS), OFDM was a technically promising candidate. The OFDM-based proposal [51] incorporated differential modulation and, as a future extension, coherent demodulation. Synchronization was proposed to be accomplished by the concept described in this thesis. The OFDM-based proposal was, however, abandoned in favor of the two final *code-division multiple access* (CDMA) proposals. Secondly, OFDM is also subject of research for use in wireless local-area networks. In 1997, ETSI announced a new standardization project for *broadband radio access networks* (BRANs) [52]. OFDM is one of the candidates for this new standard which is scheduled to be completed during 1999.

The synchronization concept presented in this thesis applies to general OFDM signals with a cyclic prefix. None of the above applications is, therefore, excluded from the estimation concept as such. A number of system aspects, however, influence how the concept actually would be embedded in a system or receiver design. This thesis addresses a few of these system aspects. In particular, it evaluates the time and frequency offset estimators in a number of practical, dispersive and fading channels. It also investigates how the concept could be used for tracking in multiuser OFDM systems such as the above UMTS proposal or future, fourth generation personal communication systems.

Channel estimators that are designed using the proposed methods in this thesis, are applicable to those of the above OFDM applications employing coherent demodulation of the subcarriers. In particular, DVB receivers could be equipped with channel estimators based on the channel estimation concept in this thesis. Investigation of the explicit application to DVB is, however, beyond the scope of this thesis.

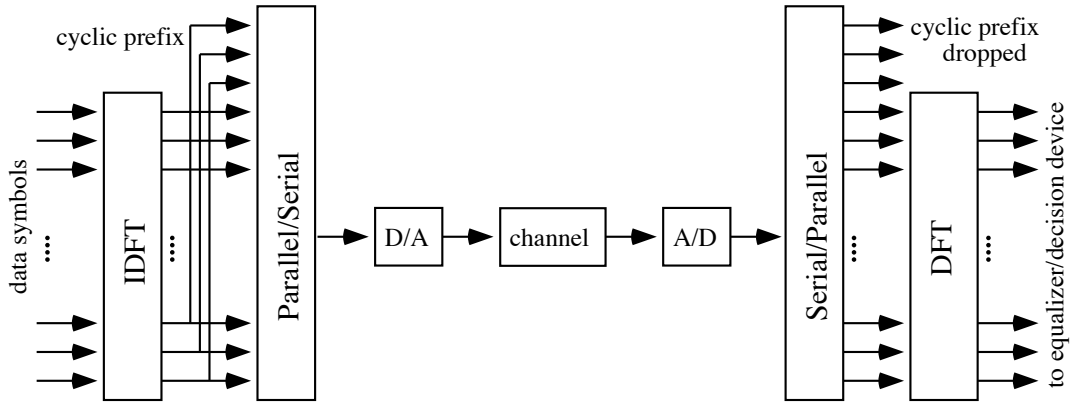

Figure 1: An OFDM system.

2 Cyclic-prefix based synchronization (Parts 2–4)

This prologue focuses on how the different parts of this thesis are related. In particular, the choice of OFDM signal models, the assumptions, etc. are highlighted. In this section the sensitivity of OFDM systems to synchronization errors and the synchronization contributions of this thesis are outlined. Section 3 addresses the effect of channel dispersion on OFDM systems and outlines the channel estimation concept. Finally, Section 4 of this prologue summarizes the more important contributions of this thesis.

2.1 Modeling synchronization errors in OFDM systems

OFDM is a block transmission system where data symbols are transmitted in parallel on a large number of subcarriers. A baseband OFDM system model, shown in Figure 1, illustrates the transmission concept. The complex data symbols are modulated on N subcarriers by an *inverse discrete Fourier transform* (IDFT). To form the OFDM symbol the last L samples are copied and put into a preamble usually referred to as the *cyclic prefix*. This data vector is digital-to-analog converted and transmitted over a channel, whose impulse response we assume is shorter than the length of the cyclic prefix. One OFDM symbol thus has duration $(N+L)T_s$ where T_s is the system's sampling period. In spite of the loss of transmission power and bandwidth associated with the cyclic prefix, the simple channel equalization it yields generally motivates its use [32].

At the receiver the signal is sampled, the cyclic prefix is removed, and the resulting data vector is demodulated by a *discrete Fourier transform* (DFT). In this thesis, the data symbols then pass a frequency domain equalizer and a decision device. Channel coding, usually necessary in fading radio environments, is not addressed in this thesis. We evaluate system performance by the uncoded symbol error rate.

Part 1 of this thesis introduces OFDM. It will be published as [1] and describes OFDM, its prevalent problems, and recent research associated with these.

Parts 2–4 address two uncertainties at the OFDM receiver, the first of which is illustrated by the block transmission characteristics in Figure 1. During each time period of duration $(N+L)T_s$ the receiver captures N samples from the serial stream of incom-

ing samples to be processed by the DFT. The block marked 'Serial/Parallel' includes this operation. In general, it is not obvious at the receiver which N-block of samples is the most suitable to capture. Because of propagation delays in the channel and sample clock imperfections at the receiver front-end, the receiver usually must track the symbol timing.

The second receiver uncertainty, not illustrated in Figure 1, is due to oscillator imperfections in the receiver front-end and Doppler effects in the radio channel. These affect the received baseband OFDM signal and increase the symbol error rate of the system, if left uncompensated. Often, a receiver needs to track these frequency variations.

We model the above two uncertainties as follows. First, the *symbol time offset* is modeled as the unknown index of the first sample of the OFDM symbol on an arbitrary but fixed time scale. The various adopted signal models assume perfect sample clocks – in [53], for instance, the effects of sample clock offsets in OFDM systems are investigated.

Secondly, carrier frequency variations are modeled by an unknown, constant *carrier frequency offset*. If not explicitly stated otherwise, the frequency offset is normalized to the carrier spacing of adjacent OFDM subcarriers. We disregard any other frequency effects. The effects of phase noise are investigated in, *e.g.*, [33, 54–56].

The signal models in Parts 2–4 form the basis for the derivation of estimators based on the *maximum likelihood* (ML) criterion. With the choice of our signal models, the causes of the symbol time offset and carrier frequency offset are transparent to the ML estimator. For instance, a time offset estimator, derived from one of the signal models in this thesis, does not distinguish between time uncertainties introduced by radio propagation or those caused by a receiver symbol clock offset. Similarly, a frequency offset estimator does not distinguish between offsets caused by the radio channel or those caused by transmitter or receiver oscillators.

The estimators assist the synchronization of the OFDM communication link. How to compensate for the offsets depends on the type of system. In a broadcast system the time offset estimate is typically used to identify the suitable block of samples making up the OFDM symbol to the receiver DFT. In addition to compensation of frequency offsets in the analog receiver front-end, frequency compensation can take place digitally, in front of the receiver DFT, with the aid of the frequency offset estimate.

In the uplink of a multiuser system that divides users across the subcarriers, these ways of synchronization at the receiver are not applicable. In this case *all* transmitted signals must be time- and frequency-aligned. Therefore, multiuser synchronization is more difficult than broadcast or downlink synchronization [57].

2.2 The effects of time and frequency offset

In OFDM systems *orthogonality* of the subcarriers is crucial. Whereas the cyclic prefix is a means to maintain orthogonality in a dispersive channel, symbol time and carrier frequency offsets may also cause the loss of subcarrier orthogonality. If not compensated for, thay can limit the performance of an OFDM system because they cause *intersymbol interference* (ISI) and *intercarrier interference* (ICI). Figures 2, 3 and 4 illustrate the effect of synchronization errors on an OFDM system with 256 subcarriers and a 10-sample cyclic prefix. The subcarriers are modulated with 16-QAM symbols.

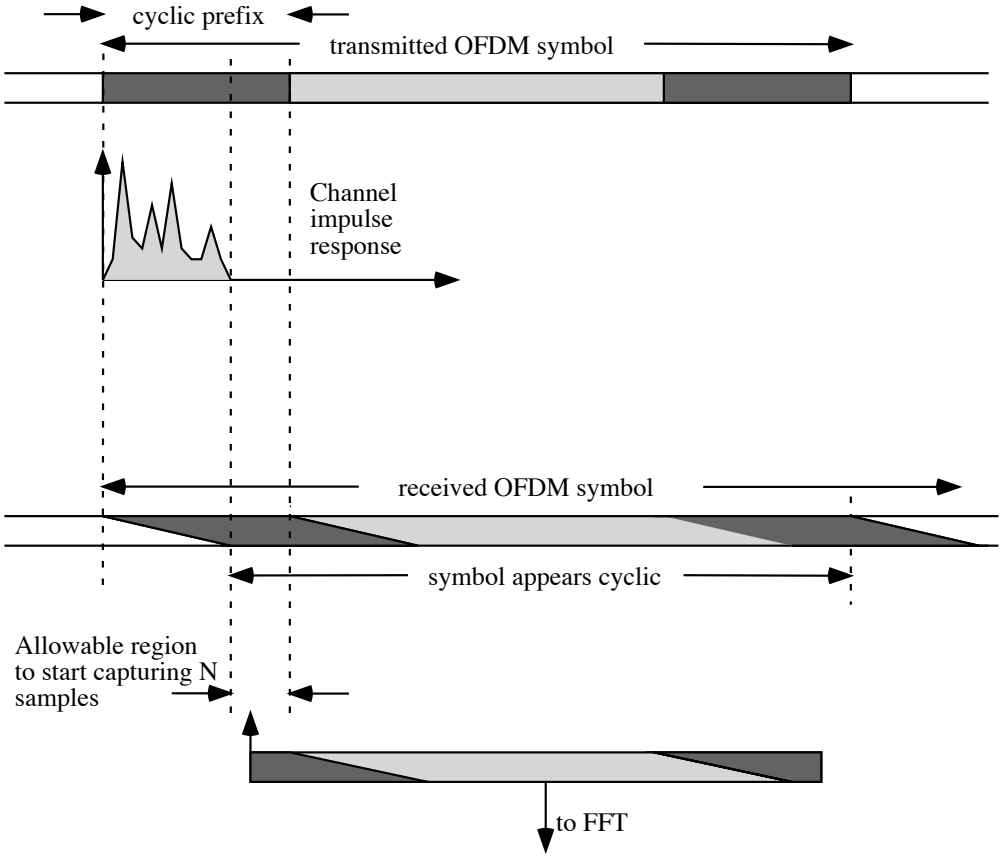

Figure 2: The symbol time offset requirements. The transmitted OFDM symbol with a cyclic prefix whose length exceeds that of the channel impulse response (top). The cyclic prefix and the symbol's tail are identical (the dark areas). As long as a receiver captures an OFDM symbol starting in the allowable region, the OFDM symbol appears cyclic, orthogonality is maintained, and ISI and ICI are avoided (bottom).

Symbol timing offsets degrade the system's performance in a non-graceful way. Because the OFDM signal is extended with a cyclic prefix, a receiver can capture an OFDM symbol, after it has passed through a dispersive channel, anywhere in a region where the symbol appears cyclic without sacrificing orthogonality, see Figure 2. Capturing a symbol outside this interval, however, causes ISI and ICI, and, consequently, a performance degradation.

A small time offset is translated by the receiver DFT into a linear phase distortion across the subcarriers without causing ISI or ICI. The left part of Figure 3 shows the effect of a small time offset on a transmitted signal which is only affected by synchronization errors (neither channel dispersion nor additive Gaussian noise distort the symbols). It shows the complex-valued data symbols after the receiver demodulation by the DFT.

Because a symbol time offset is indistinguishable from delays introduced by a dispersive channel, a channel estimator may identify small time offsets as being part of the channel dispersion. A channel equalizer fed with the channel estimates thus acts as a fine time-synchronizer by backrotating the received symbols in the left part of Figure 3. In differentially modulated systems [58], small time offsets do not cause a large performance

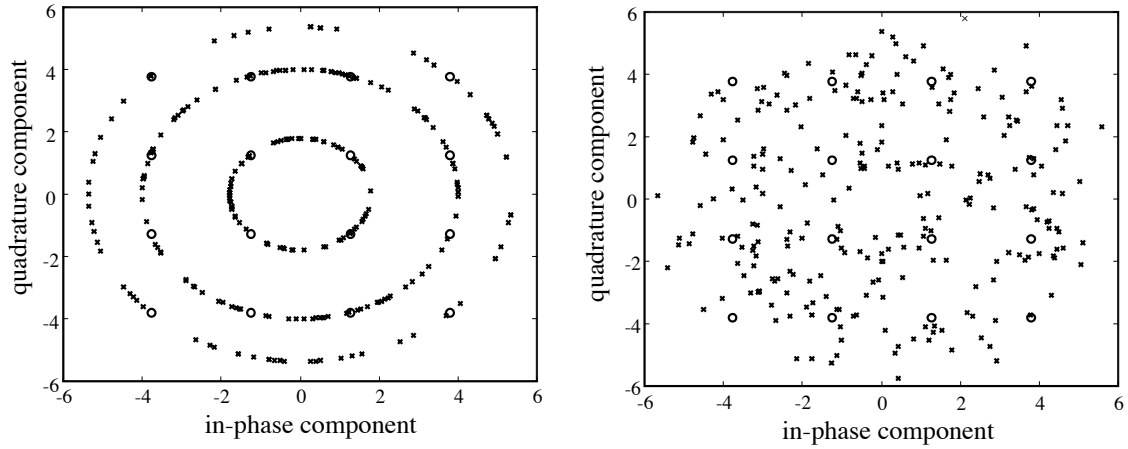

Figure 3: The input symbols of a 16-QAM constellation to the detector for two symbol time offsets in a system with a 10-sample cyclic prefix. Left: the effect of 1 sample offset; Right: the effect of 25 samples offset. No additive noise.

degradation either, because they only result in small phase differences between adjacent subcarriers or consecutive OFDM symbols.

The right part of Figure 3 shows the effect of a large time offset, that exceeds the length of the cyclic prefix. In this case, random distortion due to ISI and ICI dominates the phase rotation of the symbols. This distortion is in practice hard to counteract and is investigated in, *e.g.*, [59, 60].

Figure 4 shows the effect of a frequency offset on the same example system. The data symbols suffer from both a common phase rotation and ICI. This property is also recognized and investigated in, *e.g.*, [33]. A channel estimator cannot distinguish between phase distortions due to channel time dispersion and phase distortions due to oscillator impairments. Therefore, the above common rotation of the subcarriers may be identified by a channel estimator and compensated for by the channel equalizer. In [33], the distortion is shown to be similar to additive Gaussian noise. Therefore ICI is often addressed by the degradation of the *signal-to-noise ratio* (SNR) it causes.

2.3 Maximum likelihood offset estimation

The above synchronization effects have motivated many people to search for synchronization schemes for OFDM systems, see, *e.g.*, [36–41, 57, 61–64]. Estimation methods described in the literature belong to one of two groups: those that base the estimates on pilot information, see, *e.g.*, [57, 61–64] and those that base the estimates on the signal's statistical properties, see, *e.g.*, [36–41]. The offset estimation concept presented in Parts 2–4 of this thesis belongs to the latter group.

Part 2 of this thesis presents the joint ML estimator of the symbol time and carrier frequency offsets in OFDM systems employing a cyclic prefix for the *additive white Gaussian noise* (AWGN) channel. The ML estimator operates on the received signal in front of the receiver DFT. It does not need pilot information, is independent of how the subcarriers are modulated, and dependent on the SNR and the length of the cyclic prefix

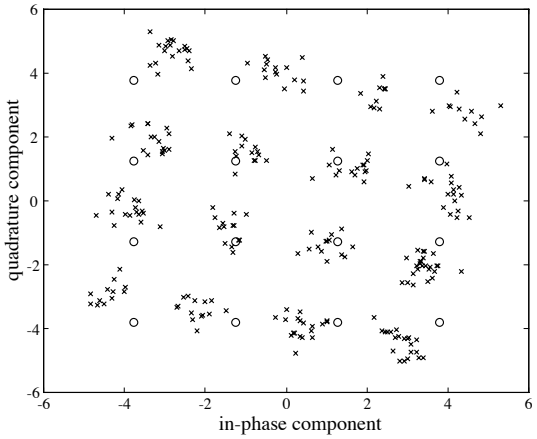

Figure 4: The input symbols of a 16-QAM constellation to the detector for a 7% frequency offset. No additive noise.

L. By simulation the performance of the estimator is illustrated both for the AWGN channel and for a dispersive channel.

By the time it was published as [2], some other contributions had independently reported estimators that exploited the cyclic prefix, see, *e.g.*, [36, 37]. Later, other such contributions were published in [38–41]. A recent conference paper compares several cyclic prefix-based methods in an indoor radio channel [65]. The paper shows that the ML estimator performs best in these channels if the receiver is assumed to know the average SNR.

We model the received OFDM signal $r(k)$ as

$$r(k) = s(k-\theta)e^{j2\pi\varepsilon k/N} + n(k), \tag{1}$$

where the signal $s(\cdot)$ models the transmitted OFDM signal. It is distorted by additive white Gaussian noise $n(\cdot)$. The model accounts for uncertainties in the symbol time and carrier frequency. The uncertainty in the arrival time of the OFDM symbol is modeled as a delay in the channel of θ samples, where θ is integer-valued and unknown. The uncertainty in carrier frequency is modeled as a complex multiplication of the received data by $e^{j2\pi\varepsilon k/N}$, where ε is the normalized frequency offset (normalized to the intercarrier spacing $1/(NT_s)$), and N is, as before, the number of subcarriers.

The assumptions about the statistical structure of the transmitted OFDM signal $s(\cdot)$ are crucial in this model. They allow explicit expressions of the joint ML estimator of θ and ε from the received signal $r(\cdot)$ without the need for additional pilot information. We assume that the transmitted OFDM signal is Gaussian, because it is the sum of many independent, similarly distributed stochastic variables [66, pp. 368–369]. Because of the cyclic prefix, $s(\cdot)$ is not stationary, but contains correlations between the signal's redundant samples.

In many practical systems the model (1) may be too much of an abstraction of reality and the performance of the ML estimator may not be satisfactory. Therefore, we also indicate how the above estimator performs in a fading and dispersive channel. We illustrate that the performance in such channels is limited by an error floor. This aspect is further addressed and elaborated in Part 3.

2.4 Pulse shaping, multiple symbols, and channel dispersion

The estimator in Part 2 is optimal for the AWGN channel. The choice of this model yields a useful estimator structure, but some of its simplifications limit the performance in practical systems. Part 3, published as [3], extends the results of Part 2 by the choice of more general signal models and investigates means to improve the performance of the ML estimator for model (1) in more practical situations.

The work in Part 3 explores the balance between the extent to which OFDM models are simplified and how useful resulting ML estimators are in terms of performance and complexity. On one hand, simplified models of the OFDM system allow for simple, explicit ML offset estimators. On the other hand, we show that by incorporating more sytem characteristics the estimator performance may sometimes improve significantly without compromising estimator complexity too much. Whether the presented estimators in Part 3 are of much practical value or not, thay all give, an illustrative view on the offset estimation problem and comprehension of how a maximum likelihood estimator exploits signal correlations for offset estimation.

The received OFDM signal is modeled in three different ways. First, some proposed OFDM systems include pulse shaping of the OFDM signal at the transmitter in order to suppress the out-of-band emission [51,60]. Other contributions report pulse shaping to be beneficial for system robustness against Doppler effects in the radio channel, and against frequency or timing errors, see, *e.g.*, [67]. Shaping of the transmitted signal changes its correlation properties. This property is not included in the signal model (1) in Part 2 and could degrade the performance of the associated ML estimator. Therefore, in Part 3, we first adopt the signal model

$$r(k) = g(k-\theta)s(k-\theta)e^{j2\pi\varepsilon k/N} + n(k), \tag{2}$$

where $g(\cdot)$ is the transmitter pulse shape. In Part 2 $g(\cdot)$ is a rectangular window. We restrict ourselves to the kind of pulse shaping that windows the transmitted OFDM signal as in (2), and do not address pulse shaping by filtering the transmitted signal as proposed in, *e.g.*, [67].

A second model insufficiency in Part 2 is that in many radio applications, time and frequency offsets vary only slowly in time. Consecutive OFDM symbols suffer, therefore, from approximately the same offsets. This property is not recognized by the signal model (1), but can be used to improve the performance of the offset estimator. The second model in Part 3 recognizes this property, and differs only from model (1) by the correlation properties of the transmitted signal. We model the received signal as

$$r(k) = \tilde{s}(k-\theta)e^{j2\pi\varepsilon k/N} + n(k), \tag{3}$$

where $\tilde{s}(\cdot)$ is the transmitted signal which we now assume contains M consecutive OFDM symbols that are affected by the same symbol time and carrier frequency offsets.

Finally, in a dispersive, fading channel environment the estimator based on (1) is still applicable but its performance shows an error floor, as illustrated in Part 2, and it is no longer optimal. (Besides, in an AWGN channel the OFDM system designer would typically refrain from using a cyclic prefix and the above estimator would not be of

any use.) Therefore, Part 3 investigates, for dispersive channels, the potential of using channel knowledge in the estimator design. The received signal is modeled by

$$r(k) = (h * s)(k - \theta) + n(k), \tag{4}$$

where $h(\cdot)$ is the known channel impulse response. For two reasons, we refrain from incorporating the frequency offset in this model. First, for many practical systems, the frequency offset estimator in Part 2 has sufficient performance. Secondly, we have not found tractable estimator structures for a model incorporating a frequency offset *and* channel dispersion.

We assume receiver knowledge of the channel. While this assumption holds for some applications (such as copper wire channels), the receiver will have to track a time-varying channel in others (such as DAB and DVB). With our assumption the resulting ML estimator performance gives an upper bound on the performance of an estimator that does not use pilots and is therefore useful when evaluating other estimators' performances.

Part 3 presents the three ML estimators, based on the models (2)–(4) above, and suggests an implementation structure for each of them. It also illustrates by simulation how each of the estimators improves the performance of the estimator based on model (1).

2.5 Multiuser synchronization

OFDM has attractive properties for multiuser systems because it intrinsically supports both time-division multiple access and frequency-division multiple access (across the subcarriers). The OFDM-based radio interface [51], proposed for the UMTS is such a multiuser system. Along with its evaluation in ETSI during 1997 came the need for algorithms synchronizing multiple users in the uplink. Multiuser synchronization is more difficult than downlink or broadcast synchronization because each user has its own synchronization errors and orthogonality is only maintained if *all* users are synchronized with the remote base station receiver, and thus with each other.

Not many contributions address this problem in the literature. The possibilities of multiuser OFDM, the requirements, and a synchronization scheme are investigated in [57].

Part 4, published as [4], shows the feasibility of uplink tracking synchronization of a multiuser OFDM system. It focuses on the system aspects of time and frequency synchronization and describes a synchronization scheme using a cyclic prefix based estimator for a multiuser OFDM system. In this paper, we think of the received signal as

$$r(k) = \sum_{m=0}^{M-1} s_m(k - \theta_m) e^{j2\pi\varepsilon_m k/N} + n(k), \tag{5}$$

where M is the number of transmitted signals. We assume that different users are assigned to different subcarriers and that the subcarriers of each user are grouped together.

We describe a multiuser offset estimator based on the concept presented in Parts 2 and 3. Rather than the optimality of the estimator, this paper focuses on its applicability in a particular system scenario. We present a synchronization scheme and a base station

receiver structure for a multiuser scenario. The work in Part 4 supported the OFDM-based proposal for the UMTS radio interface [51]. In conjunction with this work, the related technical documents [7–11] were presented within ETSI.

3 Transform-based channel estimation (Parts 5–6)

3.1 The effects of channel dispersion

One of the key properties of OFDM systems is that channel dispersion affects the transmitted data symbols multiplicatively – the subchannels appear as orthogonal, flat fading channels. Differential demodulation of the subcarriers (in time or in frequency) is a feasible way to exploit this system property [49, 58].

Receivers with coherent demodulation may also gain from the mentioned system property: equalization can effectively be performed by a one-tap equalizer for each subcarrier. In such a system a channel equalizer must, however, be fed estimates of the channel attenuations. The transmission of pilot symbols that support the channel estimation decreases the data rate of the system compared to differential systems. On the other hand, coherent systems often have lower symbol error rates than differential systems.

In this thesis we assume that the radio channel is slowly fading, that is, we assume that the channel does not change during the transmission of one OFDM symbol. In Parts 5 and 6, we adopt a multipath channel model [31]

$$g(\tau) = \sum_m \alpha_m \delta(\tau - \tau_m T_s) \tag{6}$$

where α_k are zero-mean complex Gaussian variables, and T_s is, as before, the sampling period of the system. We assume that the channel is shorter than the cyclic prefix, $\tau_m < L$. The insertion of a cyclic prefix then avoids ISI and preserves the orthogonality between the subcarriers. The OFDM system can equivalently be modeled with the simple input-output relation [32]

$$y_k = h_k x_k + n_k, \qquad k = 0, \ldots, N-1, \tag{7}$$

where x_k is the transmitted symbol, y_k is the received symbol, and n_k is a sample from a complex-valued AWGN process at the kth subcarrier. The complex-valued channel attenuation h_k is given by

$$h_k = G(\frac{k}{NT_s}), \tag{8}$$

where $G(\cdot)$ is the frequency response of the channel $g(\tau)$.

Two properties of the channel attenuations, can be used in to design good channel estimators. Both properties are related to the fact that the channel delay spread is short compared to the symbol length. First, the N frequency samples h_k are correlated. Secondly, suitable transformation of the attenuation vector $[h_0 h_1 \ldots h_{N-1}]^T$ concentrates the channel channel power into a subspace with a small dimension. The first property allows to improve on the performance of channel estimators, not using the correlation; the second property allows to make tractable approximations of this improved estimator. Parts 5 and 6 each address one particular choice of transformation.

3.2 DFT-based channel estimation

Effective compensation of the channel dispersion in coherent systems is usually performed via the estimation of the subchannel attenuations, seed, *e.g.*, [35, 44–48]. The concept in Parts 5 and 6 allows the design of low-complexity channel estimators the performance of which is close to the optimal *linear minimum mean-squared error* (LMMSE) channel estimator.

Channel estimators described in the literature are either assisted by pilot symbols [45] or used in a decision-directed scheme [35, 44]. In the estimation concept of Parts 5 and 6 we assume that all transmitted data symbols in an OFDM symbol are known by the receiver. This may either be due to the insertion of an entirely known OFDM symbol or in a decision-directed scheme where we assume correct decisions. A straightforward estimate of the channel attenuation of the kth subcarrier is, from (7),

$$\widehat{h}_k = \frac{y_k}{x_k}. \tag{9}$$

This *least-squares* (LS) estimator, does not recognize or exploit correlation between channel attenuations. Exploiting the correlation may smooth and improve estimator performance, significantly.

The LMMSE estimator of the channel attenuations exploits the channel frequency correlation optimally in terms of mean-squared error (among all linear estimators) but is of little practical value because of its computational complexity.

This has been recognized in [21, 46, 47] where an estimator is proposed which also exploits the frequency correlation of the channel. This estimator uses a transform-based design procedure, where the channel attenuations are transformed into the time-domain by means of a DFT. Channel estimation is then performed in the time-domain and the channel estimates are transformed back to the subcarrier domain.

Part 5, which will be published as [5], analyzes these DFT-based channel estimators. One of the conclusions is that the symbol error rate performance of systems employing DFT-based channel estimators experiences an error floor if the channel is not sample-spaced, that is, for non-integer τ_m in (6). Radio channels are generally not sample-spaced and DFT-based channel estimators must be designed with care. Part 5 also suggests ways to design such channel estimators and compares their performances both in terms of system symbol error rate and computational complexity.

3.3 SVD-based channel estimation

Part 6, published as [6], introduces the *singular value decomposition* (SVD) as a transformation tool in the design of channel estimators. The resulting estimator structures are similar to the DFT-based channel estimators in Part 5. In the ideal situation where the channel correlation and the SNR are known, the proposed estimator design yields optimal low-rank approximations of the LMMSE estimator in terms of mean-squared error.

Since the channel correlations and the SNR usually are not known at the receiver a channel estimator is proposed to be designed generically, *i.e.*, for particular fixed assumed

correlations and SNR, as also proposed in, *e.g.*, [45]. Part 6 analyzes the effects of mismatch between true and assumed values in the estimator design. As for the DFT-based estimators in Part 5, an error floor bounds the performance of the low-rank estimators. The estimation concept is presented for the case where all the symbols in an OFDM symbol are known. The concept is, however, also applicable in a pilot-symbol assisted modulation scheme [68]. This is illustrated by comparison of the proposed concept to another channel estimation scheme [45].

Part 6 shows that SVD-based, generically designed estimators can combine low complexity with high performance. The relevance of this estimation concept was recently confirmed in [48] where it was further evaluated and extended to include time correlation.

4 Contributions

Summarizing, the more important contributions of this thesis are:

- This thesis presents the joint ML estimator of time and frequency offsets for OFDM systems with a cyclic prefix in an AWGN channel. The estimator's performance is independent of the type of modulation of the subcarriers and does not require pilot information. Simulations show the performance of the estimator in both the AWGN channel and in a dispersive and fading channel. (Part 2)

- This thesis shows the feasibility of uplink tracking synchronization of a multiuser OFDM system. It describes a multiuser symbol time and carrier frequency synchronization scheme – including a structure for the base station – incorporating an estimator based on the cyclic prefix. This synchronization scheme was a part of the OFDM-based UMTS proposal [51]. (Part 4)

- The theory of optimal rank reduction by the SVD yields a new tool to design low-rank channel estimators. A channel estimator is proposed to be designed generically, *i.e.*, for particular fixed assumed correlations and SNR. Such an SVD-based generic channel estimator combines low complexity with high performance. (Part 6)

References

[1] J.J. van de Beek, P.O. Börjesson, P. Ödling, and S.K. Wilson, 'Orthogonal frequency-division multiplexing (OFDM)', in W.R. Stone (editor), *Review of Radio Science 1997-1999*, International Union of Radio Science (URSI), Oxford University Press, in press.

[2] J.J. van de Beek, M. Sandell, and P.O. Börjesson, 'ML estimation of time and frequency offset in OFDM systems', *IEEE Transactions on Signal Processing*, vol. 45, no. 7, pp. 1800-1805, July 1997.

[3] J.J. van de Beek, P.O. Börjesson, M.L. Boucheret, J. Martinez Arenas, D. Landström, P. Ödling, and S.K. Wilson, 'Three non-pilot-based time and frequency estimators for OFDM', Research Report 1998:08, Division of Signal Processing, Luleå University of Technology, September 1998.

[4] J.J. van de Beek, P.O. Börjesson, M.L. Boucheret, J. Martinez Arenas, D. Landström, P. Ödling, C. Östberg, M. Wahlqvist, and S.K. Wilson, 'A time and frequency synchronization scheme for multiuser OFDM', Research Report 1998:06, Division of Signal Processing, Luleå University of Technology, August 1998.

[5] O. Edfors, M. Sandell, J.J. van de Beek, S.K. Wilson, and P.O. Börjesson, 'Analysis of DFT-based channel estimators for OFDM', *Wireless Personal Communications*, Kluwer Academic Publishers, in press.

[6] O. Edfors, M. Sandell, J.J. van de Beek, S.K. Wilson, and P.O. Börjesson, 'OFDM channel estimation by singular value decomposition', *IEEE Transactions on Communications*, vol. 46, no. 7, pp. 931–939, July 1998.

[7] M. Wahlqvist, C. Östberg, J.J. van de Beek, O. Edfors, and P.O. Börjesson, 'A conceptual study of OFDM-based multiple access schemes: part 1 - air interface requirements', Technical Document Tdoc 117/96, ETSI STC SMG2 meeting no. 18, Helsinki, Finland, May 28–31, 1996. Available from the ETSI Secreteriat, F-06921 Sophia Antipolis Cedex, France.

[8] J.J. van de Beek, O. Edfors, P.O. Börjesson, M. Wahlqvist, and C. Östberg, 'A conceptual study of OFDM-based multiple access schemes: part 2 - channel estimation in the uplink', Technical Document Tdoc 116/96, ETSI STC SMG2 meeting no. 18, Helsinki, Finland, May 28–31, 1996. Available from the ETSI Secreteriat, F-06921 Sophia Antipolis Cedex, France.

[9] J.J. van de Beek, O. Edfors, P.O. Börjesson, M. Wahlqvist, and C. Östberg, 'A conceptual study of OFDM-based multiple access schemes: part 3 - performance evaluation of a coded system', Technical Document Tdoc 166/96, ETSI STC SMG2 meeting no. 19, Düsseldorf, Germany, September 2–6, 1996. Available from the ETSI Secreteriat, F-06921 Sophia Antipolis Cedex, France.

[10] J.J. van de Beek, P.O. Börjesson, D. Landström, M. Wahlqvist, P. Ödling, and C. Östberg, 'A conceptual study of OFDM-based multiple access schemes: part 4 - time and frequency tracking', Technical Document Tdoc 250/96, ETSI STC SMG2 meeting no. 20, Nice, France, December 16–20, 1996. Available from the ETSI Secreteriat, F-06921 Sophia Antipolis Cedex, France.

[11] M. Wahlqvist, M. Ericsson, C. Östberg, L. Olsson, M. Johansson, W. Ye, P. Ödling, O. Edfors, D. Landström, J.J. van de Beek, and J. Martinez Arenas, 'Description of Telias OFDM based proposal (working document in the OFDM concept group)', Technical Document Tdoc 180/97, ETSI STC SMG2 meeting no. 22, Bad Aibling, Germany, May 12–16, 1997. Available from the ETSI Secreteriat, F-06921 Sophia Antipolis Cedex, France.

[12] J.J. van de Beek, M. Sandell, P.O. Börjesson, 'ML Estimation of Timing and Frequency Offset in Multicarrier Systems', Research Report TULEA 1996:09, Division of Signal Processing, Luleå University of Technology, April 1996. Later published as [2].

[13] M. Sandell, J.J. van de Beek, and P.O. Börjesson, 'Timing and frequency synchronization in OFDM systems using the cyclic prefix', in *Proceedings of the IEEE International Symposium on Synchronization*, Essen, Germany, December 14–15, 1995, pp. 16–19.

[14] J.J. van de Beek, M. Sandell, M. Isaksson, and P.O. Börjesson, 'Low-complex frame synchronization in OFDM systems', in *Proceedings of the IEEE International Conference on Universal Personal Communications (ICUPC'95)*, Tokyo, Japan, November 6–10, 1995, pp. 982–986.

[15] J.J. van de Beek, M. Sandell, and P.O. Börjesson, 'On synchronization in OFDM systems using the cyclic prefix', in *Proceedings of the Radiovetenskaplig Konferens (RVK'96)*, Luleå, Sweden, June 3–6, 1996, pp. 663–667.

[16] D. Landström, J. Martinez Arenas, J.J. van de Beek, P.O. Börjesson, M.-L. Boucheret, and P. Ödling, 'Time and frequency offset estimation in OFDM systems employing pulse shaping', in *Proceedings of the IEEE International Conference Universal Personal Communications (ICUPC'97)*, San Diego, USA, October 12–16, 1997, pp. 279–283.

[17] J. Martinez Arenas, D. Landström, J.J. van de Beek, P.O. Börjesson, M.-L. Boucheret, and P. Ödling, 'Synchronization in OFDM systems – Sensitivity to the choice of pulse shape', in *Proceedings of the 16th GRETSI Symposium on Signal and Image Processing*, Grenoble, France, September 15–19, 1997, pp. 315-319.

[18] J.J. van de Beek, P.O. Börjesson, M.-L. Boucheret, D. Landström, J. Martinez Arenas, P. Ödling, 'On Synchronization in an OFDM based UMTS proposal', in *Proceedings of the COST 254 Workshop 'Emerging Techniques for Communication Terminals'*, Toulouse, France, July 7–9, 1997, pp. 315–320. (also presented as Technical Document (97)63, at the 3rd MC Meeting of COST 259, Lisbon, Portugal, September 24–26, 1997.)

[19] J.J. van de Beek, P.O. Börjesson, M.-L. Boucheret, D. Landström, J. Martinez Arenas, P. Ödling, S.K. Wilson, C. Östberg, and M. Wahlqvist, 'Synchronization of a TDMA-OFDM frequency hopping system', in *Proceedings of the IEEE International Vehicular Technology Conference (VTC'98)*, Ottawa, Canada, May 18–21, 1998, pp. 1290–1294. (also presented as Technical Document (98)33, at the 4rd MC Meeting of COST 259, Bern, Schweiz, February 2–4, 1998.)

[20] O. Edfors, M. Sandell, J.J. van de Beek, S.K. Wilson, P.O. Börjesson, 'Analysis of DFT-based Channel Estimators for OFDM', Research Report TULEA 1996:17, Division of Signal Processing, Luleå University of Technology, September 1996. Later published as [5].

[21] J.J. van de Beek, O. Edfors, M. Sandell, S.K. Wilson, and P.O. Börjesson, 'On channel estimation in OFDM systems', in *Proceedings of the IEEE Vehicular Technology Conference (VTC'95)*, Chicago, USA, July 25–28, 1995, pp. 815–819.

[22] J.J. van de Beek, O. Edfors, P.O. Börjesson, M. Wahlqvist, C. Östberg, 'Channel Estimation in the Uplink of an OFDM System', in *Proceedings of the Nordic Radio Symposium (NRS'96)*, Lund, Sweden, August 1996, pp 32-35.

[23] O. Edfors, M. Sandell, J.J. van de Beek, S.K. Wilson, P.O. Börjesson, 'OFDM Channel Estimation by Singular Value Decomposition', Research Report TULEA 1996:18, Division of Signal Processing, Luleå University of Technology, September 1996. Later published as [6].

[24] O. Edfors, M. Sandell, J.J. van de Beek, S.K. Wilson, and P.O. Börjesson, 'OFDM channel estimation by singular value decomposition', in *Proceedings of the IEEE 46th International Vehicular Technology Conference (VTC'96)*, Atlanta, USA, April 28–May 1, 1996, pp. 923-927.

[25] O. Edfors, M. Sandell, J.J. van de Beek, S.K. Wilson, and P.O. Börjesson, 'An application of the singular value decomposition to OFDM channel estimation', in *Proceedings of the Radiovetenskaplig Konferens (RVK'96)*, Luleå, Sweden, June 3–6, 1996, pp. 678–682.

[26] O. Edfors, M. Sandell, J.J. van de Beek, D. Landström, and F. Sjöberg, 'An Introduction to Orthogonal Frequency-Division Multiplexing', Research Report TULEA 1996:16, Division of Signal Processing, Luleå University of Technology, September 1996.

[27] J.J. van de Beek, *Estimation of Synchronization Parameters*, Licentiate Thesis 1996:14, Division of Signal Processing, Luleå University of Technology, April 1996.

[28] J.J. van de Beek, P.O. Börjesson, H. Eriksson, J.-O. Gustavsson, L. Olsson, 'MMSE Estimation of Arrival Time with Application to Ultrasonic Signals', Research Report TULEA 1993:15, Division of Signal Processing, Luleå University of Technology, April 1993.

[29] W.C. Jakes, *Microwave Mobile Communications*, John Wiley & Sons, New York, 1974.

[30] H. Meyr and G. Ascheid, *Synchronization in Digital Communications*, John Wiley & Sons, New York, vol. 1, 1990.

[31] J.G. Proakis, *Digital Communications*, 3rd edition, McGraw-Hill, New York, 1995.

[32] J.A.C. Bingham, 'Multicarrier modulation for data transmission: an idea whose time has come', *IEEE Communications Magazine*, vol. 28, no. 5, pp. 5–14, May 1990.

[33] T. Pollet, M. van Bladel, and M. Moeneclaey, 'BER sensitivity of OFDM systems to carrier frequency offset and Wiener phase noise', *IEEE Transactions on Communications*, vol. 43, no. 2/3/4, pp. 191–193, February/March/April 1995.

[34] T.M. Schmidl and C. Cox, 'Robust frequency and timing synchronization for OFDM', *IEEE Transactions on Communications*, vol. 45, no. 12, pp. 1613–1621, December 1997.

[35] V. Mignone and A. Morello, 'CD3-OFDM: a novel demodulation scheme for fixed and mobile receivers', *IEEE Transactions on Communications*, vol. 44, no. 9, pp. 1144–1151, September 1996.

[36] P.J. Tourtier, R. Monnier, and P. Lopez, 'Multicarrier modem for digital HDTV terrestrial broadcasting', *Signal Processing: Image Communication*, vol. 5, no. 5/6, pp. 379–403, December 1993.

[37] F. Daffara and O. Adami, 'A new frequency detector for orthogonal multicarrier transmission techniques', in *Proceedings of the Vehicular Technology Conference (VTC'95)*, Chicago, USA, July 25–28, 1995, pp. 804–809.

[38] T.M. Schmidl, *Synchronization Algorithms for Wireless Data Transmission Using Orthogonal Frequency Division Multiplexing (OFDM)*, PhD thesis, Stanford University, USA, 1997.

[39] D. Lee and K. Cheon, 'A new symbol timing recovery algorithm for OFDM systems', *IEEE Transactions on Consumer Electronics*, vol. 43, no. 3, pp. 767–775, August 1997.

[40] T. Seki, Y. Sugita, and T. Ishikawa, *OFDM Synchronization Demodulation Unit*, United States Patent, no. 5,602,835, February 1997.

[41] J. Martinez Arenas, *Procédés de Synchronisation Adaptés aux Systèmes á Porteuses Multiples Orthogonales*, PhD thesis, Ecole Nationale Supérieure de Télécommunications, Toulouse, France, April 1998, in English.

[42] M. Sandell, *Design and Analysis of Estimators for Multicarrier Modulation and Ultrasonic Imaging*, PhD Thesis 1996:205D, Luleå University of Technology, Luleå, Sweden, September 1996.

[43] O. Edfors, *Low-Complexity Algorithms in Digital Receivers*, PhD Thesis 1996:206D, Luleå University of Technology, Luleå, Sweden, September 1996.

[44] S.K. Wilson, R.E. Khayata, and J.M. Cioffi, '16-QAM modulation with orthogonal frequency-division multiplexing in a Rayleigh-fading environment', in *Proceedings of the IEEE Vehicular Technology Conference (VTC'94)*, Stockholm, Sweden, June 8–10, 1994, pp. 1660–1664.

[45] P. Höher, 'TCM on frequency-selective land-mobile fading channels', in E. Biglieri and M. Luise (editors), *Proceedings of the Tirrenia International Workshop on Digital Communications, 'Coded Modulation and Bandwidth-Efficient Transmission'*, Tirrenia, Italy, September 8–12, 1991, Elsevier, 1992, pp. 317-328.

[46] A. Chini, *Multicarrier Modulation in Frequency Selective Fading Channels*, PhD thesis, Carleton University, Ottawa, Canada, 1994.

[47] A. Chini, M.S. El-Tanany, and S.A. Mahmoud, 'Transmission of high rate ATM packets over indoor radio channels', *IEEE Journal on Selected Areas in Communications*, vol. 14, no. 3, pp. 469–476, April 1996.

[48] Y. Li, L.J. Cimini, Jr., and N.R. Sollenberger, 'Robust channel estimation for OFDM systems with rapid dispersive fading channels', *IEEE Transactions on Communications*, vol. 43, no. 7, pp. 1320–1324, July 1998.

[49] European Telecommunications Standards Institute (ETSI), *Radio Broadcasting Systems; Digital Audio Broadcasting (DAB) to Mobile, Portable and Fixed Receivers*, European Telecommunication Standard ETS 300 401, 1st edition, reference DE/JTC-DAB, February 1995. Available from the ETSI Secreteriat, F-06921 Sophia Antipolis Cedex, France.

[50] European Telecommunications Standards Institute (ETSI), *Digital Video Broadcasting (DVB); Framing Structure, Channel Coding and Modulation for Digital Terrestrial Television*, European Telecommunications Standard, ETS 300 744 1st edition, reference DE/JTC-DVB-8, March 1997. Available from the ETSI Secreteriat, F-06921 Sophia Antipolis Cedex, France.

[51] European Telecommunications Standards Institute (ETSI), *OFDMA Evaluation Report – The Multiple Access Scheme Proposal for the UMTS Terrestrial Radio Air Interface (UTRA)*, Technical Document Tdoc 896/97, ETSI SMG meeting no. 24, Madrid, December 1997. Available from the ETSI Secreteriat, F-06921 Sophia Antipolis Cedex, France.

[52] European Telecommunications Standards Institute (ETSI), *Broadband Radio Access Networks (BRAN); Inventory of Broadband Radio Technologies and Techniques*, Technical Report, reference DTR/BRAN-030001, February 1998. Available from the ETSI Secreteriat, F-06921 Sophia Antipolis Cedex, France.

[53] T. Pollet, P. Spruyt, and M. Moeneclaey, 'The BER performance of OFDM systems using non-synchronized sampling', in *Proceedings of the IEEE Global Telecommunications Conference (GLOBECOM'94)*, San Fransisco, USA, November 27–December 1, 1994, pp. 253–257.

[54] C. Muschallik, 'Influence of RF oscillators on an OFDM signal', in *IEEE Transactions on Consumer Electronics*, vol. 41, no. 3, pp. 592–603, August 1995.

[55] A. Garcia Armada and M. Calvo, 'Phase noise and sub-carrier spacing effects on the performance of an OFDM communication system', *IEEE Communications Letters*, vol. 2, no. 1, pp. 11–13, January 1998.

[56] T. Pollet, M. Moeneclaey, I. Jeanclaude, and H. Sari, 'Comparison of single-carrier and multi-carrier QAM system performance in the presence of carrier phase jitter', *Wireless Personal Communications*, vol. 8, no. 2, pp. 205-218, September 1998.

[57] L. Wei and C. Schlegel, 'Synchronization requirements for multi-user OFDM on satellite mobile and two-path Rayleigh fading channels', *IEEE Transactions on Communications*, vol. 43, no. 2/3/4, pp. 887–895, February/March/April 1995.

[58] V. Engels and H. Rohling, 'Multilevel differential modulation techniques (64-DAPSK) for multicarrier transmission systems', *European Transactions on Telecommunications*, vol. 6, no. 6, pp. 633–640, November/December 1995.

[59] T. Pollet and M. Moeneclaey, 'Synchronizability of OFDM signals', in *Proceedings of the IEEE Global Telecommunications Conference (GLOBECOM'95)*, Singapore, November 13–17, 1995, pp. 2054–2058.

[60] M. Gudmundson and P-O. Anderson, 'Adjacent channel interference in an OFDM system', in *Proceedings of the Vehicular Technology Conference (VTC'96)*, Atlanta, USA, April 28–May 1, 1996, pp. 918–922.

[61] W.D. Warner and C. Leung, 'OFDM/FM frame synchronization for mobile radio data communication', *IEEE Transactions on Vehicular Technology*, vol. 42, no. 3, pp. 302–313, August 1993.

[62] P.H. Moose, 'A technique for orthogonal frequency division multiplexing frequency offset correction', *IEEE Transactions on Communications*, vol. 42, no. 10, pp. 2908–2914, October 1994.

[63] F. Classen and H. Meyr, 'Frequency synchronization algorithms for OFDM systems suitable for communication over frequency-selective fading channels', in *Proceedings of the IEEE Vehicular Technology Conference (VTC'94)*, Stockholm, Sweden, June 8–10, 1994, pp. 1655–1659.

[64] M. Luise and R. Reggiannini, 'Carrier frequency acquisition and tracking for OFDM systems', *IEEE Transactions on Communications*, vol. 44, no. 11, pp. 1590–1598, November 1996.

[65] S.H. Müller, 'On the optimality of metrics for coarse frame synchronization in OFDM: a comparison', in *Proceedings of the International Symposium on Personal, Indoor, and Mobile Radio Communications (PIMRC'98)*, Boston, USA, September 8–11, 1998.

[66] P. Billingsley, *Probability and Measure*, 2nd edition, John Wiley & Sons, New York, 1986.

[67] R. Haas and J.C. Belfiore, 'A time-frequency well-localized pulse for multiple carrier transmission', *Wireless Personal Communications*, vol. 5, no. 1, pp. 1–18, July 1997.

[68] J.K. Cavers, 'An analysis of pilot-symbol assisted modulation for Rayleigh-fading channels', *IEEE Transactions on Vehicular Technology*, vol. 40, no. 4, pp. 686–693, November 1991.

Part 1

This part will be published as

J.J. van de Beek, P. Ödling, S.K. Wilson, and P.O. Börjesson, 'Orthogonal Frequency-Division Multiplexing (OFDM)', in W.R. Stone (editor), *Review of Radio Science 1996–1999*, International Union of Radio Science (URSI), Oxford University Press, 1999, in press.

Orthogonal Frequency-Division Multiplexing (OFDM)

J.J. van de Beek, P. Ödling, S.K. Wilson, and P.O. Börjesson

1 Introduction

Orthogonal Frequency-Division Multiplexing (OFDM) is the modulation technique for European standards such as the *Digital Audio Broadcasting* (DAB) [1] and the *Digital Video Broadcasting* (DVB) [2] systems. As such it has received much attention and has been proposed for many other applications, including local area networks [3] and personal communication systems [4]. OFDM is a type of multichannel modulation that divides a given channel into many parallel subchannels or subcarriers, so that multiple symbols are sent in parallel. Earlier overviews of OFDM can be found in [5, 6].

The first multichannel modulation systems appeared in the 1950's as military radio links, systems best characterized as frequency-division multiplexed systems. The first OFDM schemes were presented by Chang [7] and Saltzberg [8]. Actual use of OFDM was limited and the practicability of the concept was questioned. However, OFDM was made more practical through work of Chang and Gibby [9], Weinstein and Ebert [10], Peled and Ruiz [11], and Hirosaki [12]. The type of OFDM that we will describe in this article uses the *discrete Fourier transform* (DFT) [10] with a cyclic prefix [11]. The DFT (implemented with a *fast Fourier transform* (FFT)) and the cyclic prefix have made OFDM both practical and attractive to the radio link designer. A similar multichannel modulation scheme, *discrete multitone* (DMT) modulation, has been developed for static channels such as the digital subscriber loop [13]. DMT also uses DFTs and the cyclic prefix but has the additional feature of bit-loading which is generally not used in OFDM, although related ideas can be found in [14].

The choice for OFDM as transmission technique could be justified by comparative studies with single carrier systems. However, few such studies have been documented in the literature, see, *e.g.*, [15]. OFDM is often motivated by two of its many attractive features: it is considered to be spectrally efficient and it offers an elegant way to deal with equalization of dispersive slowly-fading channels. We concentrate here on such channels.

Multiuser systems that use OFDM must be extended with a proper multiple-access scheme as must single carrier transmission systems. Compared to single carrier systems, OFDM is a versatile modulation scheme for multiple access systems in that it intrinsically facilitates both time-division multiple access and frequency-division (or 'subcarrier-division') multiple access [4]. In addition, considerable attention has been given to the combination of the OFDM transmission technique and *code-division multiple access* (CDMA) in multicarrier-CDMA systems, MC-CDMA, see [16] and the references

therein.

OFDM also has some drawbacks. Because OFDM divides a given spectral allotment into many narrow subcarriers each with inherently small carrier spacing, it is sensitive to carrier frequency errors. Furthermore, to preserve the orthogonality between subcarriers, the amplifiers need to be linear. OFDM systems also have a high peak-to-average power ratio or crest-factor, which may require a large amplifier power back-off and a large number of bits in the *analog-to-digital* (A/D) and *digital-to-analog* (D/A) designs. All these requirements can put a high demand on the transmitter and receiver design.

OFDM has been successfully used in both the European DAB and DVB systems [1,2]. DAB is expected to be fully launched during 1998-2000 and is already broadcast on a trial basis in many countries. OFDM has also been a topic of research for use in wireless local-area networks and is a candidate for the European broadband radio access network standard [3] currently being developed by the *European Telecommunications Standard Institute* (ETSI).

For the standardization of the European third generation personal communications system within ETSI, the *universal mobile telecommunications system* (UMTS), OFDM was a technically promising candidate stressing versatility of services and resource allocation [4]. The OFDM-based proposal was, however, abandoned in favor of the two final CDMA-based proposals that were more thoroughly investigated and had broad support. OFDM is now under investigation for the fourth generation mobile communication system.

In addition to these radio systems, multicarrier techniques have also been used for broadband wired applications. Multicarrier modulation, in the form of the DMT modulation applied to the twisted copper-pair channel, has been adopted as the modulation technique for the *asynchronous digital subscriber loop* (ADSL) [13] in the US and is now one of two candidates for the *very high bit rate digital subscriber loop* (VDSL) being standardized by the *American National Standards Institute* (ANSI) and by ETSI [17].

This paper proceeds as follows. We describe the principles of the OFDM transmission technique in Section 2. In Section 3 we describe how to generate OFDM signals by means of an FFT, how to suppress out-of-band emission and how to reduce the dynamics of the transmitted signal. Section 4 describes receiver operations such as synchronization, channel estimation and equalization.

2 Principles of OFDM

OFDM is a block transmission technique. In the baseband, complex-valued data symbols modulate a large number of tightly grouped carrier waveforms. The transmitted OFDM-signal multiplexes several low-rate data streams – each data stream is associated with a given subcarrier. The main advantage of this concept in a radio environment is that each of the data streams experiences an almost flat fading channel. The *intersymbol interference* (ISI) and *intercarrier interference* (ICI) within an OFDM symbol can be avoided completely with a small loss of transmission energy using the concept of a cyclic prefix.

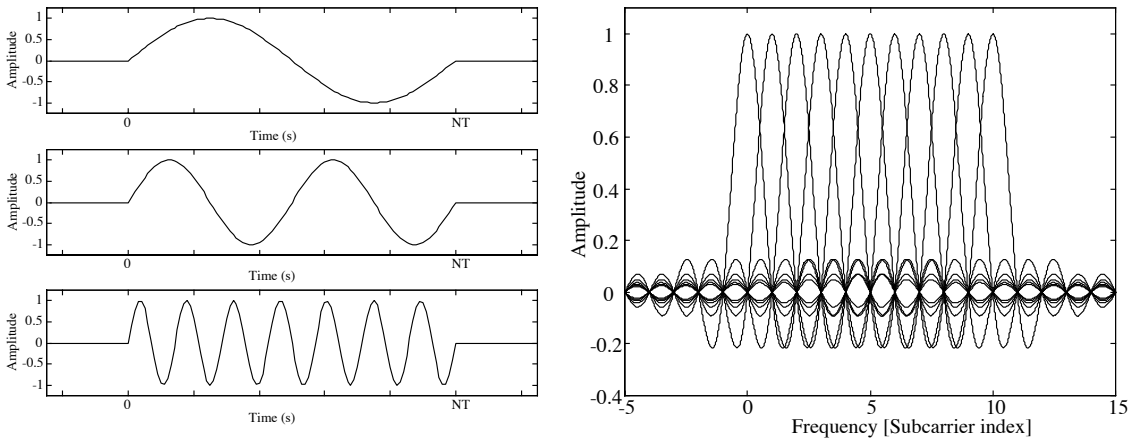

Figure 1: The real parts of three of the basis functions (with indexes 1,2 and 7) that constitute a baseband OFDM signal (left) and the concept of densely packed subcarriers in OFDM (right).

2.1 Signal characteristics

An OFDM signal consists of N orthogonal subcarriers modulated by N parallel data streams. Each baseband subcarrier is of the form

$$\phi_k(t) = e^{j2\pi f_k t}, \tag{1}$$

where f_k is the frequency of the kth subcarrier. One baseband OFDM symbol (without a cyclic prefix) multiplexes N modulated subcarriers:

$$s(t) = \frac{1}{\sqrt{N}} \sum_{k=0}^{N-1} x_k \phi_k(t) \qquad 0 < t < NT, \tag{2}$$

where x_k is the kth complex data symbol (typically taken from a PSK or QAM symbol constellation) and NT is the length of the OFDM symbol. The subcarrier frequencies f_k are equally spaced

$$f_k = \frac{k}{NT}, \tag{3}$$

which makes the subcarriers $\phi_k(t)$ on $0 < t < NT$ orthogonal. The signal (2) separates data symbols in frequency by overlapping subcarriers thus using the available spectrum in an efficient way. The left half of Figure 1 illustrates the quadrature component of some of the subcarriers of an OFDM symbol. The right half of Figure 1 illustrates how the subcarriers are packed in the frequency domain.

Figure 2 shows time and frequency characteristics of an OFDM signal with 1024 subcarriers. As the OFDM signal is the sum of a large number of independent, identically distributed components its amplitude distribution becomes approximately Gaussian by the central limit theorem. Therefore, it suffers from large peak-to-average power ratios. In addition, OFDM signals of the form (2) can have large out-of-band power as illustrated in Figure 2. Large peak-to-average power ratios also cause out-of-band emission because

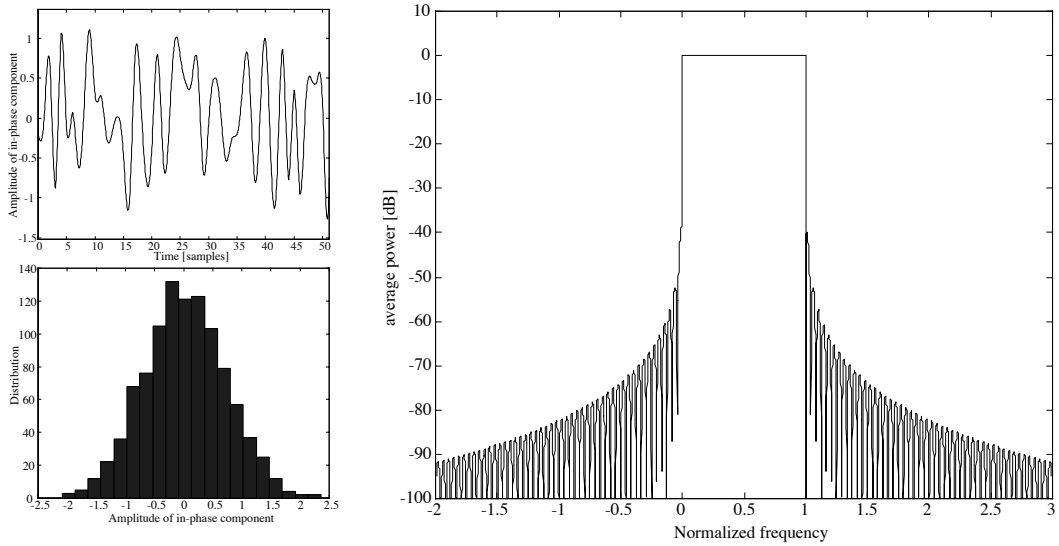

Figure 2: Time and frequency characteristics of an OFDM signal with 1024 subcarriers.

of amplifier non-linearities. Section 3 discusses ways to deal with high peak-to-average power ratios and out-of-band power.

The OFDM symbol (2) could typically be received using a bank of matched filters. However, an alternative demodulation is used in practice. T-spaced sampling of the in-phase and quadrature components of the OFDM symbol yields (ignoring channel impairments such as additive noise or dispersion)

$$s(nT) = \frac{1}{\sqrt{N}} \sum_{k=0}^{N-1} x_k e^{j2\pi \frac{nk}{N}}, \qquad 0 \le n \le N-1, \tag{4}$$

which is the *inverse discrete Fourier transform* (IDFT) of the constellation symbols x_k. Accordingly, the sampled data is demodulated with a DFT. This is one of the key properties of OFDM, first proposed by Weinstein and Ebert [10]. The DFT, typically implemented with an FFT, actually realizes a sampled matched-filter receiver in systems without a cyclic prefix.

2.2 OFDM with a cyclic prefix

Two difficulties arise when the signal in (2) is transmitted over a dispersive channel. One difficulty is that channel dispersion destroys the orthogonality between subcarriers and causes *intercarrier interference* (ICI). In addition, a system may transmit multiple OFDM symbols in a series so that a dispersive channel causes *intersymbol interference* (ISI) between successive OFDM symbols. The insertion of a silent guard period between successive OFDM symbols would avoid ISI in a dispersive environment but it does not avoid the loss of the subcarrier orthogonality. Peled and Ruiz [11] solved this problem with the introduction of a cyclic prefix. This cyclic prefix both preserves the orthogonality of the subcarriers and prevents ISI between successive OFDM symbols. Therefore, equalization at the receiver is very simple. This often motivates the use of OFDM in wireless systems.

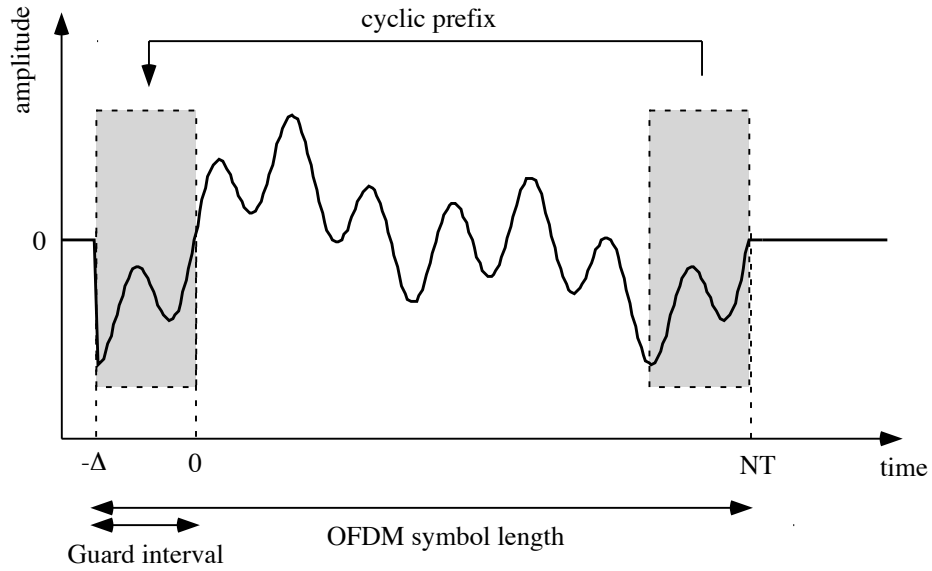

Figure 3: The concept of a cyclic prefix: the last part of the OFDM symbol is copied as a prefix of duration Δ.

The cyclic prefix, illustrated in Figure 3, works as follows. Between consecutive OFDM symbols a guard period is inserted that contains a cyclic extension of the OFDM signal. The OFDM signal (2) is extended over a period Δ so that

$$s(t) = \frac{1}{\sqrt{N}} \sum_{k=0}^{N-1} x_k e^{j2\pi f_k t}, \qquad -\Delta < t < NT. \tag{5}$$

The signal then passes through a channel, modeled by a finite-length impulse response limited to the interval $[0, \Delta_h]$. If the length of the cyclic prefix Δ is chosen such that $\Delta > \Delta_h$ the received OFDM symbol *evaluated on the interval* $[0, NT]$, ignoring any noise effects, becomes

$$r(t) = s(t) * h(t) = \frac{1}{\sqrt{N}} \sum_{k=0}^{N-1} H_k x_k e^{j2\pi f_k t} \qquad 0 < t \leq NT \tag{6}$$

where

$$H_k = \int_0^{\Delta_h} h(\tau) e^{-j2\pi f_k \tau} d\tau \tag{7}$$

is the Fourier transform of $h(t)$ evaluated at the frequency f_k. Note that within this interval the received signal is similar to the original signal except that $H_k x_k$ modulates the kth subcarrier instead of x_k. In this way the cyclic prefix preserves the orthogonality of the subcarriers.

Equation (6) suggests that the OFDM signal can be demodulated as described in the previous section, taking an FFT of the sampled data over the interval $[0, NT]$, ignoring the received signal before and after $0 < t \leq NT$. The received data (disregarding additive noise) then has the form

$$y_k = H_k x_k, \qquad k = 0, \ldots, N-1. \tag{8}$$

The received data in Equation (8) can be recovered with N parallel one-tap equalizers. This simple channel equalization motivates the use of a cyclic prefix and often the use of OFDM itself. Because we ignore the signal within the cyclic prefix this prefix also acts as the above mentioned silent guard interval preventing ISI between successive OFDM symbols.

The use of a cyclic prefix in the transmitted signal has the disadvantage of requiring more transmit energy. The loss of transmit energy (or loss of *signal-to-noise ratio* (SNR)) due to the cyclic prefix is

$$\mathcal{E}_{\text{loss}} = \frac{NT}{NT + \Delta}. \tag{9}$$

This is also a measure of the bit rate reduction required by a cyclic prefix. That is, if each subcarrier can transmit b bits, the overall bit rate in an OFDM system is $\frac{Nb}{NT+\Delta}$ bits per second as compared to the bit rate of $\frac{b}{T}$ in a system without a cyclic prefix. If latency requirements allow, these losses can be made small by choosing a symbol period NT much longer than the length of the cyclic prefix Δ.

2.3 Channel noise and Doppler spread

In this paper we devote little space to the radio channel as it is described in length and detail in other parts of this book. However, we mention a few channel impairments that are important for OFDM. OFDM systems often experience not only channel dispersion as addressed above, but also *additive white Gaussian noise* (AWGN), Doppler spreading and synchronization errors. Many of these impairments can be modeled as AWGN if they are relatively small. Synchronization errors such as carrier frequency offsets, carrier phase noise, sample clock offsets and symbol timing offsets are discussed in Section 4.

The inclusion of Gaussian noise in the signal model (2) yields a received OFDM signal $r(t) = s(t) * h(t) + n_t(t)$ and Equation (8) extended with a noise term becomes

$$y_k = H_k x_k + n_k \qquad\qquad k = 0, \ldots, N-1, \tag{10}$$

where n_k is the FFT of the sampled noise terms $n_t(nT), n = 0, \ldots, N-1$. If the received noise $n_t(t)$ is white, the noise n_k after the FFT will also be white.

In a fading channel the channel variations affect the performance of the OFDM system. For a fixed sampling period, the OFDM symbol length increases with the number of subcarriers and so does its sensitivity to channel variations. To illustrate the effects, consider an OFDM system in a flat-fading channel, a channel with a time-varying one-tap impulse response $a(t)$. The transmitted OFDM signal is multiplied with this time-varying scalar which yields the received $r(t) = a(t)s(t)$. The multiplication appears as a convolution in the frequency domain causing spreading of the subcarriers and, consequently, ICI. The sampled signal after the DFT is of the form [18]

$$y_l = \sum_{k=0}^{N-1} x_k A(k-l) \tag{11}$$

where $A(k-l)$ is the DFT of the now time-varying channel tap $a(nT)$, $n = 0, \ldots, N-1$.

In some cases the above spreading may be desirable as it is a way to introduce diversity [18]. A frequency domain channel equalizer can exploit such diversity. Other systems requiring orthogonality between subcarriers may suffer from the spreading. For a fixed sampling time the ICI due to the Doppler spreading increases with the number of carriers. Russell and Stüber [19], using a central limit theorem argument, characterize the effect of the ICI as an additive Gaussian noise with a variance that increases with the number of subcarriers. This noise is correlated in time, but white across the subcarriers. The ICI leads to an error floor which may be unacceptable. Antenna diversity or coding are suggested to reduce this error floor [19].

2.4 Design of OFDM signals

The number of subcarriers N, the bandwidth of each subcarrier $\frac{1}{NT}$, the bandwidth of the system $B \approx \frac{1}{T}$, and the length of the cyclic prefix Δ are all important parameters in the design of an OFDM system.

First, the length of the cyclic prefix should be chosen to be a small fraction of the OFDM symbol length to minimize the loss of SNR (or data rate) in (9). Because the size of the cyclic prefix is directly related to the delay spread τ of the channel, a rule of thumb is that the length of the OFDM symbol $NT \gg \tau$ or, equivalently, the number of subcarriers $N \gg \tau B$. However, if the OFDM symbol length NT is too long the ICI caused by Doppler spreading in the fading channel can become performance limiting. If the intercarrier spacing $\frac{1}{NT}$ is chosen much larger than the maximum Doppler frequency f_d, the system is relatively insensitive to the Doppler spread and the associated ICI. Therefore, the number of subcarriers should satisfy $f_d \ll \frac{1}{NT}$ or equivalently $N \ll \frac{B}{f_d}$. The above two constraints result in the following restriction on the number of subcarriers

$$\tau B \ll N \ll \frac{B}{f_d}. \tag{12}$$

Equation (12) also states a requirement on the delay- and Doppler-spread of the physical channel for proper design of an OFDM system. The far left hand side and the far right hand side also lead to $f_d\tau \ll 1$, which means that the more the channel is underspread, *i.e.*, the more correlated in either time or frequency, the easier it is to find a suitable number of subcarriers N.

> **Example 1:** The UMTS has been assigned frequencies in the 2.2 GHz band. Operators expect to be assigned 5 MHz for uplink and 5 MHz for downlink transmission and therefore in the following we assume a sample frequency of 5 MHz. A proper design of a radio interface based on OFDM depends on the characteristics of the radio environment in these bands. For the evaluation of the UMTS, ETSI has developed a set of channel models that describe the environment for different transmission situations (indoor, pedestrian, vehicular) [20]. The system should typically be used in all these environments and therefore we base our design on the worst values for the Doppler frequencies and channel delay spreads.

The vehicular channel models all adopt a mobile speed of 120 km/h. This speed corresponds to a maximum Doppler frequency of about 250 Hz. Furthermore, if we want our system to accommodate echoes up to about 10 μsec, we require (12)

$$50 \ll N \ll 20 \cdot 10^3 \tag{13}$$

Since the effects on the system performance of violating either the left or right hand requirement are different, it is not obvious how to choose N. One possible design could be, for instance, the geometric mean of the boundary values: $N \approx 1000$. A typical UMTS radio interface thus could use 1024 subcarriers implemented with an 1024-point FFT.

The length of the cyclic prefix must be larger than the channel impulse response, that is $\Delta > 10$ μsec. A possible design example of a 64-sample cyclic prefix (12.8 μsec) leads to a reduction of the data rate and transmission power of 6%. If we modulate each subcarrier with a QPSK symbol, we have $b = 2$ bits per subcarrier giving us an overall raw data rate of $\frac{bN}{NT+\Delta} = 9.4$ Mbits/sec. Similarly, an extension to 16-QAM symbols would give 18.8 Mbits/sec raw data rate.

2.5 Coding

Error control coding is an essential part of an OFDM system for mobile communication. OFDM in a fading environment is almost always used with coding to improve its performance and as such is often referred to as Coded OFDM or COFDM [6]. For an uncoded OFDM system in a frequency selective Rayleigh-fading environment, each OFDM subcarrier has a flat-fading channel. Accordingly, the average probability of error for an uncoded OFDM system is the same as that for a flat-fading single-carrier system with the same average geometric mean of the subcarriers' SNRs.

Just as we can introduce time diversity through coding and interleaving in a flat-fading single carrier system, we can introduce frequency diversity through coding and interleaving across subcarriers in an OFDM system [4, 21]. However, since OFDM in itself does not increase the system bandwidth, it can never introduce frequency diversity on flat fading channels.

With coding and interleaving across subcarriers, the strong subcarriers help the weak ones. Over a single OFDM signal, we cannot guarantee that the interleaved subcarriers are all independent. In [22, 23] we find that the achievable frequency diversity in a COFDM system is limited by the number of resolvable independent paths in the channel impulse response. One heuristic explanation is as follows. Coding diversity requires independent SNRs on each path to get the full diversity of the code. In an OFDM system the SNRs of different subcarriers are usually correlated because the channel length is small compared to the OFDM symbol length NT. How correlated the subcarriers are depends on the number of resolvable taps. In the extreme case of a one-tap channel, the SNR on all the subcarriers is the same. So regardless of the interleaving or power of the code interleaving in frequency will not increase the diversity. As the number of taps in

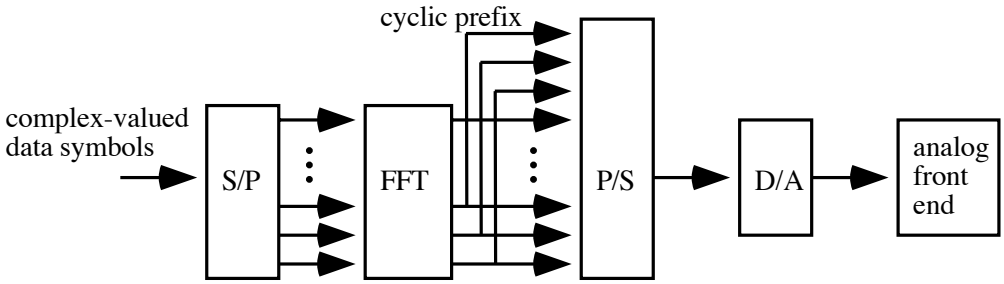

Figure 4: A block diagram of an OFDM transmitter.

the channel increases the correlation between subcarriers decreases but they will never be totally independent.

3 OFDM transmission

3.1 Signal generation

Equation (2) shows an ideal OFDM signal. which could be generated by a bank of oscillators. Such an implementation could, however, become prohibitively complex as the number of subcarriers becomes large. Similar to the demodulation of the data samples with the DFT, the baseband signal can be generated digitally by means of an IDFT [10]. Figure 4 shows such an OFDM transmitter. This has paved the way for practical use of OFDM. Consider the signal

$$\tilde{s}(t) = \sum_{n=0}^{lN-1} s_n g(t - \frac{nT}{l}) \qquad \text{for all } t, \tag{14}$$

where

$$s_n = \frac{1}{\sqrt{N}} \sum_{k=0}^{N-1} x_k e^{\frac{j2\pi kn}{lN}} \qquad n = 0, \ldots, lN-1, \tag{15}$$

is the oversampled IDFT of the constellation symbols x_k, the integer $l \geq 1$, and $g(t)$ is an interpolating filter. The output signal from the D/A, $\tilde{s}(t)$, can be made very close to the ideal signal $s(t)$ as defined in (2). The quality of the approximation depends on, for example, the characteristics of the D/A including the interpolation filter and the IDFT.

A spectrum of an OFDM signal is shown in Figure 2. The spectrum decays with $1/f$ and spectral leakage into neighboring bands is sometimes too large to meet regulation requirements. Several approaches have been taken to combat this out-of-band emission. The most straightforward is perhaps to use a large number of subcarriers to narrow the spectra, however at the cost of increased complexity, increased sensitivity to Doppler effects, and higher demands on the accuracy of synchronization.

Another approach is to use pulse shaping of the OFDM symbol to change the spectral occupancy. Pulse shaping can be done either by applying a time window [4] to the OFDM symbol or by passing the OFDM signal through a filter [28], typically combined with the

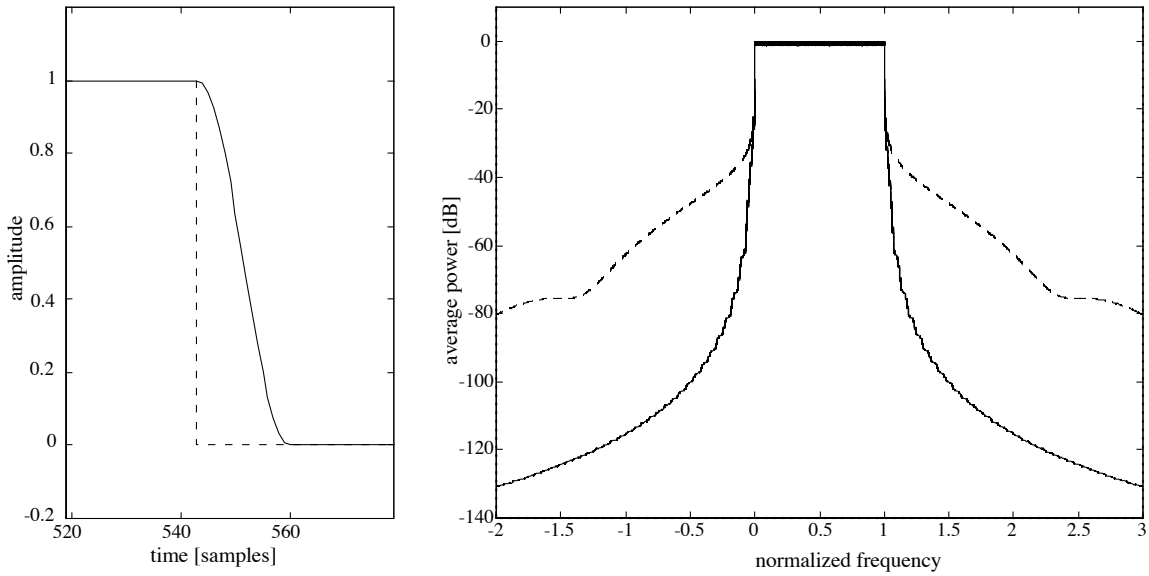

Figure 5: The OFDM signal shaped with cosine roll-off edges (solid) and with a rectangular window (dashed). The edge of the OFDM symbol for both pulses (left) and the OFDM power spectrum (right)

interpolation filter above. Pulse shaping has to be applied with care since orthogonality between the subcarriers is rarely maintained.

An example of using a time-window to shape the symbol is shown in the left half of Figure 5. Compared with the rectangular window, the symbol has been cyclically extended with a number of extra samples shaped with a raised cosine window [4]. The original symbol is left unchanged in the center. The associated power spectra for the two signals are shown in the right half of Figure 5.

Whereas the application of pulse shaping can improve the spectral occupancy of an OFDM system, its effect on other system characteristics has also motivated some recent studies towards design of suitable pulse shapes [24, 25, 27]. Much of this work focuses on the choice of new sets of basis functions for the modulation of parallel channels and on how such pulses improve an OFDM system's robustness to Doppler effects, carrier frequency variations, and time synchronization. The application of wavelet theory to multicarrier communications and pulse shaping is documented in, *e.g.*, [26].

3.2 Techniques to reduce the peak-to-average power ratio

An OFDM signal has an approximately Gaussian amplitude distribution when the number of subcarriers is large. Therefore, very high peaks in the transmitted signal can occur. This property is often measured via the signal's peak-to-average power ratio, which for the OFDM signal is high. To be able to transmit and receive these peaks without clipping, the A/D and D/A need to be designed with high demands on range and precision.

If the dynamic ranges of the A/D and D/A are increased, the resolution also needs to be increased in order to maintain the same quantization noise level. Therefore, an

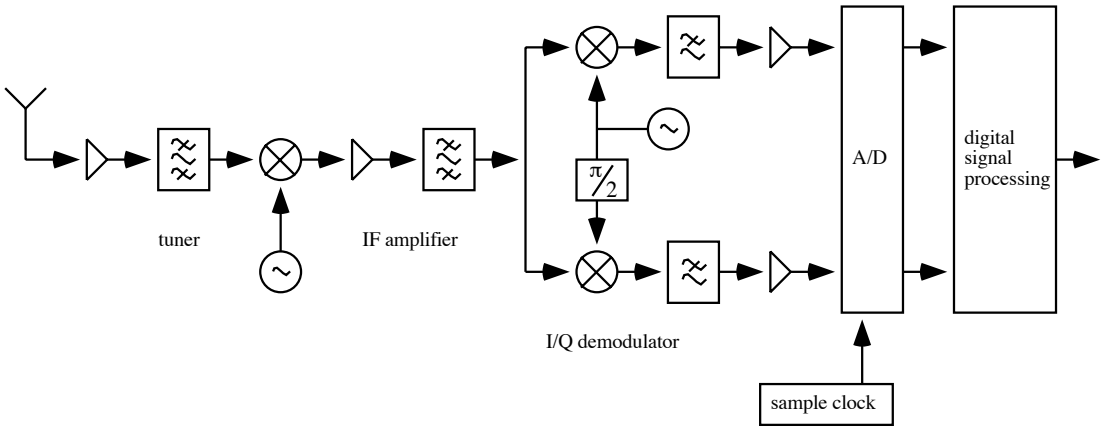

Figure 6: Example of the front end of an OFDM receiver employing one intermediate frequency.

OFDM signal may require expensive A/Ds and D/As compared to many other modulation formats, and for some applications suitable A/Ds and D/As may not be available at all. Also, a large power back-off of the amplifiers is necessary. Intentional or accidental clipping of the OFDM signal often occurs in practice. The clipping of a received sample affects all subcarriers in the system. The sensitivity to clipping effects is investigated by, *e.g.*, Gross and Veeneman [29].

At least three concepts for reducing the peak-to-average power ratio have been proposed [30–34]. In the first concept one signal with a low peak-to-average power ratio out of a set of signals is transmitted. In [31], for instance, it is observed that by appropriately choosing the phase of each subcarrier the peak-to-average power ratio can be reduced.

The second concept reduces the peak-to-average power ratio by coding. Block codes can accomplish this, see, *e.g.*, [32], and in [33] it is shown that complementary codes have good properties to combine peak-to-average power reduction and forward error correction.

Finally, in [34] impulse-like time-domain signals are iteratively subtracted from the original signal to reduce the peaks. These time-domain signals are generated by a set of reserved, unused symbols in the DFT domain. Subcarriers which are not used to transmit data symbols are used to transmit symbols, chosen to generate a transmitted signal with low peak-to-average power ratio.

4 OFDM reception

In Section 2 we have discussed aspects of the demodulation of data in OFDM. Two other important parts of the processing of the received OFDM signal are synchronization and channel estimation. Here, we address these topics.

4.1 Synchronization

At the front-end of the receiver OFDM signals are subject to synchronization errors due to oscillator impairments and sample clock differences. The demodulation of the received

Table 1: Loss of SNR in OFDM because of various synchronization impairments: 1) a carrier frequency offset ε, 2) carrier phase noise for oscillator with linewidth β, 3) a sample-clock offset Δf_s (in ppm) for the nth subcarrier and 4) a symbol-timing offset.

Impairment	SNR-loss (dB)
Carrier frequency offset[1] ε in AWGN channel [35]	$D \approx \frac{10}{3\ln 10}(\pi\varepsilon)^2 \frac{E_s}{N_0}$
Carrier frequency offset[1] ε in fading channel [36]	$D \leq 10\log_{10}\left(\frac{1+0.5947\frac{E_s}{N_0}\sin^2\pi\varepsilon}{\mathrm{sinc}^2\varepsilon}\right)$
Phase noise[1] of oscillator, bandwidth β [28]	$D \approx \frac{11}{6\ln 10}(4\pi\beta)\frac{E_s}{N_0}$
Sample clock frequency offset[2] Δf_s at the nth subcarrier [37].	$D_n \approx 10\log_{10}\left(1+\frac{1}{3}\frac{E_s}{N_0}(\pi n 10^{-6}\Delta f_s)^2\right)$
Symbol timing offset[3] [38]	–

[1]normalized to the intercarrier spacing $\frac{1}{NT}$
[2]normalized to the sample clock frequency, in ppm
[3]normalized to the OFDM symbol length $NT + \Delta$

radio signal to baseband, possibly via an intermediate frequency, involves oscillators whose frequencies may not be perfectly aligned with the transmitter frequencies. This results in a carrier frequency offset. Figure 6 illustrates the front-end of an OFDM receiver where these errors can occur. Also, demodulation (in particular the radio frequency demodulation) usually introduces phase noise acting as an unwanted phase modulation of the carrier wave. Carrier frequency offset and phase noise degrade the performance of an OFDM system.

When the baseband signal is sampled at the A/D, the sample clock frequency at the receiver may not be the same as that at the transmitter. Not only may this sample clock offset cause errors, it may also cause the duration of an OFDM symbol at the receiver to be different from that at the transmitter. If the symbol clock is derived from the sample clock this generates variations in the symbol clock. Since the receiver needs to determine when the OFDM symbol begins for proper demodulation with the FFT, usually a symbol synchronization algorithm at the receiver is usually necessary. Symbol synchronization also compensates for delay changes in the channel.

The effects of synchronization errors are investigated in, among others, [28], [35–41]. Table 1 summarizes some of the important results.

The most important effect of a frequency offset between transmitter and receiver is a loss of orthogonality between the subcarriers resulting in ICI. The characteristics of this ICI are similar to white Gaussian noise and lead to a degradation of the SNR [35]. For both AWGN and fading channels, this degradation increases with the square of the number of subcarriers. Table 1 illustrates this degradation as a function of the frequency offset normalized to the intercarrier spacing, ε.

Like frequency offsets, phase noise and sample clock offsets cause ICI and thus a

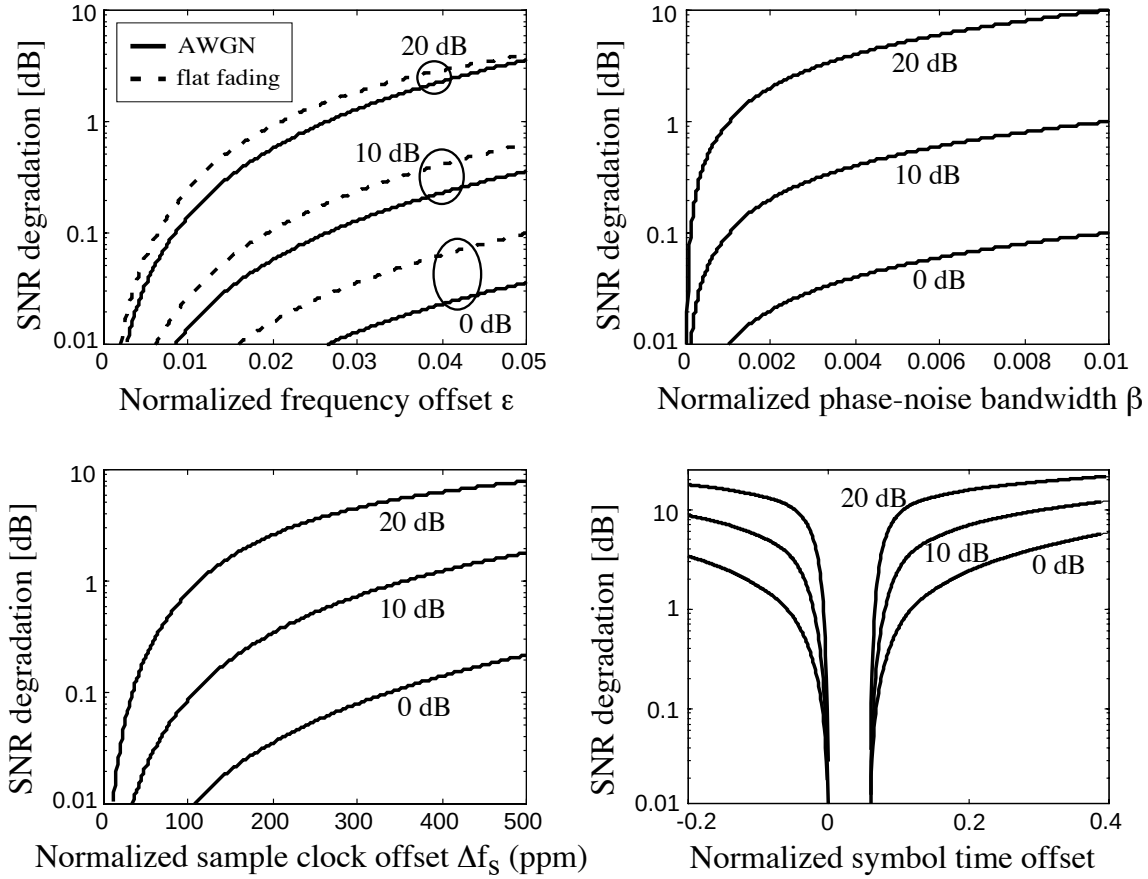

Figure 7: SNR-degradation for three operating SNRs versus 1) a frequency offset ε, normalized to the intercarrier spacing (upper left), 2) phase-noise bandwidth β, normalized to the intercarrier spacing (upper right), 3) a sample clock offset Δf_s for the nth subcarrier, normalized to the sample clock frequency (lower left), and 4) a symbol clock offset, normalized to the OFDM symbol length $NT + \Delta$ (lower right).

degradation of the SNR. The extent of these degradations is indicated in Table 1. The table shows the phase noise degradation for a phase noise bandwidth β. This bandwidth is normalized to the intercarrier spacing $\frac{1}{NT}$. The degradation due to a sample clock frequency offset δf_s, also normalized to the sample clock frequency and denoted in parts per million (ppm), is shown, too. For a DVB-like OFDM system Muschallik [39] concludes that phase noise is not performance limiting in properly designed consumer receivers for OFDM. Pollet, *et al.*, [37] show that the degradation due to a sample clock frequency offset differs from subcarrier to subcarrier, the highest subcarrier experiencing the largest SNR-loss.

Finally, the degradation due to symbol timing errors is not graceful. If the length of the cyclic extension exceeds the length of the channel impulse response a receiver can capture an OFDM symbol anywhere in a region where the symbol appears cyclic, without sacrificing orthogonality. A small error only appears as pure phase-rotations of the data symbols and may be compensated by the channel equalizer, still preserving the system's orthogonality. A large error resulting in capturing a symbol outside this

allowable interval, on the other hand, causes ISI, ICI, and a performance degradation.

Example 2: For the UMTS system in Example 1 the distortion expressions from Table 1 are illustrated by the curves in Figure 7. A typical sample clock offset of $\Delta f_s = 10$ ppm results in an SNR degradation of less than 0.1 dB. A phase noise bandwidth of 50 Hz ($\beta = 0.01$) results in an SNR degradation of about 1 dB. In [41] it is shown that a channel equalizer may compensate for a part of this degradation.

The sensitivity to frequency offsets in the UMTS scenario determines the performance requirements of a frequency tracking scheme. In order to keep the distortion less than 1 dB, the frequency offset may not exceed 2% of the subcarrier spacing. Finally, the sensitivity to symbol time offsets determines the performance requirements of a time tracking scheme. Due to the presence of the cyclic prefix that is 64 samples long, time offsets on the order of 10 samples do not affect our system's performance. The remaining samples of the cyclic prefix are needed to keep the system's orthogonality in dispersive channels

Summarizing, oscillator phase noise and sample-clock variations generate ICI but seldom limit system performance. Frequency offsets and symbol clock offsets, however, generally need to be tracked at the receiver. We now give a brief review of some recently proposed frequency and timing estimators for OFDM and then describe one of these methods, based on the cyclic prefix, in more detail.

We model the uncertainty about the start of the baseband OFDM symbol as an unknown delay and the uncertainty about the transmitter carrier frequency as a rotation of the complex-valued transmitted signal. We ignore the channel dispersion, isolating the offset problem. The model for the received signal becomes

$$r(k) = s(k-\theta)e^{j2\pi\varepsilon k/N} + n(k), \tag{16}$$

where θ is the unknown integer-valued delay and ε is the unknown carrier frequency offset relative to the intercarrier spacing. The received signal now contains unknown time and frequency offsets and, of course, the unknown data symbols (via $s(k)$).

Time and frequency offset estimators have been addressed in a number of publications, see [36, 40] and [42–53]. We divide these estimators conceptually into two groups. The first group [36, 42–44] assumes that transmitted data symbols are known at the receiver. This can in practice be accomplished by transmitting known pilot symbols according to some protocol. The unknown symbol timing and carrier frequency offset may then be estimated from the received signal. The insertion of pilot symbols usually implies a reduction of the data rate. An example of such a pilot-based algorithm is found in [42], joint time and frequency offset estimators based on this concept are described in [43, 44], and in [36] the repetition of an OFDM symbol supports the estimation of a frequency offset.

A second approach [45–49] uses statistical redundancy in the received signal. The transmitted signal $s(k)$ is modeled as a Gaussian process. The offset values are then estimated by exploiting the intrinsic redundancy provided by the L samples constituting

the cyclic prefix. The basic idea behind these methods is that the cyclic prefix of the transmitted signal (5) yields information about where an OFDM symbol is likely to start. Moreover, the transmitted signal's redundancy also contains useful information about the carrier frequency offset. In [45] the authors recognize that the statistic

$$\zeta(m) \triangleq \sum_{k=m}^{m+L-1} |r(k) - r(k+N)| \tag{17}$$

contains information about the time offset θ. This statistic, implemented with a sliding sum, identifies samples of the cyclic prefix by the sum of L consecutive differences. The statistic is likely to become small when the index m is close to the start of the OFDM symbol. Therefore, Tourtier, *et al.*, [45] propose the time offset estimator

$$\widehat{\theta} = \arg\min_{\theta} \{\zeta(\theta)\}. \tag{18}$$

Sandell *et al.* [47], van de Beek *et al.* [48], and later Lee and Cheon [49] use the statistic

$$\gamma(m) \triangleq \sum_{k=m}^{m+L-1} r(k) r^*(k+N), \tag{19}$$

to estimate the time offset. This statistic is the sum of L consecutive correlations and its magnitude is likely to become large when the index m is close to the start of the OFDM symbol. Furthermore, the phase of the statistic $\gamma(m)$ at the time $m = \widehat{\theta}$ is related to the frequency offset. In [49], this offset is estimated by

$$\widehat{\varepsilon} = -\frac{1}{2\pi} \angle\gamma\left(\widehat{\theta}\right)., \tag{20}$$

where $\angle$ denotes the angle of its complex-valued argument. From (16), (19), and (20), the frequency estimate is the argument of a sum of complex numbers. Without additive noise and correct time estimate $\widehat{\theta}$, each term $r(k)r^*(k+N)$ has the same argument: $2\pi\varepsilon$. Hence, each term contributes coherently to the sum, while the additive noise contributes incoherently. Because of this implicit averaging the variance of the frequency estimator is usually low. The concept of using statistics based on the pairwise correlation in the received signal $r(k)$ due to the cyclic prefix for the estimation of time and frequency offsets is patented in [50].

The joint *maximum likelihood* (ML) estimator of the time and frequency offsets for the AWGN channel is derived by van de Beek, *et al.* [48]. This optimal estimator is shown to be based on the sufficient statistic $\gamma(m)$ in (19) together with the additional statistic

$$\Phi(m) \triangleq \frac{1}{2} \sum_{k=m}^{m+L-1} |r(k)|^2 + |r(k+N)|^2. \tag{21}$$

The joint ML estimate is

$$\widehat{\theta}_{\mathrm{ML}} = \arg\max_{\theta} \{|\gamma(\theta)| - \rho\Phi(\theta)\}, \tag{22}$$

$$\widehat{\varepsilon}_{\mathrm{ML}} = -\frac{1}{2\pi} \angle\gamma\left(\widehat{\theta}_{\mathrm{ML}}\right), \tag{23}$$

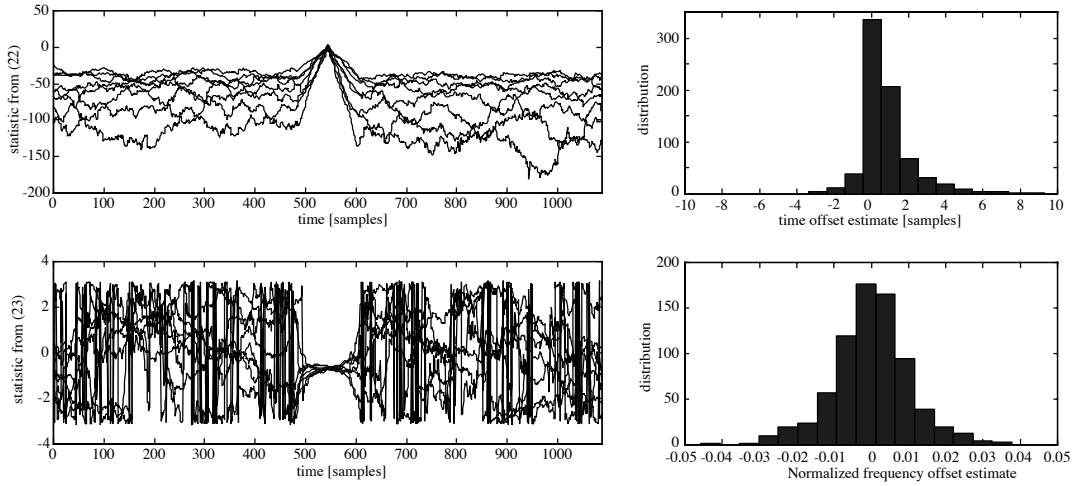

Figure 8: Statistics for the joint ML-estimation of θ and ε in Example 3. The statistic $|\gamma(\theta)| - \rho\Phi(\theta)$, whose maximizing argument points at the start of an OFDM symbol (top) and the statistic $\angle\gamma(\theta)$, whose value at these instants is proportional to the frequency offset (bottom).

where $\rho = \mathrm{SNR}/(\mathrm{SNR}+1)$ is the magnitude of the correlation coefficient at the receiver between a sample in the tail of the OFDM symbol and its copy in the cyclic prefix.

> **Example 3:** Consider the downlink of the UMTS system in Examples 1 and 2 for the 'Vehicular B' channel for UMTS [20]. Each mobile can track its time and frequency offsets with the ML estimator (22) and (23). Figure 8 shows the 'eye-diagram' of the statistics $|\gamma(\theta)| - \rho\Phi(\theta)$ and $\angle\gamma(\theta)$. The indexes at which the upper statistic peak provide the most likely start of the OFDM symbols, while the values of the lower statistic at these indexes give the most likely frequency offsets.
>
> The distribution of these estimates is shown in the right half of Figure 8. The time offset estimates are within about 10 samples of the true time instant and the frequency offset estimates are within about 2% of the true offset. See Figure 7 and Example 2 for the consequences of this estimation for the system performance.

Synchronization schemes are discussed in, *e.g.*, [45, 51, 52]. Figure 9 shows a possible receiver structure that compensates for time and frequency offsets. In addition to controlling a voltage controlled oscillator in the analog receiver front-end, frequency correction can also be performed digitally by multiplying the received signal in front of the FFT with the estimate-based signal $\exp(-j2\pi\widehat{\varepsilon}\frac{k}{N})$. Timing correction is typically performed in conjunction with the removal of the cyclic prefix and the FFT.

4.2 Channel estimation

Some OFDM systems (as, for instance, the DAB standard [1]) modulate the subcarriers differentially [54]. The information symbols may be encoded differentially from

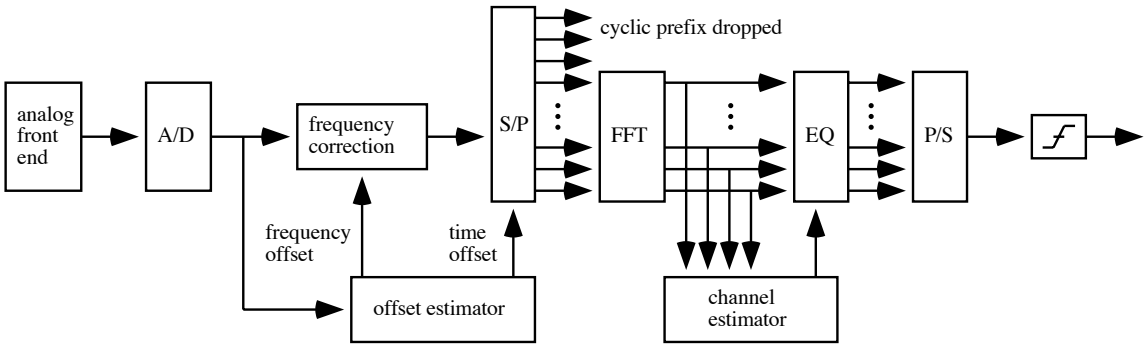

Figure 9: Time/frequency offset correction and channel estimation/equalization in an OFDM receiver.

one OFDM symbol to the next within one subcarrier, or differentially between adjacent subcarriers within one OFDM symbol. Even in a fading channel environment, such a modulation does not need the tracking of the subcarrier attenuations (tracking of the carrier frequencies has still to be done). The performance sacrifice associated with this modulation scheme compared to coherent modulation schemes is often motivated by its simple receiver structure and its avoidance of pilot symbols. However, if the subcarriers are coherently modulated as in the DVB standard [2] estimation of the channel's attenuations of each subcarrier is necessary. These estimates are used in the channel equalizer, which, in an OFDM receiver, may consist of one complex multiplication for each subcarrier in an OFDM symbol. Figure 9 shows the receiver structure for a coherent OFDM receiver.

Channel estimation in OFDM is usually performed with the aid of pilot symbols. Since each subcarrier is flat fading, techniques from single carrier flat fading systems are directly applicable to OFDM. For such systems *pilot-symbol assisted modulation* (PSAM) on flat fading channels [55, 56] involves the sparse insertion of known pilot symbols in a stream of data symbols. The attenuation of the pilot symbols is measured and the attenuations of the data symbols in between these pilot symbols are typically estimated/interpolated using time correlation properties of the fading channel.

The concept of PSAM in OFDM systems also allows the use of the frequency correlation properties of the channel. The time-frequency grid in Figure 10 illustrates three ways of inserting pilots symbols among data symbols. The first pilot pattern inserts entirely known OFDM symbols in the OFDM signal. The second modulates pilot symbols on a particular set of subcarriers. The third pattern uses scattered pilot symbols, as in the DVB standard.

In OFDM systems where Doppler effects are kept small (that is, the OFDM symbol is short compared with the coherence time of the channel) the time correlation between the channel attenuations of consecutive OFDM symbols is high. Furthermore, in a properly designed OFDM system the subcarrier spacing is small compared with the coherence bandwidth of the channel (see Section 2). Therefore, there is also a substantial frequency correlation between the channel attenuations of adjacent subcarriers. Both of these time and frequency correlations can be exploited by a channel estimator. The choice of pilot

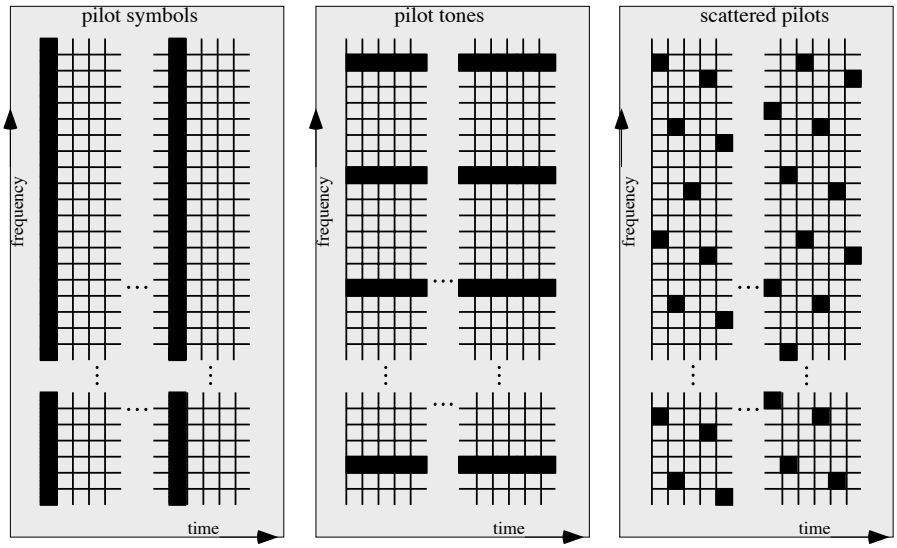

Figure 10: Time-frequency grid for an OFDM system with three pilot patterns: entirely known OFDM symbols (left), pilot subcarriers (middle) and scattered pilots (right).

pattern determines the form of the channel estimator.

Most documented channel estimation concepts consist of two steps, one or both of which use the correlation of the channel. First, the attenuations at the pilot positions are measured and possibly smoothed using the channel correlation. These measurements then serve to estimate (interpolate) the complex-valued attenuations of the data symbols in the second step. This second step uses the channel correlation properties either with interpolation filters or with a decision-directed scheme. Depending on the pilot pattern (see Figure 10) the estimation strategies diverge here.

Höher [57], for instance, proposes a scattered pilot pattern. The interpolation in the presented scheme uses the channel measurements with two FIR Wiener filters. The first Wiener filter interpolates and smoothes the channel attenuations in frequency. A second Wiener filter then interpolates and smoothes the channel attenuations in time. This scheme exploits the channel correlation properties in the design of the interpolating Wiener filters. In general, the correlation properties and the SNR needed to design the estimator are not known. Therefore, Hoeher [57] proposes to design the estimator for fixed, assumed values of the channel correlations and SNR.

Recent publications by Edfors *et al.* [58, 59] and Li *et al.* [60], focus on the first pilot pattern of Figure 10, where completely known OFDM symbols are sparsely inserted in the stream of OFDM symbols. The channel attenuations in between these OFDM symbols are then either interpolated using the channel time correlation or the estimator is applied on consecutive OFDM symbols in a decision-directed scheme [22, 61, 62].

We first adopt a matrix formulation of Equation (8) and collect the channel attenuations of one OFDM symbol (the Fourier transform of $h(t)$ evaluated at the frequency f_k) in the vector $\mathbf{h}$. The observed symbols after the receiver DFT become

$$\mathbf{y} = \mathbf{X}\mathbf{h} + \mathbf{n}, \tag{24}$$

where the diagonal matrix $\mathbf{X}$ contains the transmitted symbols on its diagonal (either

known pilot symbols or receiver decisions of information symbols which we in the following assume are correct), and the vector $\mathbf{y}$ contains the observed outputs of the DFT. In this matrix notation the *least-squares* (LS) channel estimate (minimizing $\|\mathbf{y} - \mathbf{X}\widehat{\mathbf{h}}\|^2$ for all possible $\widehat{\mathbf{h}}$) becomes

$$\widehat{\mathbf{h}}_{ls} = \mathbf{X}^{-1}\mathbf{y} = \left[\begin{array}{cccc} \frac{y_0}{x_0} & \frac{y_1}{x_1} & \cdots & \frac{y_{N-1}}{x_{N-1}} \end{array} \right]^T. \tag{25}$$

This estimator simply divides the received symbol on each subcarrier by the transmitted symbol to obtain an estimate of the channel attenuation. From the system property (8), this is an estimator that intuitively makes sense.

The frequency correlation can now be used to smooth and improve the LS channel estimate. Various strategies can be adopted to use the frequency correlation. The optimal *linear minimum mean-squared error* (LMMSE) estimate of $\mathbf{h}$ (minimizing $E\left\{\|\widehat{\mathbf{h}} - \mathbf{h}\|^2\right\}$ for all possible linear estimators $\widehat{\mathbf{h}}$) becomes

$$\widehat{\mathbf{h}}_{lmmse} = \mathbf{A}\widehat{\mathbf{h}}_{ls}, \tag{26}$$

where

$$\mathbf{A} = \mathbf{R}_{hh_{ls}}\mathbf{R}^{-1}_{h_{ls}h_{ls}} = \mathbf{R}_{hh}\left(\mathbf{R}_{hh} + \sigma_n^2\left(\mathbf{X}\mathbf{X}^H\right)^{-1}\right)^{-1}, \tag{27}$$

and $\mathbf{R}_{hh} = E\left\{\ \mathbf{h}\mathbf{h}^H\right\}$ is the channel autocorrelation matrix, that is, the matrix containing the correlations of the channel attenuations of the subcarriers, see [58,59]. Similarly, $\mathbf{R}_{hh_{ls}}$ denotes the correlation matrix between the channel attenuations and their LS-estimates, and $\mathbf{R}_{h_{ls}h_{ls}}$ denotes the autocorrelation matrix of the LS-estimates.

This LMMSE estimator is, for complexity reasons, of little practical value. Not only does Equation (26) assume knowledge of the channel correlation and the SNR, it also requires N multiplications per estimated attenuation and the dependency on the pilots or decisions $\mathbf{X}$ may require frequent recalculation of the matrix $\mathbf{A}$. However, the LMMSE estimator (or any other high-performance and complex estimator) can be used as a basis for the design of more feasible estimators. In [23, 58–60] generic low-complexity approximations of (26) are developed. Their performances can be made very close to that of the optimal LMMSE estimator. They are generic in the sense that they use assumed (fixed) channel correlation and SNR for the design of $\mathbf{A}$. They are low-complexity in the sense that they require significantly less than N multiplications per estimated attenuation.

Example 4: For the UMTS example system developed in Examples 1–3, we now adopt a multiple access scheme that separates users both in time and in frequency. As a minimal access entity each user modulates 22 adjacent subcarriers during one OFDM symbol. Let us consider how we could design a channel estimator for one user with a 64 kbit/s downlink.

This user is assigned 22 adjacent subcarriers every third OFDM symbol. Of the 22 subcarriers, four are used for transmission of pilot symbols, as shown in Figure 11. The other subcarriers carry QPSK data symbols, yielding an uncoded data rate of 165.44 kbit/s. First, we estimate the channel

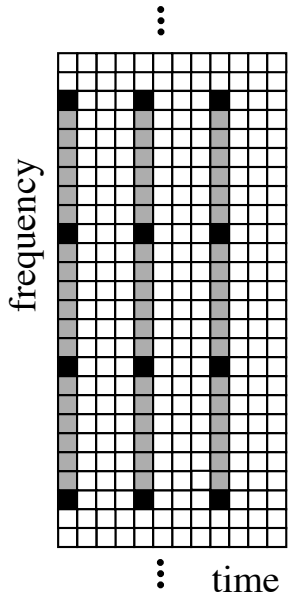

Figure 11: OFDM symbols from the multiple-access example scenario in a time-frequency grid. The pilot symbols are black, the data symbols are grey, and unused symbols (by this user) are white.

attenuations on the pilot positions using the LS estimator (25). Because the number of pilots is small, we can choose a channel estimator based on (27) that assumes a fixed channel correlation. The channel estimation requires 4 multiplications per transmitted data symbol.

5 Summary

This paper reviews the OFDM transmission technique. We have described its key properties, the FFT and the cyclic prefix, and we have addressed many of the recent research developments associated with OFDM. This paper discusses receiver operations such as synchronization, channel estimation and equalization. It also outlines the problems of out-of-band emission, and how to reduce the dynamics of the transmitted signal. For further reading, the reference list below covers many important recent contributions.

6 Acknowledgements

We would like to gratefully acknowledge the helpful comments and suggestions of Ove Edfors, Lund University, Magnus Sandell, Lucent Technologies, Julia Martinez Arenas, Ericsson Radio Systems AB, Tony Ottosson, Chalmers University of Technology, and the six anonymous reviewers. Much of the knowledge drawn upon here has been developed together with the present and former staff of Telia Research AB, Luleå, Sweden.

References

[1] European Telecommunications Standards Institute (ETSI), *Radio Broadcasting Systems; Digital Audio Broadcasting (DAB) to Mobile, Portable and Fixed Receivers*, European Telecommunication Standard ETS 300 401, 1st edition, reference DE/JTC-DAB, February 1995. Available from the ETSI Secreteriat, F-06921 Sophia Antipolis Cedex, France.

[2] European Telecommunications Standards Institute (ETSI), *Digital Video Broadcasting (DVB); Framing Structure, Channel Coding and Modulation for Digital Terrestrial Television*, European Telecommunications Standard, ETS 300 744 1st edition, reference DE/JTC-DVB-8, March 1997. Available from the ETSI Secreteriat, F-06921 Sophia Antipolis Cedex, France.

[3] European Telecommunications Standards Institute (ETSI), *Broadband Radio Access Networks (BRAN); Inventory of Broadband Radio Technologies and Techniques*, Technical Report, reference DTR/BRAN-030001, February 1998. Available from the ETSI Secreteriat, F-06921 Sophia Antipolis Cedex, France.

[4] European Telecommunications Standards Institute (ETSI), *OFDMA Evaluation Report – The Multiple Access Scheme Proposal for the UMTS Terrestrial Radio Air Interface (UTRA)*, Technical Document Tdoc 896/97, ETSI SMG meeting no. 24, Madrid, December 1997. Available from the ETSI Secreteriat, F-06921 Sophia Antipolis Cedex, France.

[5] J.A.C. Bingham, 'Multicarrier modulation for data transmission: an idea whose time has come', *IEEE Communications Magazine*, vol. 28, no. 5, pp. 5–14, May 1990.

[6] W.Y. Zou, and Y. Wu, 'COFDM: an overview', *IEEE Transactions on Broadcasting*, vol. 41, no. 1, pp. 1–8, March 1995.

[7] R.W. Chang, 'Synthesis of band-limited orthogonal signals for multichannel data transmission', *Bell System Technical Journal*, vol. 45, pp. 1775–1796, December 1966.

[8] B.R. Saltzberg, 'Performance of an efficient parallel data transmission system', *IEEE Transactions on Communications*, vol. 15, no. 6, pp. 805–811, December 1967.

[9] R.W. Chang and R.A. Gibby, 'Theoretical study of performance of an orthogonal multiplexing data transmission scheme', *IEEE Transactions on Communications*, vol. 16, no. 4, pp. 529–540, August 1968.

[10] S.B. Weinstein and P.M. Ebert, 'Data transmission by frequency-division multiplexing using the discrete Fourier transform', *IEEE Transactions on Communications*, vol. 19, no. 5, pp. 628–634, October 1971.

[11] A. Peled and A. Ruiz, 'Frequency domain data transmission using reduced computational complexity algorithms', in *Proceedings of the IEEE International Conference*

on Acoustics, Speech, and Signal Processing (ICASSP), Denver, Colorado, 1980, pp. 964–967.

[12] B. Hirosaki, 'An orthogonally multiplexed QAM system using the discrete Fourier transform', *IEEE Transactions on Communications*, vol. 29, no. 7, pp. 982–989, July 1981.

[13] 'Network and customer installation interfaces – asymmetric digital subscriber line (ADSL) metallic interface', ANSI standard T1.413-1995.

[14] R. Wesel, 'Fundamentals of coding for broadcast OFDM', in *Proceedings of the 29th Asilomar Conference on Signals, Systems & Computers*, October 1995.

[15] M. Gosh, 'Analysis of the effect of impulse noise on multicarrier and single-carrier QAM systems', *IEEE Transactions on Communications*, vol. 44, no. 2, pp. 145–147, 1996.

[16] S. Hara and R. Prasad, 'Overview of multicarrier CDMA', *IEEE Communications Magazine*, vol. 35, no. 12, pp. 126–133, December 1997.

[17] VDSL Alliance, 'VDSL Alliance SDMT VDSL draft standard proposal', ANSI contribution T1E1.4/97-332, Sacramento, December 1997.

[18] L.J. Cimini, 'Analysis and simulation of a digital mobile channel using orthogonal frequency-division multiplexing', *IEEE Transactions on Communications*, vol. 33, no. 7, pp. 665–675, July 1985.

[19] M. Russell and G. Stüber, 'Interchannel interference analysis of OFDM in a mobile environment', in *Proceedings of the Vehicular Technology Conference (VTC'95)*, Chicago, USA, July 1995, pp. 820–824.

[20] ETSI SMG, 'Selection procedures for the choice of radio transmission technologies for the UMTS', ETR/SMG 30.03, v.3.0.0, Valbonne, France, 1997.

[21] M. Sandell, S.K. Wilson, and P.O. Börjesson, 'Performance analysis of coded OFDM on fading channels with non-ideal interleaving and channel knowledge', in *Proceedings of the IEEE Vehicular Technology Conference (VTC'97)*, Phoenix, USA, 1997, pp. 1380–1384.

[22] S.K. Wilson, *Digital Audio Broadcasting in a Fading and Dispersive Channel*, PhD thesis, Stanford University, August 1994.

[23] A. Chini, *Multicarrier Modulation in Frequency Selective Fading Channels*, PhD thesis, Carleton University, September 1994.

[24] B. Le Floch, M. Alard, and C. Berrou, 'Coded orthogonal frequency division multiplex', *Proceedings of the IEEE*, vol. 83, no. 6, pp. 982–996, 1995.

[25] S.D. Sandberg and M.A. Tzannes, 'Overlapped discrete multitone modulation for high speed copper wire communications', *IEEE Journal on Selected Areas in Communications*, vol. 13, no. 9, pp. 1571–1585, December 1995.

[26] G. Wornell, 'Emerging applications of multirate signal processing and wavelets in digital communications', *Proceedings of the IEEE*, vol. 84, no. 4, pp. 586–603, April 1996.

[27] R. Haas and J.C. Belfiore, 'A time-frequency well-localized pulse for multiple carrier transmission', *Wireless Personal Communications*, vol. 5, no. 1, pp. 1–18, July 1997.

[28] T. Pollet and M. Moeneclaey, 'Synchronizability of OFDM signals', in *Proceedings of the IEEE Global Telecommunications Conference (GLOBECOM'95)*, Singapore, November 1995, pp. 2054–2058.

[29] R. Gross and D. Veeneman, 'Clipping distortion in DMT ADSL systems', *Electronics Letters*, vol. 29, no. 24, pp. 2080–2081, 1993.

[30] S.H. Müller and J.B. Huber, 'A comparison of peak power reduction schemes for OFDM', in *Proceedings of the IEEE Global Telecommunications Conference (GLOBECOM'97)*, Phoenix, Arizona, USA, 1997, pp. 1–5.

[31] S. Narahashi and T. Nojima, 'A new phasing scheme for multitone signal systems to reduce peak-to-average power ratio', *Electronics and Communications in Japan*, Part 1, vol. 80, no. 1, pp. 89–97, 1997.

[32] A.J. Jones, T.A. Wilkinson, and S.K. Barton, 'Block coding scheme for reduction of peak to mean envelop power ratio of multicarrier transmission schemes', *Electronics Letters*, vol. 30, no. 25, pp. 2098–2099, 1994.

[33] R.D.J. van Nee, 'OFDM codes for peak-to-average power reduction and error correction', in *Proceedings of the IEEE Global Telecommunications Conference (GLOBECOM'96)*, London, England, November 1996, pp. 740–744.

[34] J. Tellado and J.M. Cioffi, 'PAR reduction in multicarrier transmission systems', ANSI T1E1.4/97-367, Sacramento, USA, 1997.

[35] T. Pollet, M. van Bladel, and M. Moeneclaey, 'BER sensitivity of OFDM systems to carrier frequency offset and Wiener phase noise', *IEEE Transactions on Communications*, vol. 43, no. 2/3/4, pp. 191–193, February/March/April 1995.

[36] P.H. Moose, 'A technique for orthogonal frequency division multiplexing frequency offset correction', *IEEE Transactions on Communications*, vol. 42, no. 10, pp. 2908–2914, October 1994.

[37] T. Pollet, P. Spruyt, and M. Moeneclaey, 'The BER performance of OFDM systems using non-synchronized sampling', in *Proceedings of the IEEE Global Telecommunications Conference (GLOBECOM'94)*, San Francisco, USA, November 1994, pp. 253–257.

[38] M. Gudmundson and P-O. Anderson, 'Adjacent channel interference in an OFDM system', in *Proceedings of the Vehicular Technology Conference (VTC'96)*, Atlanta, USA, April 1996, pp. 918–922.

[39] C. Muschallik, 'Influence of RF oscillators on an OFDM signal', *IEEE Transactions on Consumer Electronics*, vol. 41, no. 3, pp. 592–603, August 1995.

[40] L. Wei and C. Schlegel, 'Synchronization requirements for multi-user OFDM on satellite mobile and two-path rayleigh fading channels', *IEEE Transactions on Communications*, vol. 43, no. 2/3/4, pp. 887–895, February/March/April 1995.

[41] A. Garcia Armada and M. Calvo, 'Phase noise and sub-carrier spacing effects on the performance of an OFDM communication system', *IEEE Communications Letters*, vol. 2, no. 1, pp. 11–13, January 1998.

[42] W.D. Warner and C. Leung, 'OFDM/FM frame synchronization for mobile radio data communication', *IEEE Transactions on Vehicular Technology*, vol. 42, no. 3, pp. 302–313, August 1993.

[43] F. Classen and Meyr, 'Frequency synchronization algorithms for OFDM systems suitable for communication over frequency-selective fading channels', in *Procceedings of the IEEE Vehicular Technology Conference (VTC'94)*, Stockholm, Sweden, 1994, pp. 1655–1659.

[44] T.M. Schmidl and Cox, 'Robust frequency and timing synchronization for OFDM', *IEEE Transactions on Communications*, vol. 45, no. 12, pp. 1613–1621, December 1997.

[45] P.J. Tourtier, R. Monnier, and P. Lopez, 'Multicarrier modem for digital HDTV terrestrial broadcasting', *Signal Processing: Image Communication*, vol. 5, no. 5/6, pp. 379–403, December 1993.

[46] F. Daffara and O. Adami, 'A new frequency detector for orthogonal multicarrier transmission techniques', in *Proceedings of the Vehicular Technology Conference (VTC'95)*, Chicago, USA, July 1995, pp. 804–809.

[47] M. Sandell, J.J. van de Beek, and P.O. Börjesson, 'Timing and frequency synchronization in OFDM systems using the cyclic prefix', in *Proceedings of the IEEE International Symposium on Synchronization*, Essen, Germany, December 1995, pp. 16–19.

[48] J.J. van de Beek, M. Sandell, and P.O. Börjesson, 'ML estimation of time and frequency offsets in OFDM systems', *IEEE Transactions on Signal Processing*, vol. 45, no. 7, pp. 1800–1805, July 1997.

[49] D. Lee and K. Cheon, 'A new symbol timing recovery algorithm for OFDM systems', *IEEE Transactions on Consumer Electronics*, vol. 43, no. 3, pp. 767–775, August 1997.

[50] T. Seki, Y. Sugita, and T. Ishikawa, *OFDM Synchronization Demodulation Unit*, United States Patent, no. 5,602,835, February 1997.

[51] H. Nogami and T. Nagashima, 'A frequency and timing period acquisition technique for OFDM systems', in *Proceedings of the Conference on Personal, Indoor, and Mobile Radio Communications* (PIMRC'95), September 1995, pp. 1010–1015.

[52] C.-R. Sheu, Y.-L. Huang and C.-C. Huang, 'Joint symbol frame, and carrier synchronization for Eureka 147 DAB system', in *Proceedings of the International Conference on Universal Personal Communications (ICUPC'97)*, San Diego, USA, October 1997, pp. 693–697.

[53] T.M. Schmidl, *Synchronization Algorithms for Wireless Data Transmission using Orthogonal Frequency Division Multiplexing (OFDM)*, PhD thesis, Stanford University, USA, June 1997.

[54] V. Engels and H. Rohling, 'Multilevel differential modulation techniques (64-DAPSK) for multicarrier transmission systems', *European Transactions on Telecommunications*, vol. 6, no. 6, pp. 633–640, November/December 1995.

[55] M.L. Moher and J.H. Lodge, 'TCMP – A Modulation and Coding Strategy for Rician-Fading Channels', *IEEE Journal on Selected Areas in Communications*, vol. 7, no. 9, pp. 1347–1355, December 1989.

[56] J.K. Cavers, 'An analysis of pilot-symbol assisted modulation for Rayleigh-fading channels', *IEEE Transactions on Vehicular Technology*, vol. 40, no. 4, pp. 686–693, November 1991.

[57] P. Höher, 'TCM on frequency-selective land-mobile fading channels', in *Proceedings of the Tirrenia International Workshop on Digital Communications*, Tirrenia, Italy, September 1991, pp. 317-328.

[58] O. Edfors, M. Sandell, J.J. van de Beek, S.K. Wilson, and P.O. Börjesson, 'OFDM channel estimation by singular value decomposition', *IEEE Transactions on Communications*, vol. 46, no. 7, pp. 931–939, July 1998.

[59] O. Edfors, M. Sandell, J.J. van de Beek, S.K. Wilson, and P.O. Börjesson, 'Analysis of DFT-based channel estimators for OFDM', *Wireless Personal Communications*, Kluwer Academic Publishers, in press.

[60] Y. Li, L.J. Cimini, Jr., and N.R. Sollenberger, 'Robust channel estimation for OFDM systems with rapid dispersive fading channels', *IEEE Transactions on Communications*, vol. 46, no. 7, pp. 902–915, July 1998.

[61] S.K. Wilson, R.E. Khayata, and J.M. Cioffi, '16-QAM modulation with orthogonal frequency-division multiplexing in a Rayleigh-fading environment', in *Proceedings of the IEEE Vehicular Technology Conference (VTC'94)*, Stockholm, Sweden, June 1994, pp. 1660–1664.

[62] V. Mignone and A. Morello, 'CD3–OFDM: a novel demodulation scheme for fixed and mobile receivers', *IEEE Transactions on Communications*, vol. 44, no. 9, pp. 1144–1151, September 1995.

Part 2

This part has been published as

J.J. van de Beek, M. Sandell, and P.O. Börjesson, 'ML Estimation of Time and Frequency Offset in OFDM Systems', *IEEE Transactions on Signal Processing*, vol. 45, no. 7, pp. 1800–1805, July 1997.

ML Estimation of Time and Frequency Offset in OFDM Systems

J.J. van de Beek, M. Sandell, and P.O. Börjesson

Abstract – We present the joint *maximum likelihood* (ML) symbol-time and carrier-frequency offset estimator in *orthogonal frequency-division multiplexing* (OFDM) systems. Redundant information contained within the cyclic prefix enables this estimation without additional pilots. Simulations show that the frequency estimator may be used in a tracking mode and the time estimator in an acquisition mode.

1 Introduction

Orthogonal frequency-division multiplexing (OFDM) systems have recently gained increased interest. OFDM is used in the European digital broadcast radio system and is being investigated for other wireless applications such as digital broadcast television and mobile communication systems, as well as for broadband digital communication on existing copper networks. See [1] and [2] and the references therein.

We address two problems in the design of OFDM receivers. One problem is the unknown OFDM symbol arrival time. Sensitivity to a time offset is higher in multicarrier systems than in single-carrier systems and has been discussed in [3] and [4]. A second problem is the mismatch of the oscillators in the transmitter and receiver. The demodulation of a signal with an offset in the carrier frequency can cause a high bit error rate and may degrade the performance of a symbol synchronizer [3, 5].

A symbol clock and a frequency offset estimate may be generated at the receiver with the aid of pilot symbols known to the receiver [6, 7], or, as in [8], by maximizing the average log-likelihood function. Redundancy in the transmitted OFDM signal also offers the opportunity for synchronization. Such an approach is found in [7, 9, 10] for a time offset and in [10–12] for a frequency offset. We present and evaluate the joint *maximum likelihood* (ML) estimation of the time and carrier-frequency offset in OFDM systems. The key element that will rule the discussion is that the OFDM data symbols already contain sufficient information to perform synchronization. Our novel algorithm exploits the cyclic prefix preceding the OFDM symbols, thus reducing the need for pilots.

2 The OFDM system model

Figure 1 illustrates the baseband, discrete-time OFDM system model we investigate. The complex data symbols are modulated by means of an *inverse discrete Fourier transform*

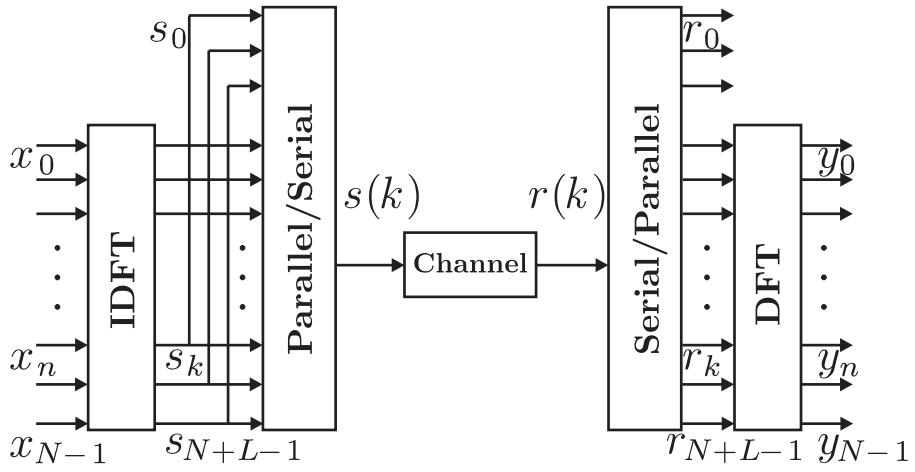

Figure 1: The OFDM system, transmitting subsequent blocks of N complex data.

(IDFT) on N parallel subcarriers. The resulting OFDM symbol is serially transmitted over a discrete-time channel, whose impulse response we assume is shorter than L samples. At the receiver, the data are retrieved by means of a *discrete Fourier transform* (DFT)

An accepted means of avoiding *intersymbol interference* (ISI) and preserving orthogonality between subcarriers is to copy the last L samples of the body of the OFDM symbol (N samples long) and append them as a preamble — the cyclic prefix — to form the complete OFDM symbol [1, 2]. The effective length of the OFDM symbol as transmitted is this cyclic prefix plus the body ($L + N$ samples long). The insertion of a cyclic prefix can be shown to result in an equivalent parallel orthogonal channel structure that allows for simple channel estimation and equalization [13]. In spite of the loss of transmission power and bandwidth associated with the cyclic prefix, these properties generally motivate its use [1, 2].

In the following analysis we assume that the channel is nondispersive and that the transmitted signal $s(k)$ is only affected by complex *additive white Gaussian noise* (AWGN) $n(k)$. We will, however, evaluate our estimator's performance for both the AWGN channel and a time-dispersive channel.

Consider two uncertainties in the receiver of this OFDM symbol: the uncertainty in the arrival time of the OFDM symbol (such ambiguity gives rise to a rotation of the data symbols) and the uncertainty in carrier frequency (a difference in the local oscillators in the transmitter and receiver gives rise to a shift of all the subcarriers). The first uncertainty is modeled as a delay in the channel impulse response $\delta(k - \theta)$, where θ is the integer-valued unknown arrival time of a symbol. The latter is modeled as a complex multiplicative distortion of the received data in the time domain $e^{j2\pi\varepsilon k/N}$, where ε denotes the difference in the transmitter and receiver oscillators as a fraction of the inter-carrier spacing ($1/N$ in normalized frequency). Notice that all subcarriers experience the same shift ε. These two uncertainties and the AWGN thus yield the received signal

$$r(k) = s(k - \theta)e^{j2\pi\varepsilon k/N} + n(k). \tag{1}$$

Two other synchronization parameters are not accounted for in this model. First,

an offset in the carrier phase may affect the symbol error rate in coherent modulation. If the data is differentially encoded, however, this effect is eliminated. An offset in the sampling frequency will also affect the system performance. We assume that such an offset is negligible. The effect of non-synchronized sampling is investigated in [14].

Now consider the transmitted signal $s(k)$. This is the DFT of the data symbols x_k, which we assume are independent. Hence, $s(k)$ is a linear combination of independent, identically distributed random variables. If the number of subcarriers is sufficiently large, we know from the central limit theorem that $s(k)$ approximates a complex Gaussian process whose real and imaginary parts are independent. This process, however, is not white, since the appearance of a cyclic prefix yields a correlation between some pairs of samples, that are spaced N samples apart. Hence, $r(k)$ is not a white process, either, but because of its probabilistic structure, it contains information about the time offset θ and carrier frequency offset ε. This is the crucial observation that offers the opportunity for joint estimation of these parameters based on $r(k)$.

A synchronizer cannot distinguish between phase shifts introduced by the channel and those introduced by symbol time delays [4]. Time error requirements may range from the order of one sample (wireless applications, where the channel phase is tracked and corrected by the channel equalizer) to a fraction of a sample (in, *e.g.*, high bit-rate digital subscriber lines, where the channel is static and essentially estimated only during startup).

Without a frequency offset, the frequency response of each subchannel is zero at all other subcarrier frequencies, *i.e.*, the subchannels do not interfere with one other [2]. The effect of a frequency offset is a loss of orthogonality between the tones. The resulting *intercarrier interference* (ICI) has been investigated in [11]. The effective *signal-to-noise ratio* (SNR_e) due to both additive noise and ICI is shown to be lower bounded by

$$\mathrm{SNR}_e(\varepsilon) \geq \frac{\mathrm{SNR}}{1 + 0.5947 \;\; \mathrm{SNR} \sin^2 \pi\varepsilon} \left(\frac{\sin \pi\varepsilon}{\pi\varepsilon} \right)^2 \tag{2}$$

where $\mathrm{SNR} = \sigma_s^2/\sigma_n^2$, $\sigma_s^2 \triangleq E\left\{|s(k)|^2\right\}$ and $\sigma_n^2 \triangleq E\left\{|n(k)|^2\right\}$. The difference between the SNR and the SNR_e is a measure of the sensitivity to a frequency offset ε. Notice that in the absence of additive noise the frequency offset must satisfy $|\varepsilon| \leq 1.3 \cdot 10^{-2}$, in order to obtain an SNR_e of 30 dB or higher. This result agrees well with the analysis of multiuser OFDM systems in [3], which states that a frequency accuracy of 1–2% of the intercarrier spacing is necessary.

3 ML estimation

Assume that we observe $2N+L$ consecutive samples of $r(k)$, *cf.* Figure 2, and that these samples contain one complete $(N + L)$ -sample OFDM symbol.

The position of this symbol within the observed block of samples, however, is unknown because the channel delay θ is unknown to the receiver. Define the index sets

$$\begin{aligned} \mathcal{I} &\triangleq \{\theta, \ldots, \theta + L - 1\} \text{ and} \\ \mathcal{I}' &\triangleq \{\theta + N, \ldots, \theta + N + L - 1\}, \end{aligned}$$

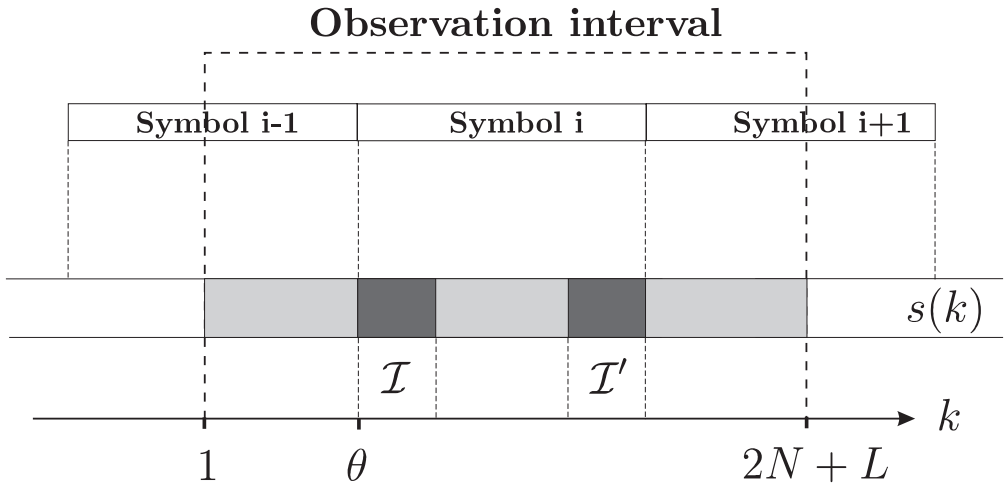

Figure 2: Structure of OFDM signal with cyclicly extended symbols, $s(k)$. The set $\mathcal{I}$ contains the cyclic prefix, *i.e.* the copies of the L data samples in $\mathcal{I}'$.

(see Figure 2). The set $\mathcal{I}'$ thus contains the indices of the data samples that are copied into the cyclic prefix, and the set $\mathcal{I}$ contains the indices of this prefix. Collect the observed samples in the $(2N+L)\times 1$ -vector $\mathbf{r} \triangleq [r(1) \ \ldots \ r(2N+L)]^T$. Notice that the samples in the cyclic prefix and their copies, $r(k), k \in \mathcal{I} \cup \mathcal{I}'$, are pairwise correlated, *i.e.*,

$$\forall k \in \mathcal{I}: \quad E\left\{r(k)r^*(k+m)\right\} = \begin{cases} \sigma_s^2 + \sigma_n^2 & m = 0 \\ \sigma_s^2 e^{-j2\pi\varepsilon} & m = N \\ 0 & \text{otherwise,} \end{cases} \tag{3}$$

while the remaining samples $r(k), k \notin \mathcal{I} \cup \mathcal{I}'$ are mutually uncorrelated.

The log-likelihood function for θ and ε, $\Lambda(\theta,\varepsilon)$, is the logarithm of the probability density function $f(\mathbf{r}|\theta,\varepsilon)$ of the $2N+L$ observed samples in $\mathbf{r}$ given the arrival time θ and the carrier frequency offset ε. In the following, we will drop all additive and positive multiplicative constants that show up in the expression of the log-likelihood function, since they do not affect the maximizing argument. Moreover, we drop the conditioning on (θ,ε) for notational clarity. Using the correlation properties of the observations $\mathbf{r}$, the log-likelihood function can be written as

$$\begin{aligned} \Lambda(\theta,\varepsilon) &= \log f(\mathbf{r}\,|\theta,\varepsilon) \\ &= \log\left(\prod_{k\in\mathcal{I}} f(r(k), r(k+N)) \prod_{k\notin\mathcal{I}\cup\mathcal{I}'} f(r(k))\right) \\ &= \log\left(\prod_{k\in\mathcal{I}} \frac{f(r(k), r(k+N))}{f(r(k))\, f(r(k+N))} \prod_{k} f(r(k))\right), \end{aligned} \tag{4}$$

where $f(\cdot)$ denotes the probability density function of the variables in its argument. Notice that it is used for both one- and two-dimensional (1-D and 2-D) distributions. The product $\prod_k f(r(k))$ in (4) is independent of θ (since the product is over all k) and ε (since the density $f(r(k))$ is rotationally invariant). Since the ML estimation of θ and

ε is the argument maximizing $\Lambda(\theta,\varepsilon)$, we may omit this factor. Under the assumption that $\mathbf{r}$ is a jointly Gaussian vector, (4) is shown in the Appendix to be

$$\Lambda(\theta,\varepsilon) = |\gamma(\theta)|\cos(2\pi\varepsilon + \angle\gamma(\theta)) - \rho\Phi(\theta), \tag{5}$$

where $\angle$ denotes the argument of a complex number,

$$\gamma(m) \triangleq \sum_{k=m}^{m+L-1} r(k)r^*(k+N), \tag{6}$$

$$\Phi(m) \triangleq \frac{1}{2}\sum_{k=m}^{m+L-1} |r(k)|^2 + |r(k+N)|^2, \tag{7}$$

and

$$\rho \triangleq \left| \frac{E\{r(k)r^*(k+N)\}}{\sqrt{E\left\{|r(k)|^2\right\}E\left\{|r(k+N)|^2\right\}}} \right| = \frac{\sigma_s^2}{\sigma_s^2+\sigma_n^2} = \frac{\mathrm{SNR}}{\mathrm{SNR}+1} \tag{8}$$

is the magnitude of the correlation coefficient between $r(k)$ and $r(k+N)$. The first term in (5) is the weighted magnitude of $\gamma(\theta)$, a sum of L consecutive correlations between pairs of samples spaced N samples apart. The weighting factor depends on the frequency offset. The term $\Phi(\theta)$ is an energy term, independent of the frequency offset ε. Notice that its contribution depends on the SNR (by the weighting-factor ρ).

The maximization of the log-likelihood function can be performed in two steps:

$$\max_{(\theta,\varepsilon)} \Lambda(\theta,\varepsilon) = \max_{\theta}\max_{\varepsilon}\Lambda(\theta,\varepsilon) = \max_{\theta}\Lambda(\theta,\widehat{\varepsilon}_{\mathrm{ML}}(\theta)). \tag{9}$$

The maximum with respect to the frequency offset ε is obtained when the cosine term in (5) equals one. This yields the ML estimation of ε

$$\widehat{\varepsilon}_{\mathrm{ML}}(\theta) = -\frac{1}{2\pi}\angle\gamma(\theta) + n, \tag{10}$$

where n is an integer. A similar frequency offset estimator has been derived in [11] under different assumptions. Notice that by the periodicity of the cosine function, several maxima are found. We assume that an acquisition, or rough estimate, of the frequency offset has been performed and that $|\varepsilon| < 1/2$; thus $n = 0$. Since $\cos(2\pi\widehat{\varepsilon}_{\mathrm{ML}}(\theta) + \angle\gamma(\theta)) = 1$, the log-likelihood function of θ (which is the compressed log-likelihood function with respect to ε) becomes

$$\Lambda(\theta,\widehat{\varepsilon}_{\mathrm{ML}}(\theta)) = |\gamma(\theta)| - \rho\Phi(\theta) \tag{11}$$

and the joint ML estimation of θ and ε becomes

$$\widehat{\theta}_{\mathrm{ML}} = \arg\max_{\theta}\{|\gamma(\theta)| - \rho\Phi(\theta)\}, \tag{12}$$

$$\widehat{\varepsilon}_{\mathrm{ML}} = -\frac{1}{2\pi}\angle\gamma\left(\widehat{\theta}_{\mathrm{ML}}\right). \tag{13}$$

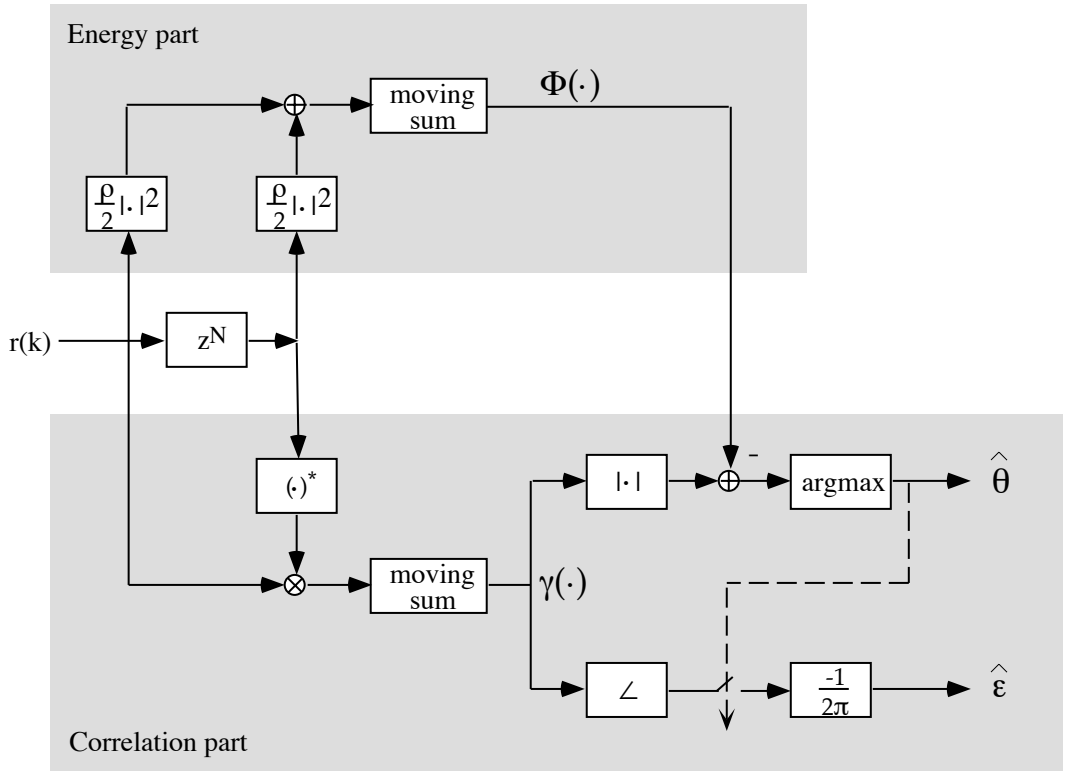

Figure 3: Structure of the estimator.

Notice that only two quantities affect the log-likelihood function (and thus the performance of the estimator): the number of samples in the cyclic prefix L and the correlation coefficient ρ given by the SNR. The former is known at the receiver, and the latter can be fixed. Basically, the quantity $\gamma(\theta)$ provides the estimates of θ and ε. Its magnitude, compensated by an energy term, peaks at time instant $\widehat{\theta}_{\mathrm{ML}}$, while its phase at this time instant is proportional to $\widehat{\varepsilon}_{\mathrm{ML}}$. If ε is *a priori* known to be zero, the log-likelihood function for θ becomes $\Lambda(\theta) = \mathrm{Re}\{\gamma(\theta)\} - \rho\Phi(\theta)$ and $\widehat{\theta}_{\mathrm{ML}}$ is its maximizing argument. This estimator and a low-complexity variant are analyzed in [9].

In an OFDM receiver, the quantity $\gamma(\theta)$, which is defined in (6), is calculated on-line, *cf.* Figure 3. The signals $\Lambda(\theta, \widehat{\varepsilon}_{\mathrm{ML}}(\theta))$ (whose maximizing arguments are the time estimates $\widehat{\theta}_{\mathrm{ML}}$) and $-(1/2\pi)\angle\gamma(\theta)$ (whose values at the time instants $\widehat{\theta}_{\mathrm{ML}}$ yield the frequency estimates) are shown in Figure 4. Notice that (12) and (13) describe an open-loop structure. Closed-loop implementations based on (5) and (11) may also be considered. In such structures the signal $\Lambda(\theta, \widehat{\varepsilon}_{\mathrm{ML}}(\theta))$ is typically fed back in a *phase-locked loop* (PLL). If we can assume that θ is constant over a certain period, the integration in the PLL can significantly improve the performance of the estimators.

4 Simulations

We use Monte Carlo simulations to evaluate the performance of the estimators, in which we consider an OFDM system with 256 subcarriers. In each simulation 125000 symbols

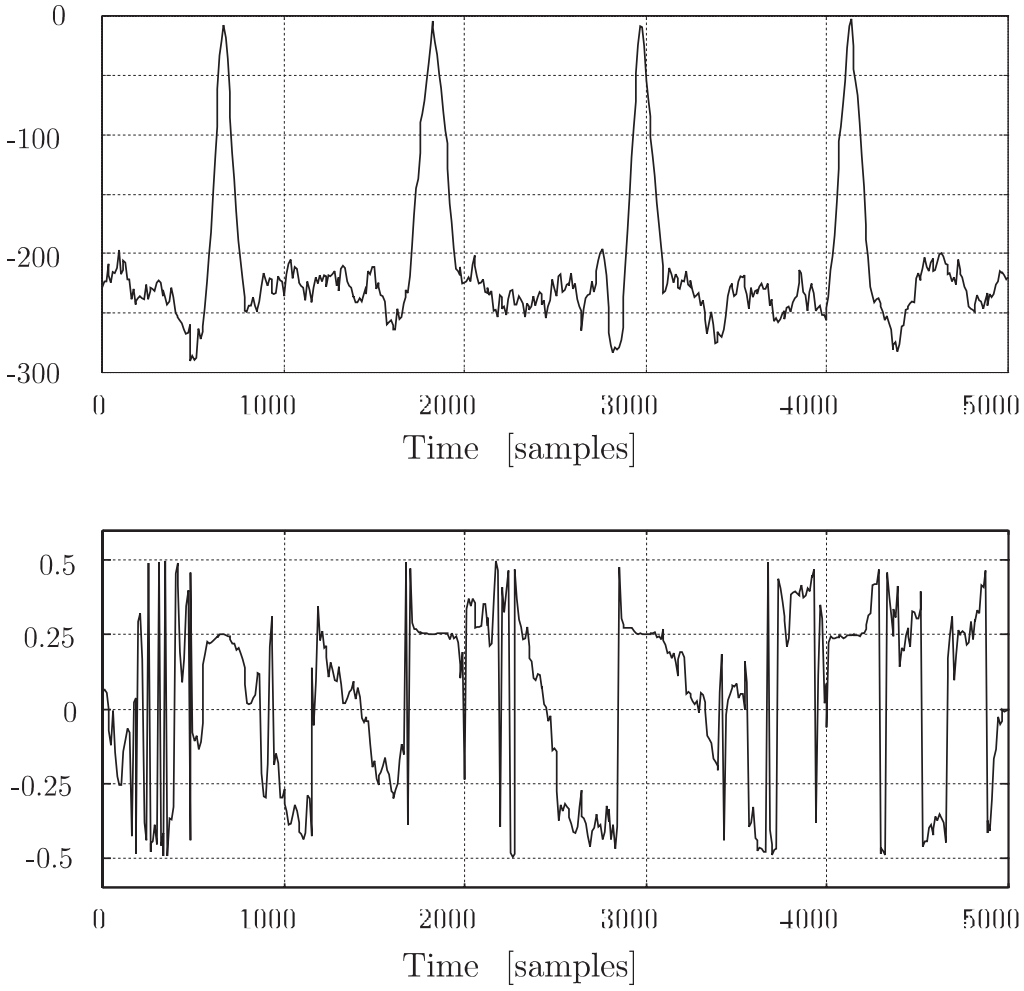

Figure 4: The signals that generate the ML-estimates ($N = 1024$, $L = 128$, $\varepsilon = 0.25$ and SNR= 15 dB): The maximizing indices of $\Lambda\left(\theta, \widehat{\varepsilon}_{\mathrm{ML}}\left(\theta\right)\right)$ (top) yield the time estimates $\widehat{\theta}_{\mathrm{ML}}$. At these time instants the arguments of $\gamma\left(\theta\right)$ (bottom) yield $\widehat{\varepsilon}_{\mathrm{ML}}$.

are used. We evaluate the performance of the estimators by means of the estimator mean-squared error.

Performance results for the AWGN channel are shown in Figures 5 and 6. First, the estimator mean-squared error as a function of L is estimated. Figure 5 shows the estimator performance for SNR values of 4 dB, 10 dB and 16 dB. Notice that the performance of the time estimator is asymptotically independent of L, provided that the cyclic prefix is longer than a certain threshold value. This threshold value decreases with the SNR. Both the time estimator and the frequency estimator exhibit such a performance threshold based on L. However, notice that as L increases beyond these respective thresholds, only the frequency estimator will show continued improvement. Thus, for the AWGN channel and from a time synchronization viewpoint, there is very little advantage in increasing the length of the cyclic prefix beyond the time estimator's threshold.

Second, the estimator variances as a function of SNR for $L = 4$, $L = 8$, and $L = 15$ are shown in Figure 6. Notice that even in these plots a threshold phenomenon as in Figure 5

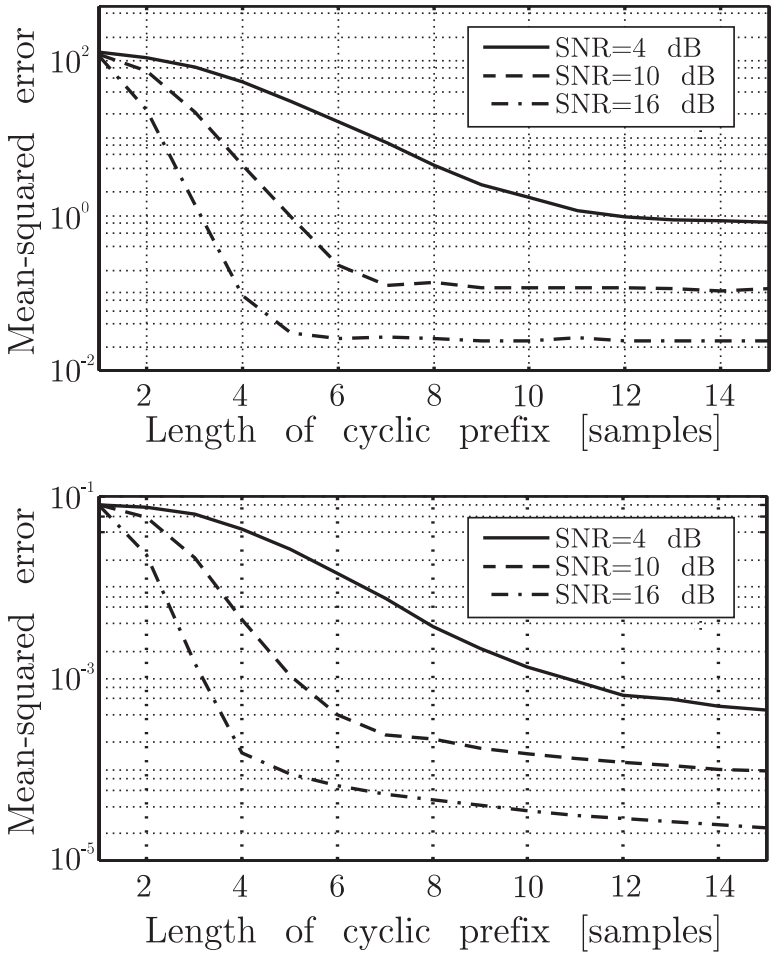

Figure 5: Performance of the time (top) and frequency (bottom) estimators for the AWGN channel (4 dB, 10 dB, and 16 dB). The dimensionless performance measure is expressed in squared units relative to the sample interval (top) and the inter-tone spacing (bottom). The number of subcarriers is $N = 256$.

occurs. This phenomenon is a property of time delay estimation and is documented in, *e.g.*, [15].

The above results do not directly apply to a time dispersive channel environment. Therefore, we also consider the performance of our estimators in a wireless system operating at 2 GHz with a bandwidth of 5 MHz. An outdoor dispersive, fading environment with micro-cell characteristics is chosen: the channel has an exponentially decaying power delay profile with root mean squared width equal to 0.4 μs (corresponding to 2 samples) and a maximum delay spread of 3 μs (corresponding to 15 samples). It is modeled to consist of 15 independent Rayleigh-fading taps [16] and additive noise. We choose a cyclic prefix consisting of 15 samples. This choice avoids ISI, while the loss of power and bandwidth due to the cyclic prefix ($L/(N+L)$) is about 5%. This system transmits about 18,000 OFDM symbols per second, each containing 256 complex information symbols. In this dispersive environment the definition of θ is ambigious. We define the true delay as the center-of-gravity of the channel impulse response. Moreover, we define the SNR

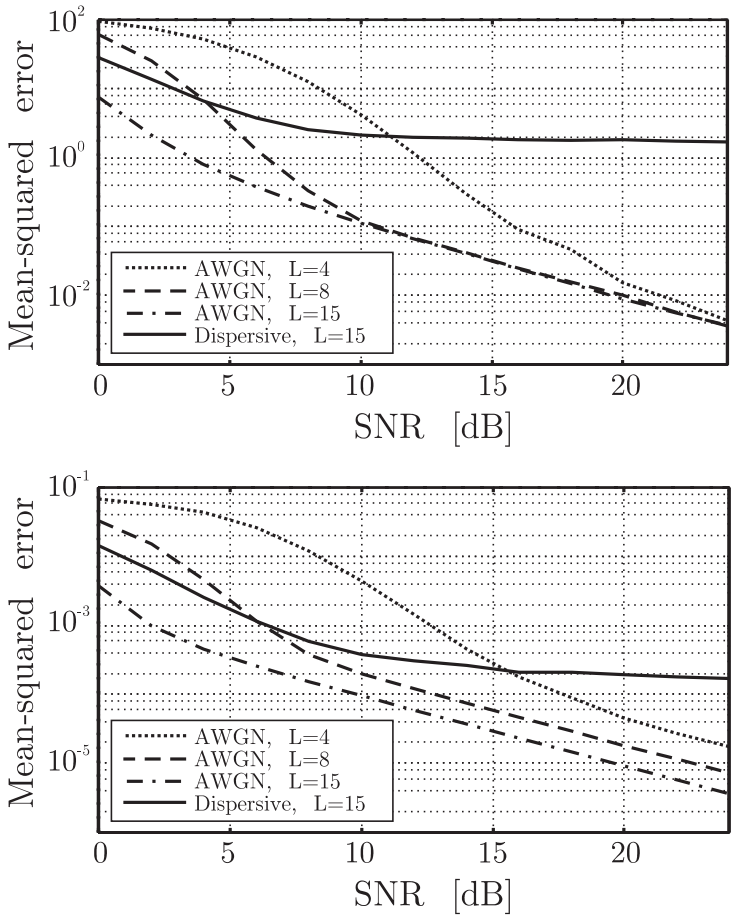

Figure 6: Performance of the time (top) and frequency (bottom) estimators for the AWGN channel ($L = 4, L = 8$, and $L = 15$) and the dispersive channel ($L = 15$). The dimensionless performance measure is expressed in squared units relative to the sample interval (top) and the inter-tone spacing (bottom). The number of subcarriers is $N = 256$.

as $\text{SNR} = \sigma_s^2 P_h / \sigma_n^2$ where P_h is the sum of the average power in all channel taps.

The error floor in Figure 6 clearly shows the performance degradation caused by the dispersive channel as compared with the corresponding curves for the AWGN channel. In the dispersive case, the estimators operate in an environment for which they are not designed (they are not optimal). Signals passed through the AWGN channel will have the simple, pairwise correlation structure (3), but signals passed through a dispersive channel generally have a more complex correlation structure.

Depending on the application and the presence of a high performance channel estimator/equalizer, the performance of the time estimate in Figure 6 (standard deviation of 1–2 samples) may be good enough to generate a stable clock. In most situations this performance will suffice at least in an acquisition mode. The frequency offset estimator shows an error standard deviation of less than 2% of the inter-tone spacing (see Figure 6), which satisfies the requirements discussed in Section 2.

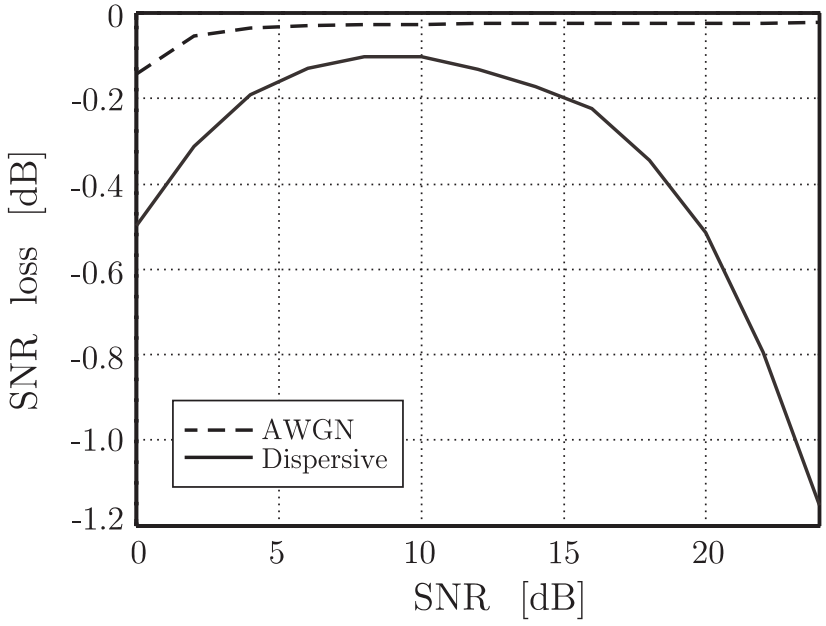

Figure 7: Performance of the frequency estimator for the AWGN channel and the dispersive channel ($L = 15$). The number of subcarriers is $N = 256$.

Finally, the performance of the frequency estimator is plotted in Figure 7 by means of the SNR loss in decibels: SNR_e-SNR. The SNR loss is (*cf.* (2)) a function of ε. We assume that a frequency offset can be corrected using the estimate $\widehat{\varepsilon}_{\text{ML}}$ and we thus use the standard deviation of the estimate as the argument in (2). The SNR loss is plotted for the AWGN channel and the dispersive channel. Notice that even for the dispersive channel this loss does not exceed 0.5 dB for SNR values between 0 dB and 20 dB.

5 Discussion

We have presented the joint ML estimator of time and frequency offset in OFDM systems. It uses the redundant information contained within the cyclic prefix. It is derived under the assumption that the channel distortion only consists of additive noise, but simulations show that it can perform well even in a dispersive channel. The ML estimator for the latter case may be derived, but it will not have the same simple structure as our proposed estimator.

The frequency estimator performs better than the time estimator because of its implicit averaging. From (6) and (10), the estimate is the argument of a sum of complex numbers. Without additive noise $n(k)$, each term $r(k)r^*(k+N)$ has the same argument, $-2\pi\varepsilon$. Hence, they contribute coherently to the sum, while the additive noise contributes incoherently. This explains why the performance will improve as the size of the cyclic prefix increases.

In wireless systems pilots are needed for channel estimation. These pilots can be used by the synchronizer in order to further increase performance. Resulting synchronizers may be hybrid structures using both pilots and the redundancy of the cyclic prefix. How

to incorporate pilot symbols in such time and frequency estimators is not straightforward and needs further research.

A The log-likelihood function

The log-likelihood function (4) can be written as

$$\Lambda(\theta,\varepsilon) = \sum_{k=\theta}^{\theta+L-1} \log\left(\frac{f\left(r(k), r(k+N)\right)}{f\left(r(k)\right) f\left(r(k+N)\right)}\right). \tag{14}$$

The numerator is a 2-D complex-valued Gaussian distribution, which, using the correlation properties (3), becomes

$$f\left(r(k), r(k+N)\right) = \frac{\exp\left(-\frac{|r(k)|^2 - 2\rho \mathrm{Re}\left\{e^{j2\pi\varepsilon} r(k) r^*(k+N)\right\} + |r(k+N)|^2}{(\sigma_s^2+\sigma_n^2)(1-\rho^2)}\right)}{\pi^2\left(\sigma_s^2+\sigma_n^2\right)^2\left(1-\rho^2\right)}, \tag{15}$$

where ρ is the magnitude of the correlation coefficient between $r(k)$ and $r(k+N)$ as defined in (8). The denominator of (14) consists of two 1-D complex Gaussian distributions

$$f\left(r(k)\right) = \frac{\exp\left(-\frac{|r(k)|^2}{(\sigma_s^2+\sigma_n^2)}\right)}{\pi\left(\sigma_s^2+\sigma_n^2\right)}, \tag{16}$$

and the log-likelihood function (14), after some algebraic manipulations, becomes

$$\Lambda(\theta,\varepsilon) = c_1 + c_2\left(\left|\gamma\left(\theta\right)\right| \cos\left(2\pi\varepsilon + \angle\gamma\left(\theta\right)\right) - \rho\Phi\left(\theta\right)\right), \tag{17}$$

where $\gamma\left(m\right)$ and $\Phi\left(m\right)$ are defined in (6) and (7), and c_1 and c_2 are constants, independent of θ and ε. Since the maximizing argument of $\Lambda\left(\theta,\varepsilon\right)$ is independent of the constants c_1 and c_2, and $c_2 > 0$, the ML-estimate $\left(\widehat{\theta}_{\mathrm{ML}}, \widehat{\varepsilon}_{\mathrm{ML}}\right)$ also maximizes (5).

Acknowledgment

The authors wish to thank M. Isaksson, Telia Research AB, Luleå, Sweden, for many stimulating discussions during the early stages of the project leading to this paper.

References

[1] W.Y. Zou and Y. Wu, 'COFDM: An Overview', *IEEE Transactions on Broadcasting*, vol. 41, no. 1, pp. 1–8, March 1995.

[2] J.A.C. Bingham, 'Multicarrier modulation for data transmission: an idea whose time has come', *IEEE Communications Magazine*, vol. 28, no. 5, pp. 5–14, May 1990.

[3] L. Wei and C. Schlegel, 'Synchronization requirements for multi-user OFDM on satellite mobile and two-path Rayleigh fading channels', *IEEE Transactions on Communications*, vol. 43, no. 2/3/4, pp. 887–895, February/March/April 1995.

[4] T. Pollet and M. Moeneclaey, 'Synchronizability of OFDM signals', in *Proceedings of the IEEE Global Telecommunications Conference (GLOBECOM'95)*, Singapore, November 1995, pp. 2054–2058.

[5] T. Pollet, M. van Bladel, and M. Moeneclaey. 'BER sensitivity of OFDM systems to carrier frequency offset and Wiener phase noise', *IEEE Transactions on Communications*, vol. 43, no. 2/3/4, pp. 191–193, February/March/April 1995.

[6] W.D. Warner and C. Leung, 'OFDM/FM frame synchronization for mobile radio data communication', *IEEE Transactions on Vehicular Technology*, vol. 42, no. 3, pp. 302–313, August 1993.

[7] P.J. Tourtier, R. Monnier, and P. Lopez, 'Multicarrier modem for digital HDTV terrestrial broadcasting', *Signal Processing: Image Communication*, vol. 5, no. 5–6, pp. 379–403, December 1993.

[8] F. Daffara and A. Chouly, 'Maximum likelihood frequency detectors for orthogonal multicarrier systems', in *Proceedings of the IEEE International Conference on Communications (ICC'93)*, May 1993, pp 766–771.

[9] J.J. van de Beek, M. Sandell, M. Isaksson, and P.O. Börjesson, 'Low-complex frame synchronization in OFDM systems', in *Proceedings of the IEEE International Conference on Universal Personal Communications (ICUPC'95)*, Tokyo, Japan, November 1995, pp 982–986.

[10] M. Sandell, J.J. van de Beek, and P.O. Börjesson, 'Timing and frequency synchronization in OFDM systems using the cyclic prefix', in *Proceedings of the IEEE International Symposium on Synchronization*, Essen, Germany, December 1995, pp. 16–19.

[11] P.H. Moose, 'A technique for orthogonal frequency division multiplexing frequency offset correction', *IEEE Transactions on Communications*, vol. 42, no. 10, pp. 2908–2914, October 1994.

[12] F. Daffara and O. Adami, 'A new frequency detector for orthogonal multicarrier transmission techniques', in *Proceedings of the Vehicular Technology Conference (VTC'95)*, Chicago, Illinois, USA, July 1995, pp. 804–809.

[13] A. Peled and A. Ruiz, 'Frequency domain data transmission using reduced computational complexity algorithms', in *Proceedings of the IEEE International Conference on Acoustics, Speech, and Signal Processing (ICASSP'80)*, Denver, Colorado, 1980, pp. 964–967.

[14] T. Pollet, P. Spruyt, and M. Moeneclaey, 'The BER performance of OFDM systems using non-synchronized sampling'. in *Proceedings of the IEEE Global Telecommunications Conference (GLOBECOM'94)*, San Francisco, USA, November 1994, pp. 253–257.

[15] G.C. Carter, 'Coherence and time delay estimation', *Proceedings of the IEEE*, vol. 75, no. 2, pp. 236–255, February 1987.

[16] W.C. Jakes, *Microwave Mobile Communications*, Classic Reissue, IEEE Press, Piscataway, NJ, 1974.

Part 3

This part has been published as

J.J. van de Beek, P.O. Börjesson, M.-L. Boucheret, D. Landström, J. Martinez Arenas, P. Ödling, and S.K. Wilson, 'Three Non-Pilot-Based Time and Frequency Estimators for OFDM", Research Report 1998:08, Division of Signal Processing, Luleå University of Technology, September 1998.

Three Non-Pilot-Based Time and Frequency Estimators for OFDM

J.J. van de Beek, P.O. Börjesson, M.-L. Boucheret, D. Landström,
J. Martinez Arenas, P. Ödling, and S.K. Wilson

Abstract – This paper presents time-domain maximum likelihood estimators of time and frequency offsets for three *orthogonal frequency-division multiplexing* (OFDM) signal models: for a pulse-shaped one-shot OFDM signal, for a stream of multiple OFDM signals and for an OFDM signal in a dispersive channel environment. We also develop structures to simplify the estimators' implementation. Simulation results indicate the relative performances and strengths of these three estimators.

1 Introduction

In this paper we focus on the estimation of symbol-time and carrier frequency offsets for *orthogonal frequency-division multiplexing* (OFDM) symbols for synchronization purposes in wireless environments. The synchronization of an OFDM transmitter and receiver is important because OFDM systems are in general more sensitive to frequency offsets than single carrier systems [1] and symbol-time synchronization is conceptually different [2]. Not only may synchronization errors cause *intersymbol interference* (ISI), they also can cause the loss of orthogonality between the subcarriers resulting in *intercarrier interference* (ICI). The sensitivity of OFDM systems to synchronization errors has been documented in, *e.g.*, [1–4]. Some documented time and frequency offset estimators for OFDM require pilot symbols, see for example [5–7]. However, insertion of many pilot symbols lower the overall information rate. Hence, methods that do not use pilots are desirable. Such methods have been investigated in [8–12] and patented in [13]. The method described in [11] differs from the other methods in that it describes the time-domain *maximum likelihood* (ML) estimator for OFDM systems with a cyclic-prefix [14] in an *additive white Gaussian noise* (AWGN) channel. This estimator exploits the redundancy in the cyclic prefix to determine both the time and frequency offset of a received OFDM symbol. One of the main contributions of [11] is the knowledge that the estimator is optimal in the ML sense and as such gives an upper bound on the performance of a time and frequency estimator.

However, the estimator in [11] was derived for an AWGN channel and, as such, it is not optimal in practical wireless OFDM channels. In this paper we describe three signal models for wireless OFDM systems and derive the ML time and frequency offset estimator associated with each of the models. We focus on the role of the signal model, rather than on a particular application. Each model incorporates some of the properties

of either the transmitted signal or the radio channel. One purpose of this paper is to provide a toolbox of techniques that can be used to improve the performance of the estimator from [11]. We derive these techniques by adapting the signal model to more accurately model the system. A second purpose is to build knowledge about the structure of ML estimators for OFDM systems which can be used to design a specific system.

The three cases are as follows. First, pulse-shaping is used in many wireless OFDM systems to reduce the out-of-band emission and for reasons of robustness against Doppler spread and frequency offsets [15–17]. Here, we focus on the kind of pulse-shaping accomplished by windowing the transmitted signal. Pulse-shaping by filtering transmitted signals is beyond the scope of this paper. Because the ML estimator in [11] was derived for OFDM systems without pulse-shaping, its performance will suffer when it is applied to a pulse-shaped OFDM signal. We present an estimator for pulse-shaped systems, see also [18, 19].

Secondly, the ML estimator's performance suffers below a given SNR threshold [11]. For example, for bandlimited signals, proposed for multiuser communication systems [20], this threshold may reduce the applicability of the estimation concept. In many practical systems the time and frequency variations in the channel vary only slowly. We present an ML estimator designed for a stream of OFDM symbols that exploits this system property and can help compensate for the above performance degradation.

Finally, wireless OFDM systems often operate in a multipath environment, and thus under a dispersive channel [21]. Applying the estimator derived in [11, 13] will result in a error floor in the performance of the time and frequency offset estimator. We develop an ML estimator that is based on knowledge of the channel dispersion.

The paper is organized as follows. In Section 2 we discuss general properties of the OFDM system that an estimator may take into account and exploit. In Section 3 we present three signal models and the associated ML estimators. First, we present the ML estimator for time and frequency offsets for systems using pulse-shaping. Secondly, we present the ML estimator of time and frequency offsets for systems in which these parameters vary slowly. Finally, we present the ML estimator of a time offset for systems with channel dispersion. The paper does not target a particular application. Instead, we will be working with signal models for a class of estimators and show how different system properties can be incorporated in the model. In Section 4 we illustrate the performance of the estimators with simulation results and we discuss these in Section 5. We show that by incorporating system properties as pulse-shaping or knowledge about the stability of the clocks and oscillators the estimator performance can significantly be improved.

2 OFDM systems and synchronization

Figure 1 shows the structure of the OFDM system where our signal models are based on. The transmitter modulates complex data symbols on a large number of subcarriers by means of an *inverse discrete Fourier transform* (IDFT). Each block of samples is cyclically extended with a prefix before it is transmitted over the channel [14]. In the receiver the cyclic prefix is removed and the data are demodulated by means of a *discrete Fourier transform* (DFT). If the cyclic prefix is longer than the length of the channel

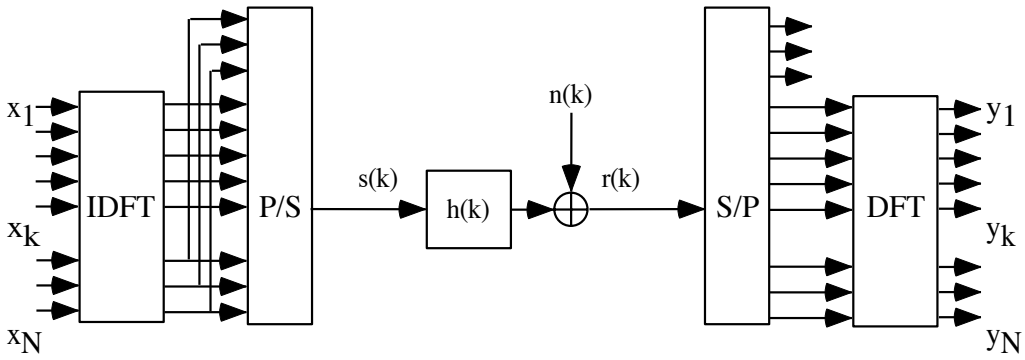

Figure 1: The OFDM system model.

impulse response it avoids ISI and ICI [14]. For the synchronization concept described in this paper the number of subcarriers N and the length of the cyclic prefix L (in samples) are important parameters. They describe the amount of redundancy in the signal that the estimator can exploit. Reference [11] investigates the estimator's performance in relation to N and L.

The sensitivity to a symbol-time offset of θ (in samples) has been investigated in [4]. The performance degradation is not graceful and an analysis must differ between small and large time offsets. If the length of the cyclic prefix exceeds the length of the channel impulse response, the system is robust against small time offsets. As long as the time delay θ and the length of the channel impulse response together do not exceed the length of the cyclic prefix L, ISI and ICI are avoided. The time offset will then appear as a linear phase distortion of the demodulated data symbols across the subcarriers but not in ISI and ICI. A channel estimator can not distinguish these rotations from channel phase distortions. Depending on the quality of the channel estimator, parts of the phase offsets will therefore in a coherent system be compensated for by the channel equalizer. In a differential system the system performance depends on how fast the channel is varying.

For large delays θ ISI and ICI occur [4]. Therefore, symbol timing requirements are relaxed by increasing the length of the cyclic prefix. Alternatively, good time synchronization allows for a tight design of the cyclic prefix leading to spectrally efficient systems.

The sensitivity to frequency offsets for the AWGN channel has analytically been investigated in, among others, [1]. A frequency offset ε (normalized to the intercarrier spacing) results in ICI. The amount of ICI is proportional to ε^2 and the *signal-to-noise ratio* (SNR). In [1] the ICI is interpreted as a degradation of the SNR and quantitatively investigated. For example, a frequency offset which is 4% of the intercarrier spacing results in interference that decreases the SNR with approximately 0.2 dB, if the original SNR is 10 dB, for an AWGN channel.

In the next section we discuss three models of the received OFDM signal. Information about the unknown offsets is found in the correlation of the received signal. A few model assumptions are crucial and similar for all the three models: in each model we assume that the transmitted discrete-time signal is Gaussian [22]. Because of the cyclic prefix this signal is not white. Each transmitted OFDM symbol contains L consecutive samples

that are pairwise correlated with L other consecutive samples N samples ahead. By observing this correlation we can tell where the OFDM symbol is likely to start. As we will see in the rest of the paper, the frequency offset can also be estimated exploiting this redundancy.

As a reference model we assume that the transmitted signal $s(k)$ is Gaussian with covariance function

$$C_s(k_1,k_2)=\begin{cases} & \text{if } k_1=k_2, \\ \sigma_s^2, & \text{if } k_1=k_2+N \text{ and } 0\le k_2<L, \\ & \text{if } k_2=k_1+N \text{ and } 0\le k_1<L, \\ 0, & \text{otherwise.}\end{cases} \tag{1}$$

Notice that this model only reflects the appearance of *one* OFDM symbol (one cyclic prefix) in the transmitted signal. In a real system the transmitted signal typically consists of a stream of OFDM symbols, each containing such a redundancy.

Based on the above assumptions our reference model of the received signal $r(k)$ is as in [11],

$$r(k)=s(k-\theta)e^{j2\pi\varepsilon k/N}+n(k) \qquad -\infty<k<\infty, \tag{2}$$

where $s(k)$ is a sample of the Gaussian process with covariance function (1), and $n(k)$ is complex AWGN with variance σ_n^2. We will compare the signal models developed in this paper with our reference model (2). We focus on the estimation of the unknown offset parameters θ and ε from the received data $r(k)$. It is possible to estimate θ and ε from $r(k)$, because much of the statistical structure of the transmitted signal $s(k)$ is transferred to the received signal $r(k)$.

The ML estimator based on (2) yields a fast one-shot estimator of θ and ε [11], which we repeat here for later reference (we slightly change notations for reasons of comparison with later results in this paper)

$$\begin{aligned}\widehat{\theta}_{\text{AWGN}} &= \arg\max_{\theta}\left\{|\gamma_N(\theta)|+\gamma_0(\theta)\right\}, \\ \widehat{\varepsilon}_{\text{AWGN}} &= -\frac{1}{2\pi}\angle\gamma_N(\widehat{\theta}_{\text{AWGN}}),\end{aligned} \tag{3}$$

where $\widehat{\theta}_{\text{AWGN}}$ is the symbol-time offset, $\widehat{\varepsilon}_{\text{AWGN}}$ is the frequency offset, and

$$\begin{aligned}\gamma_N(\theta) &= \sum_{k=\theta}^{\theta+L-1} r(k)r^*(k+N), \\ \gamma_0(\theta) &= -\frac{\rho}{2}\sum_{k=\theta}^{\theta+L-1}|r(k)|^2+|r(k+N)|^2.\end{aligned} \tag{4}$$

In these equations ρ is defined as

$$\rho=\frac{\sigma_s^2}{\sigma_s^2+\sigma_n^2}=\frac{\text{SNR}}{\text{SNR}+1}, \tag{5}$$

and $\text{SNR}=\sigma_s^2/\sigma_s^2$. This estimator extracts the information carried by the cyclic prefix by correlating the received signal and a delayed copy. The term $\gamma_N(m)$ collects this correlation. The term $\gamma_0(m)$ compensates for high contributions due to large sample values rather than a large correlation.

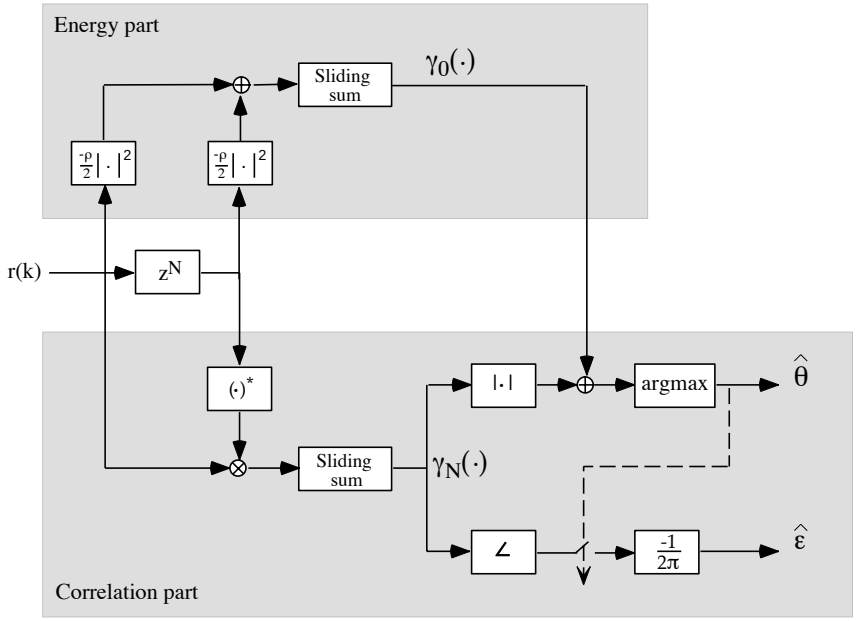

Figure 2: Structure of the estimator designed for an AWGN channel.

3 Estimators of time and frequency offsets

In this section we generalize model (2) and estimator (3) to include pulse-shaping, multiple symbols, and channel dispersion. We introduce the vector $\mathbf{r}$ for the received signal, with covariance matrix $\mathbf{C}_r$. Then, the covariance function of the received signal contains the information due to (multiple) cyclic prefixes, pulse-shaping or channel dispersion and noise. The joint ML estimate $(\widehat{\theta,\varepsilon})_{\mathrm{ML}}$ of θ and ε, given the received Gaussian data vector $\mathbf{r}$ with known covariance matrix $\mathbf{C}_r$ becomes

$$(\widehat{\theta,\varepsilon})_{\mathrm{ML}} = \arg\max_{\theta,\varepsilon} \left\{ -\mathbf{r}^H \mathbf{C}_r^{-1}(\theta,\varepsilon)\,\mathbf{r} \right\}. \tag{6}$$

For the signal models described in this section, the quadratic form can be put in explicit expressions that lead to implementable structures.

3.1 Offset estimators for pulse-shaped systems

Some OFDM systems require pulse-shaping in order to suppress the system's sidelobes and out-of-band emission. Other systems become more robust against Doppler effects and frequency offsets. The use of pulse-shaping is suggested in, *e.g.*, [4, 15–17, 23]. Two ways of pulse-shaping are addressed in literature: pulse-shaping by filtering and pulse-shaping by windowing. In this paper we address the latter group. Examples of pulse-shapes found in existing systems or system proposals are (see Figure 3) the pulse shapes given by the raised cosine shaped,

$$p_T(k) = \begin{cases} \frac{1}{2}\left(1-\cos\left(\frac{k}{P-1}\pi\right)\right), & 0 \le k < P, \\ 1, & P \le k < N+L-P, \\ \frac{1}{2}\left(1+\cos\left(\frac{k-(N+L-P)}{P-1}\pi\right)\right), & N+L-P \le k < N+L, \end{cases} \tag{7}$$

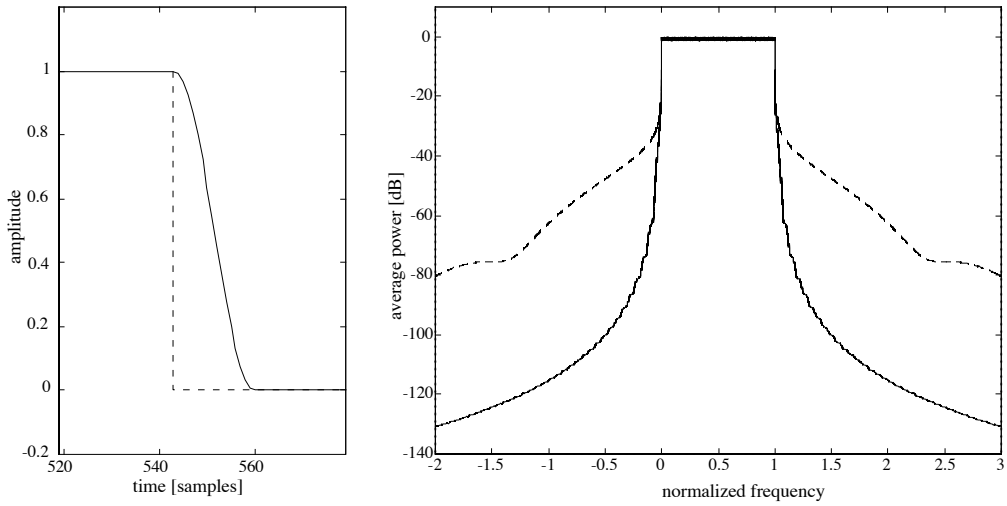

Figure 3: The OFDM signal shaped with cosine roll-off edges (solid) and with a rectangular window (dashed). The edge of the OFDM symbol for both pulses (left) and the OFDM power spectrum (right) Rectangular pulse (dashed) and raised cosine pulse (solid).

in [23], which as a special case becomes the Hanning window which is investigated in [4, 23]. For some pulse-shapes and parameter choices, the subcarriers in the OFDM symbol lose their orthogonality. The choice of pulse-shapes is beyond the scope of this paper.

For a general pulse-shape we model the received signal as

$$r(k) = g(k-\theta)s(k-\theta)e^{j2\pi\varepsilon k/N} + n(k), \qquad -\infty < k < \infty, \tag{8}$$

where θ, ε, $r(k)$, $s(k)$, and $n(k)$ are defined as in (2), and

$$g(k) = \begin{cases} p(k) & 0 \le k < N+L \\ 1 & \text{otherwise.} \end{cases}, \tag{9}$$

where $p(k)$ is the pulse-shape, for instance (7). The choice of unit power outside the interval $\{0, \ldots, N+L\}$ models our assumption that there actually are a preceding and next OFDM symbols, which is not obvious in, for instance, a system with time-division multiple access. We do, however, not rely on any correlation property of these symbols. As in the reference model (2), we model correlation properties (and now also the shape) of one OFDM symbol only ($N+L$ consecutive samples) in the transmitted signal. Equation (8) models adjacent OFDM symbols as white Gaussian with time-invariant average power. For the choice $p(k) = 1$, $k = 0 \le k < N+L$, model (8) reduces to (2).

Pulse-shaping affects the performance of an estimator in two ways, one negative and one positive. First, it changes the amplitude in some parts of the signal. For most practical pulses it reduces the amplitude in the parts of the signal that are cyclically repeated. This reduces the correlation in the signal, and thus also the performance of the estimator. Secondly, the pulse-shape introduces a time-varying signal power that also carries information about the symbol-time offset. This information may improve

the performance of an estimator. For some systems the net effect of the pulse-shaping is positive as simulations will show.

To derive the ML estimator for the pulse-shaped OFDM system, we find the pair $(\widehat{\theta,\varepsilon})$ that maximizes the log-likelihood function $\Lambda(\theta,\varepsilon) = -\mathbf{r}^{\mathrm{H}}\mathbf{C}_r^{-1}(\theta,\varepsilon)\,\mathbf{r}$. In Appendix A it is shown that this function becomes

$$\Lambda(\theta,\varepsilon) = |\gamma_N(\theta)|\cos\{2\pi\varepsilon + \angle\gamma_N(\theta)\} + \gamma_0(\theta), \tag{10}$$

where

$$\begin{aligned}\gamma_N(\theta) &= \sum_{k=-\infty}^{\infty} h_N(k-\theta)r(k)r^*(k+N), \\ \gamma_0(\theta) &= \sum_{k=-\infty}^{\infty} h_0(k-\theta)\,|r(k)|^2,\end{aligned} \tag{11}$$

and where

$$h_N(k) = \begin{cases} \frac{1}{\sigma_n^2}\frac{2\mathrm{SNR}g(k)g(k+N)}{\mathrm{SNR}(g^2(k)+g^2(k+N))+1} & 0\le k<L \\ 0 & \text{otherwise}\end{cases}, \tag{12}$$

$$h_0(k) = \begin{cases} -\frac{1}{\sigma_n^2}\frac{\mathrm{SNR}g^2(k+N)+1}{\mathrm{SNR}(g^2(k)+g^2(k+N))+1} & 0\le k<L \\ -\frac{1}{\sigma_n^2}\frac{\mathrm{SNR}g^2(k-N)+1}{\mathrm{SNR}(g^2(k)+g^2(k-N))+1} & N\le k<N+L \\ -\frac{1}{\sigma_n^2}\frac{1}{\mathrm{SNR}g^2(k)+1} & \text{otherwise}\end{cases}. \tag{13}$$

The SNR is the ratio of the average signal energy to the average noise energy ($\mathrm{SNR} = \sigma_s^2/\sigma_n^2$). The ML estimator maximizes the log-likelihood function and becomes

$$\begin{aligned}\widehat{\theta}_{\mathrm{pulse}} &= \arg\max_{\theta}\{|\gamma_N(\theta)| + \gamma_0(\theta)\}, \\ \widehat{\varepsilon}_{\mathrm{pulse}} &= -\frac{1}{2\pi}\angle\gamma_N(\widehat{\theta}_{\mathrm{pulse}}).\end{aligned} \tag{14}$$

The filter $h_0(k)$ has infinite length. In order to make the filter length finite, we add $\frac{1}{\sigma_n^2}\frac{1}{\mathrm{SNR}+1}\sum_{k=-\infty}^{\infty}|r(k)|^2$ to log-likelihood function $\Lambda(\theta,\varepsilon)$. Since this term does not depend on θ it will not change the maximizing argument $\widehat{\theta}_1$ (thus, there is no performance loss). Because we have chosen $g(1) = 1$ outside $0 \le k < N+L$ (see (9)), this yields, the same structure $\Lambda(\theta,\varepsilon)$ as in (10) where now $h_0(k)$ is reddefined as

$$h_0(k) = \begin{cases} -\rho\frac{1}{\sigma_n^2}\frac{\mathrm{SNR}g^2(k+N)+1-g^2(k)}{\mathrm{SNR}(g^2(k)+g^2(k+N))+1} & 0\le k<L \\ -\rho\frac{1}{\sigma_n^2}\frac{1-g^2(k)}{\mathrm{SNR}g^2(k)+1} & L\le k<N \\ -\rho\frac{1}{\sigma_n^2}\frac{\mathrm{SNR}g^2(k-N)+1-g^2(k)}{\mathrm{SNR}(g^2(k)+g^2(k-N))+1} & N\le k<N+L \\ 0 & \text{otherwise}\end{cases}, \tag{15}$$

where ρ is as in estimator (3). This filter now has finite length and is thus implementable. When $p(k) = 1$, the signal model (8) reduces to (2) and the estimates $\widehat{\theta}_{\mathrm{pulse}}$ and $\widehat{\varepsilon}_{\mathrm{pulse}}$ coincide with $\widehat{\theta}_{\mathrm{AWGN}}$ and $\widehat{\varepsilon}_{\mathrm{AWGN}}$. A similar estimator performing one-shot estimation in a time–division multiuser systems is investigated in [18, 19, 24]. Figure 4 shows the

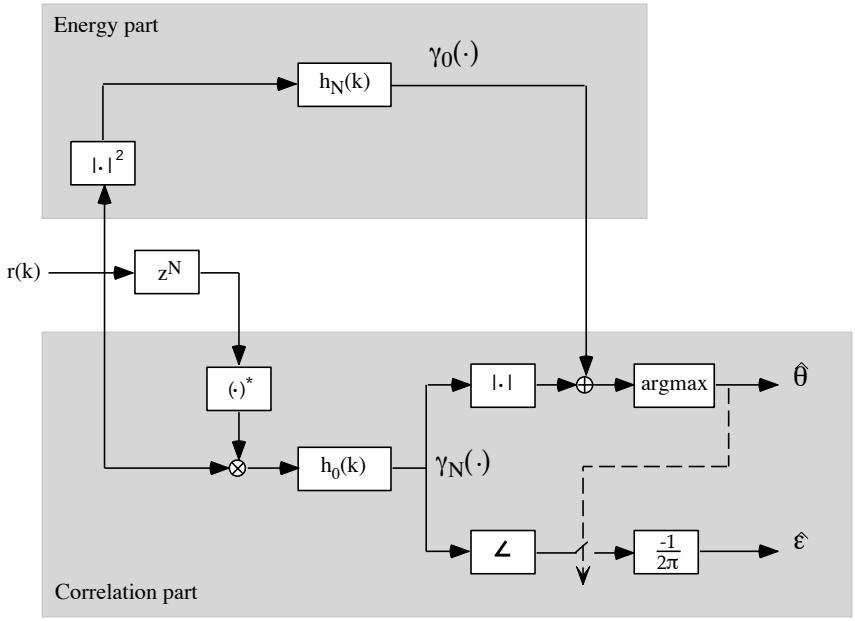

Figure 4: Structure of the estimator designed for the AWGN channel and pulse-shaping.

estimator structure. Note the similarity of the estimator structures for the AWGN model (2) and the pulse shaping model (8); the estimator only replaces sliding sums by filters.

Estimator (14) exploits two types of information. First, the correlation between the samples in the cyclic prefix is used, and collected by the filter $h_N(k)$. Moreover, the time-varying signal power contains information about θ. The estimator extracts this information by means of the filter $h_0(k)$. This filter $h_0(k)$ works much like a matched filter to $|r(k)|^2$.

3.2 Offset estimators for systems with serial transmission of OFDM symbols

The signal models (2) and (8) incorporate *a priori* knowledge about *one* transmitted OFDM symbol in the transmitted signal and use only $N + L$ samples in the estimation procedure. Estimators based on these models are one-shot estimators in the sense that they generate estimates of the time and frequency offset for each symbol by exploiting the information carried by only that symbol. In this section we describe a signal model that incorporates multiple OFDM symbols to improve the estimator performance. It benefits from the statistical structure of M consecutive OFDM symbols.

We model the received signal $r(k)$ as

$$r(k) = \tilde{s}(k-\theta)e^{j2\pi\varepsilon k/N} + n(k) \qquad -\infty < k < \infty, \tag{16}$$

where θ, ε, and $n(k)$ are defined as before. Now, we assume that the transmitted signal

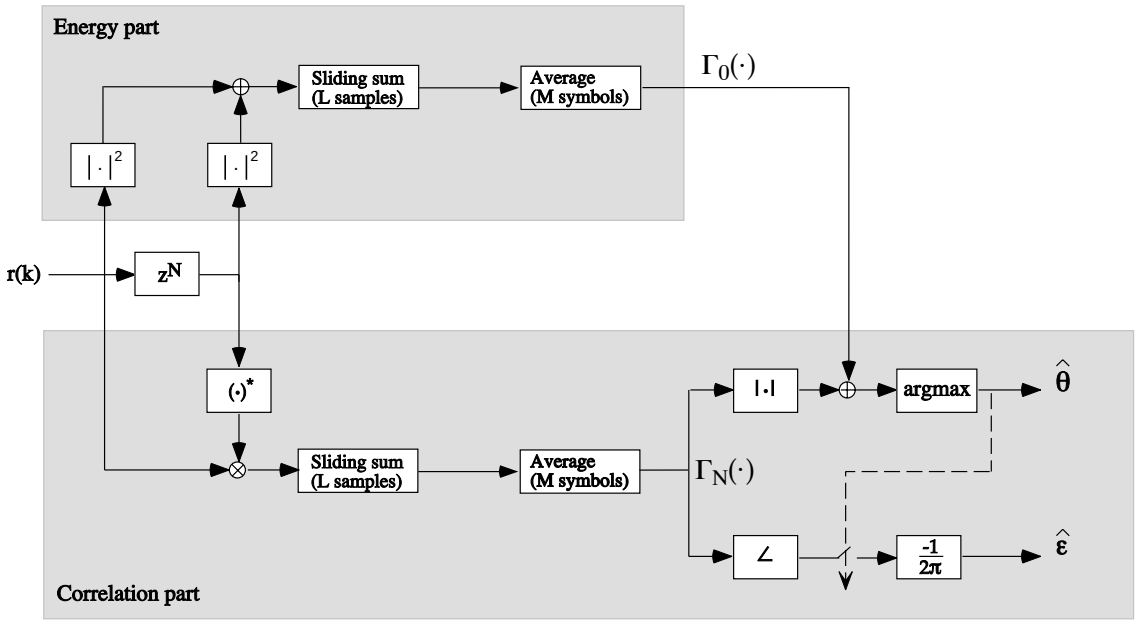

Figure 5: Structure of the estimator designed for serial transmission.

$\tilde{s}(k)$ has covariance function

$$C_{\tilde{s}}(k_1,k_2)=\begin{cases}\sigma_{\tilde{s}}^2 & \text{if } k_1=k_2\\ \sigma_{\tilde{s}}^2 & \text{if } \begin{cases} k_1=k_2+N \text{and}\\ m(N+L)\le k_2<m(N+L)+L \text{ and } m=0\dots M\end{cases}\\ \sigma_{\tilde{s}}^2 & \text{if } \begin{cases} k_2=k_1+N \text{and}\\ m(N+L)\le k_1<m(N+L)+L \text{ and } m=0\dots M\end{cases}\\ 0 & \text{otherwise}\end{cases} \tag{17}$$

The purpose of this model is to increase the information available to the estimator and to generate a stable symbol clock and oscillator. In practical applications there may be a drift in the transmitter symbol clock relative to the receiver clock. In particular, when M is large, not all of the received symbols obey the perfect clock we assume. For instance, in systems with a multiple access scheme based on time-division, the drift from one symbol to the next may be large. In most applications, however, clock drifts are such that for moderate M the assumption holds.

In Appendix B, we derive the log-likelihood function of θ and ε, yielding

$$\Lambda(\theta,\varepsilon)=|\Gamma_N(\theta)|\cos\{2\pi\varepsilon+\angle\Gamma_N(\theta)\}+\Gamma_0(\theta), \tag{18}$$

where

$$\begin{aligned}\Gamma_N(\theta) &= \sum_{m=0}^{M-1}\gamma_N(\theta+m(N+L)),\\ \Gamma_0(\theta) &= \sum_{m=0}^{M-1}\gamma_0(\theta+m(N+L)),\end{aligned} \tag{19}$$

and where $\gamma_N(\cdot)$ and $\gamma_0(\cdot)$ are as defined in (4). The optimal estimator for model (16) now becomes

$$\begin{aligned} \widehat{\theta}_{\text{serial}} &= \arg\max_{\theta} \{|\Gamma_N(\theta)| + \Gamma_0(\theta)\}, \\ \widehat{\varepsilon}_{\text{serial}} &= -\frac{1}{2\pi} \angle \Gamma_N(\widehat{\theta}_{\text{serial}}). \end{aligned} \tag{20}$$

Thus, the optimal way (in a maximum likelihood sense) to process the M consecutive symbols is to average M statistics $\gamma_N(\cdot)$ and $\gamma_0(\cdot)$ defined in (4) to create the log-likelihood function. The estimator (20) can, in a straightforward way, be extended to incorporate pulse-shaping, as well.

3.3 Offset estimators for systems with channel dispersion

In many applications, for instance the European *digital audio broadcasting* (DAB) network [25] and the *digital video broadcasting* (DVB) [26] system, channel dispersion will affect the correlation properties of the received OFDM signal. For the purpose of data detection in an OFDM receiver, this channel dispersion appears as a multiplicative distortion of the data symbols and correction is straightforward. However, the time and frequency synchronization concept targeted by this paper works on the received signal $r(k)$ before the DFT. In this section we state a signal model incorporating $r(k)$'s correlation due to the channel dispersion. As we will see though, optimal synchronization which is conceptually straightforward, is not as tractable as in the previous cases and some approximations are necessary to reach an implementable estimator.

Given a channel impulse response, $h(k)$, we model the received signal $r(k)$ as

$$r(k) = (h * s)(k - \theta) + n(k) \qquad -\infty < k < \infty, \tag{21}$$

where θ, $s(k)$ and $n(k)$ are as defined earlier. We assume that the length H of $h(k)$ is smaller than the length of the cyclic prefix L. Note that we model the radio channel by a discrete-time sample-spaced $h(k)$. Because of the dispersive channel $h(k)$ the correlation structure of $s(k)$ is not transferred so directly to the received signal $r(k)$. Although the channel colors the received signal we will show that estimation is possible.

In our derivation we present only an estimation of θ, ignoring the estimation of ε. Our motivation for this is twofold. First, from previous applied work [11] we have seen that the performance of frequency estimators based on models (2) and (8) is sufficient in a dispersive channel, whereas the performance of the time estimators, sometiimes, is not. Secondly, in this paper, we aim for a tractable estimator structure that gives an indication of likely performance in a dispersive environment so that we can gain an understanding of what synchronization information is contained in $r(k)$. For a model with a frequency offset *and* channel disersion we have not found such a tractable structure for the general statistic $-\mathbf{r}^H \mathbf{C}_r^{-1}(\theta, \varepsilon)\, \mathbf{r}$ in (6). Thus, we focus on estimation of θ.

We assume that we know the channel impulse response. While this assumption holds for some applications (such as copper wire channels), the receiver will have to track a time-varying channel in others (such as DAB, DVB). However, this assumption and the following derivation will give an upper bound on the performance of an estimator that does not use pilots and is therefore useful when evaluating other estimators' performances.

As with the previous models, the ML estimator depends on the covariance matrix $\mathbf{C}_r$ of the received data vector $\mathbf{r}$. Because of the channel dispersion and the cyclic prefix this matrix has the following structure. We can write $\mathbf{C}_r$ as

$$\mathbf{C}_r = \mathbf{H}\mathbf{C}_s\mathbf{H}^H + \sigma_n^2\mathbf{I}, \tag{22}$$

where the matrix $\mathbf{C}_s$ is the correlation matrix of the transmitted OFDM signal $s(k)$ and whose $(k_1, k_2)^{th}$ entries are $C_s(k_1, k_2)$ as in (1), and $\mathbf{H}$ is a matrix whose entries on the ith row and the columns with indexes $\{i, \ldots, i+H-1\}$ are $\{h(0), h(1), \ldots, h(H-1)\}$. We can rewrite $\mathbf{C}_r$ as the sum of three separate matrices,

$$\mathbf{C}_r = \mathbf{C}_0 + \sigma_n^2\mathbf{I} + \mathbf{C}_{cp}(\theta). \tag{23}$$

where

$$\begin{aligned} \mathbf{C}_0 &= \sigma_s^2\mathbf{H}\mathbf{H}^H, \\ \mathbf{C}_{cp}(\theta) &= \sigma_s^2\mathbf{H}\mathbf{I}(\theta)\mathbf{H}^H, \end{aligned} \tag{24}$$

and

$$\mathbf{I}(\theta)_{i,j} = \begin{cases} 1 & \text{if } i \in [\theta, \theta+L-1] \text{ and } j = i+N \\ 1 & \text{if } j \in [\theta, \theta+L-1] \text{ and } i = j+N \\ 0 & \text{otherwise} \end{cases}. \tag{25}$$

In (23), the first term $\mathbf{C}_0$ is a band matrix representing the channel correlation. The second term $\sigma_n^2\mathbf{I}$ is a matrix representing the noise correlation. The third term, $\mathbf{C}_{cp}(\theta)$, is a matrix representing the total correlation of samples located in the repeated parts, *i.e.*, the cyclic prefix. Note that only $\mathbf{C}_{cp}(\theta)$ depends on the unknown θ. The only non-zero elements of $\mathbf{C}_{cp}(\theta)$ are concentrated in a $(N+L+H)\times(N+L+H)$ submatrix, and the dependency of θ appears only in the position of this submatrix.

The ML estimator for model (21) is

$$\widehat{\theta}_{\text{dispersion}} = \arg\max_{\theta}\left\{-\mathbf{r}^H\mathbf{C}_r^{-1}(\theta)\,\mathbf{r}\right\}. \tag{26}$$

This estimator has good performance, but as the size of $\mathbf{C}_r$ increases, so does the complexity. A simplified estimator that approximates this performance exploits the structure of $\mathbf{C}_r$ and becomes (see Appendix C)

$$\widehat{\theta}_{\text{dispersion}} = \arg\max_{\theta}\left\{\sum_{i=-(N+L+H-1)}^{N+L+H-1}\gamma_i(\theta)\right\}, \tag{27}$$

where

$$\gamma_i(m) = \sum_{k=-\infty}^{\infty} h_i(k-m)r(k)r^*(k+i), \tag{28}$$

and where $h_i(k)$ is defined in Appendix C. This result is important because one can now implement the estimator with filters $h_i(k)$. Filter $h_i(k)$ has finite support of length

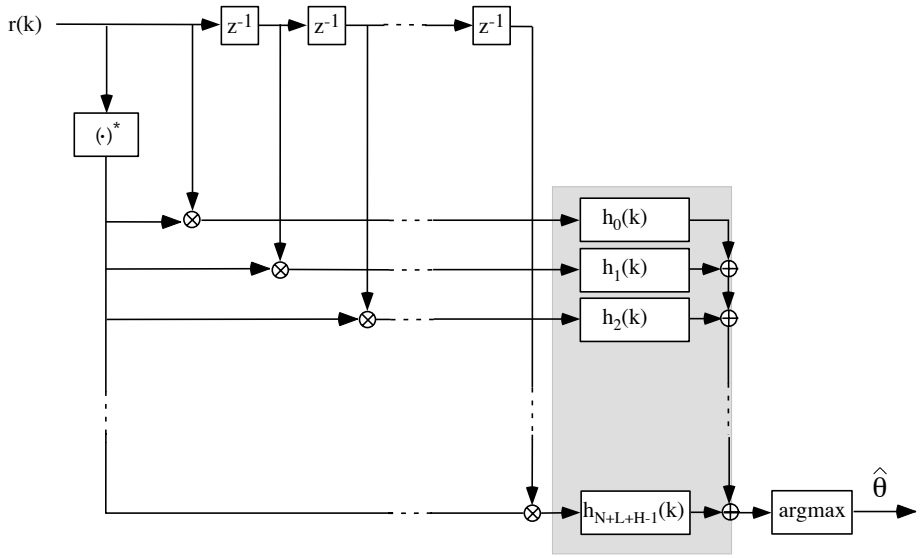

Figure 6: Structure of the estimator designed for a dispersive channel.

$(N + L + H) - |i|$. Estimator (27) suggests the implementation structure shown in Figure 6. First the products $r(k)r^*(k + i)$ are formed. These are fed into the filterbank containing filters with impulse responses $h_i(k)$.

Low-complexity approximations of (27) can be obtained by disregarding filters with a relatively small contribution to the quadratic form. Typically, for a channel with a short impulse response, the filters $h_i(k)$ with i equal or close to $-N$, 0 and N contribute most. In general, the complexity and the approximation error relative to the optimal estimator can be varied by varying the number of filters.

This estimator structure is similar to the structure (3). Without channel dispersion, only the terms $\gamma_0(m)$, $\gamma_{-N}(m)$ and $\gamma_N(m)$ contain non-zero values and estimator (27) reduces to (3) for $\varepsilon = 0$. The estimate $\widehat{\theta}_{\text{dispersion}}$ then coincides with $\widehat{\theta}_{\text{AWGN}}$. Also, the estimator (27) can, in a straightforward way be extended to incorporate pulse-shaping as well. The pulse-shape appears in the covariance matrix $\mathbf{C}_r$ and in the filters $h_i\,(k)$.

4 Simulations

4.1 Performance in a system with pulse-shaping

We illustrate the estimator concepts described in the previous sections with the following system. Consider an OFDM system with 64 subcarriers. In order to reduce ISI and ICI in a dispersive channel environment the system employs a cyclic prefix of 16 samples. Also, we assume that the transmitter shapes 8 samples of an OFDM symbol (4 samples at each side) with the raised cosine pulse-shape.

We first investigate how the pulse-shape in this system affects the estimator performance. Figure 7 shows the variance of the time-offset estimators (3), designed for no pulse-shaping, and (14), designed for pulse-shaping. Thus, one estimator does not take the pulse-shape into account and one does.

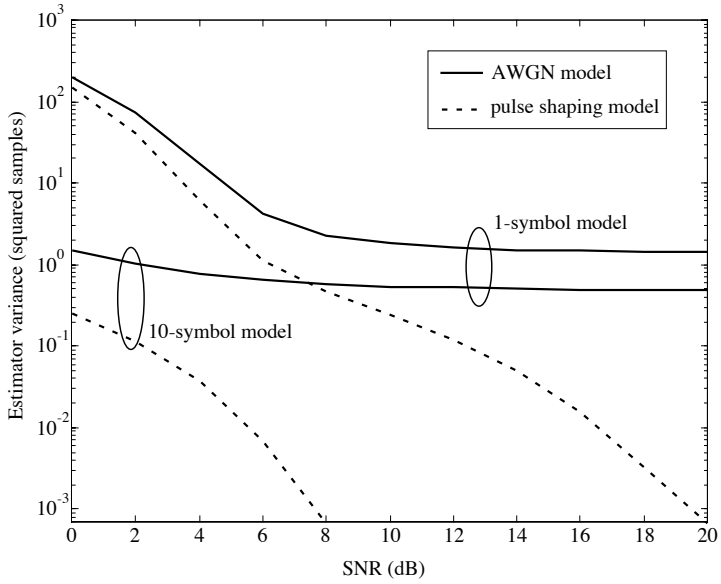

Figure 7: Variance of the time offset estimator in a system with pulse-shaping. The estimator designed without pulse-shaping with (solid) and without (dash-dotted) averaging over 10 symbols. The estimator designed for pulse-shaping with (dotted) and without (dashed) averaging over 10 symbols.

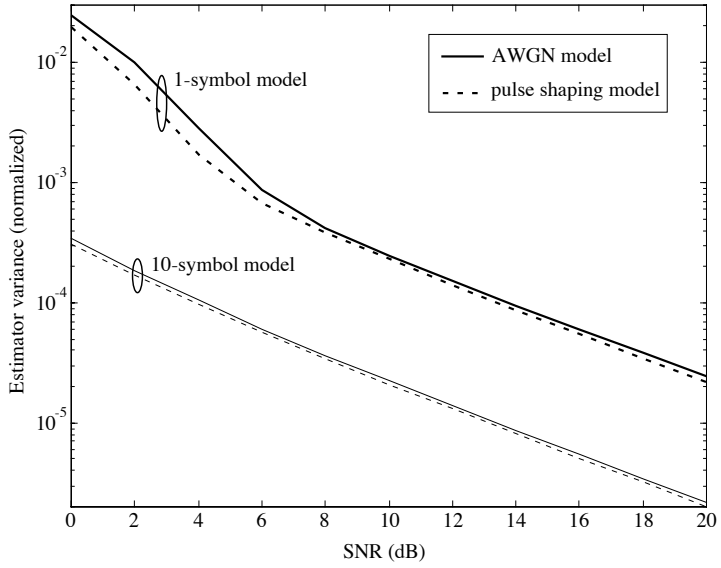

Figure 8: Variance of the frequency offset estimator in a system with pulse-shaping. The estimator designed without pulse-shaping with (solid) and without (dash-dotted) averaging over 10 symbols. The estimator designed for pulse-shaping with (dotted) and without (dashed) averaging over 10 symbols.

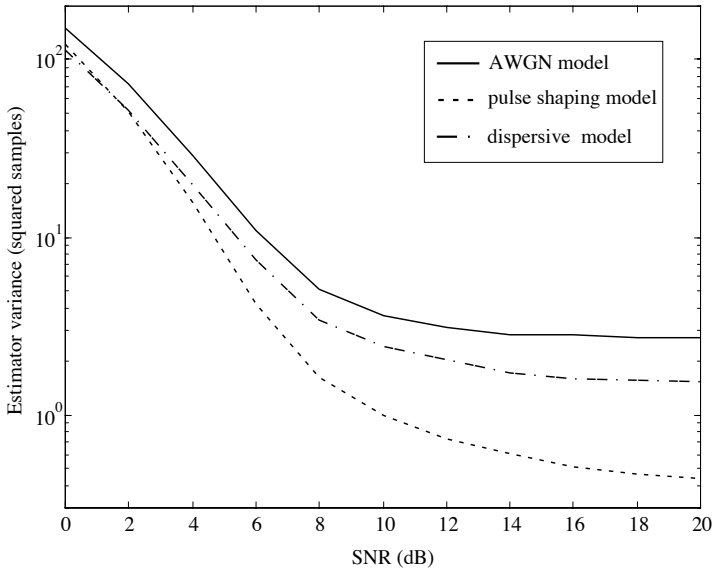

Figure 9: Variance of the time offset estimator for a system with pulse-shaping and channel dispersion. The estimator designed for the AWGN channel (solid), the estimator designed with only the knowledge about the channel dispersion (dash-dotted), and the estimator designed with only the knowledge about the pulse-shape (dashed).

Both estimators are then extended with the averaging concept (20) ($M = 10$), yielding another two estimators (see Figure 7). Ignoring the pulse-shape in the design of the estimator results in a performance error floor. This error floor can be decreased by averaging but consideration of the pulse-shape in the estimator design removes this error floor. Figure 8 shows the estimator variance for the frequency estimators designed as described above. In our system scenario the inclusion of the pulse-shape in the model does not significantly improve the performance of the frequency estimator.

4.2 Performance in a dispersive environment

We now assume that the system operates in a dispersive environment. The channel length of the channel impulse response is 8 samples. We model the channel with the following static discrete-time exponentially decaying channel impulse response

$$h(\tau) = e^{-\tau/3}, \qquad \tau = 0, \ldots, 7.$$

As above, the transmitter employs the raised cosine pulse-shape. Figure 9 shows the performance of the time offset estimators (3), designed with no knowledge of the pulse-shape nor the channel dispersion, (14), designed with no knowledge of the channel dispersion but incorporating the pulse-shape, and (26) for $\varepsilon = 0$, designed without knowledge of the pulse-shape but incorporating the channel dispersion. Thus, one estimator takes neither pulse-shaping nor dispersion into account (reference estimator), one estimator takes only the pulse-shape into account, and one estimator recognizes the channel dispersion only. The latter estimator evaluates $-\mathbf{r}^H \mathbf{C}_r^{-1}(\theta)\,\mathbf{r}$, that is, without the suggested approximations. In this scenario, the performance of each estimator experiences an error

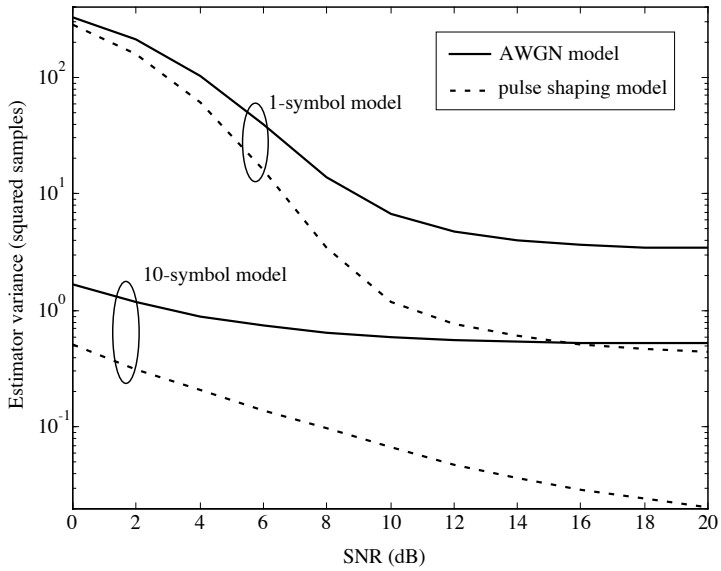

Figure 10: Variance of the time offset estimator in a system with pulse-shaping and channel dispersion.The estimator designed for the AWGN channel with (solid) and without (dash-dotted) averaging over 10 symbols. The estimator designed for pulse-shaping with (dotted) and without (dashed) averaging over 10 symbols.

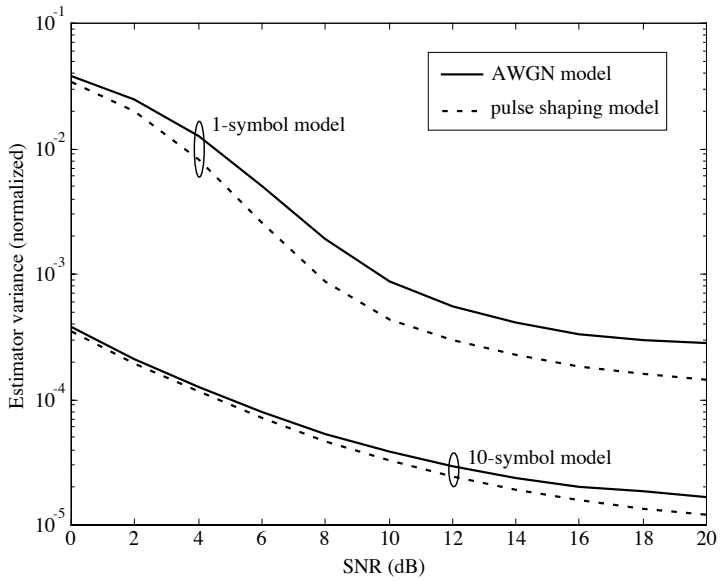

Figure 11: Variance of the frequency offset estimator for a system with pulse-shaping and channel dispersion. The estimator designed for the AWGN channel with (solid) and without (dash-dotted) averaging over 10 symbols. The estimator designed for pulse-shaping with (dotted) and without (dashed) averaging over 10 symbols.

floor because none of the estimators is perfectly matched to the true signal properties. Using knowledge of the pulse-shape property improves the performance more than using knowledge of the channel dispersion alone.

Figures 10 and 11 show the performance of the joint estimators (3) (the reference estimator) and (14) (the pulse-shaping estimator). Both estimators are also extended with the averaging concept (20). In our dispersive environment the use of estimator (14) combined with averaging decreases the error floor.

The simulation results in this section suggest that in systems with pulse-shaping, estimator performance is increased by incorporating the pulse-shape in the signal model. Moreover, in systems with channel dispersion, where time and frequency offsets vary slowly, averaging decreases the error floor.

5 Summary

We have presented three signal models and their respective ML estimators of time and frequency offsets for OFDM systems. Each of the models addresses an aspect of an OFDM system which affects the estimation of the time and frequency offsets in a wireless OFDM system based on the cyclic prefix redundancy. When applied to a wireless system, all of the estimators can improve on the performance of the ML estimator designed for the AWGN channel [11]. We have presented the ML estimator based on a signal model that considers the pulse-shape. Simulations show that the use of this estimator in systems with pulse-shaping is beneficial in both AWGN and dispersive environments. We have also found that when the clock drift is small, averaging can significantly improve the error floor of the estimator. The estimator designed for a dispersive channel can be quite complex, but is useful since it gives a bound on the achievable performance.

A The ML estimator for pulse-shaping

For model (8) the log-likelihood function $\Lambda(\theta,\varepsilon)$ can be written as

$$\Lambda(\theta,\varepsilon) = \log\left(\prod_{k\in[\theta,\theta+L-1]} f\left(r(k),r(k+N)\right)\cdot \prod_{k\notin[\theta,\theta+L-1]\cup[\theta+N,\theta+N+L-1]} f\left(r(k)\right)\right),$$

where $f\left(r(k),r(k+N)\right)$ is the joint Gaussian probability density function for the pair $(r(k),r(k+N))$, $k\in[\theta,\theta+L-1]$ (samples coupled through the cyclic extension), and $f\left(r(k)\right)$ denotes the Gaussian density function for other values of k. Now, define $\mathbf{r} = \begin{bmatrix} r(k) & r(k+N)\end{bmatrix}^T$. By calculating the densities $f\left(r(k)\right)$ and $f\left(\mathbf{r}\right)$ we find the log-likelihood function $\Lambda(\theta,\varepsilon)$. First, $r(k)$ is a complex Gaussian variable with density $f\left(r(k)\right)$ and

$$\log f\left(r(k)\right) = -\frac{1}{\sigma_n^2}\frac{|r(k)|^2}{\mathrm{SNR}g^2(k-\theta)+1} + \log c_1 \quad -\infty < k < \infty\ ,$$

where $\sigma_s^2 \equiv E\left\{|s(k)|^2\right\}$, $\sigma_n^2 \equiv E\left\{|n(k)|^2\right\}$, and c_1 is a constant independent of θ. Secondly, $\mathbf{r}$ is a complex Gaussian vector with joint density function $f\left(\mathbf{r}\right)$, where

$$\log f\left(\mathbf{r}\right) = -\mathbf{r}^H\mathbf{C}^{-1}\mathbf{r} + \log c_2,$$

$\mathbf{C}$ its covariance matrix, and c_2 is a constant independent of θ. $\mathbf{C}$ becomes

$$\begin{aligned}\mathbf{C} &= E\left\{\mathbf{r}^H\mathbf{r}\right\} \\ &= \sigma_n^2\begin{bmatrix} \mathrm{SNR}g^2(k-\theta)+1 & \mathrm{SNR}g(k-\theta)g(k+N-\theta)e^{-j2\pi\varepsilon} \\ \mathrm{SNR}g(k+N-\theta)g(k-\theta)e^{j2\pi\varepsilon} & \mathrm{SNR}g^2(k+N-\theta)+1 \end{bmatrix}.\end{aligned}$$

Thus,

$$\begin{aligned}\log f(\mathbf{r}) &= -\frac{1}{D}\left(\mathrm{SNR}g^2(k+N-\theta)+1\right)|r(k)|^2 \\ &\quad -\frac{1}{D}\left(\mathrm{SNR}g^2(k-\theta)+1\right)|r(k+N)|^2 \\ &\quad +\frac{2}{D}\mathrm{SNR}g(k-\theta)g(k+N-\theta)\mathrm{Re}\left\{e^{-j2\pi\varepsilon}r^*(k)r(k+N)\right\},\end{aligned}$$

where D is the discriminant of $\mathbf{C}$,

$$D = \sigma_n^2\left(\mathrm{SNR}\left(g^2(k-\theta)+g^2(k+N-\theta)\right)+1\right).$$

Straightforward calculations now yield

$$\begin{aligned}\Lambda(\theta,\varepsilon) &= \sum_{k\in[\theta,\theta+L-1]}\log f\left(r(k),r(k+N)\right)+\sum_{k\notin[\theta,\theta+L-1]\cup[\theta+N,\theta+N+L-1]}\log f\left(r(k)\right) \\ &= \sum_{k=-\infty}^{\infty}h_N(k-\theta)\mathrm{Re}\left\{e^{-j2\pi\varepsilon}r^*(k)r(k+N)\right\}+\sum_{k=-\infty}^{\infty}h_0(k-\theta)\left|r(k)\right|^2,\end{aligned}$$

where $h_N(k)$ and $h_0(k)$ defined in (12). Equation (10) now follows readily

B The ML estimator for M consecutive symbols

Assume that the observation interval contains M complete OFDM symbols. The arrival time θ is, as before, the index of the first sample of the first complete symbol, modelling the unknown channel delay. Consider the cyclic prefixes $\mathcal{I}_m$ and their copies $\mathcal{I}'_m$ for each symbol $m = 0,\ldots,M-1$:

$$\begin{aligned}\mathcal{I}_m &\equiv \{m(N+L)+\theta,\ldots,m(N+L)+\theta+L-1\}, \\ \mathcal{I}'_m &\equiv \{m(N+L)+\theta+N,\ldots,m(N+L)+\theta+N+L-1\},\end{aligned}$$

and define the union of all these indexes

$$\begin{aligned}\mathcal{I} &\equiv \bigcup_{m=0}^{M-1}\mathcal{I}_m, \\ \mathcal{I}' &\equiv \bigcup_{m=0}^{M-1}\mathcal{I}'_m.\end{aligned}$$

The observation samples $r(k)$ can now be divided into the samples $r(k),\ k\in\mathcal{I}\cup\mathcal{I}'$, which are pairwise dependent, and the remaining samples $r(k),\ k\notin\mathcal{I}\cup\mathcal{I}'$ which are

independent. Using these properties, the probability density function of the observation can be written as

$$\begin{aligned} f\left(\mathbf{r}\,|\theta,\varepsilon\right) &= \prod_{k\in\mathcal{I}} f\left(r(k),r(k+N)\right) \prod_{k\notin\mathcal{I}} f\left(r(k)\right) = \\ & \prod_{k\in\mathcal{I}} \frac{f\left(r(k),r(k+N)\right)}{f\left(r(k)\right) f\left(r(k+N)\right)} \prod_{k} f\left(r(k)\right). \end{aligned}$$

The last factor is independent of θ and ε and can thus be omitted. The remaining part can be rewritten as

$$\prod_{k\in\mathcal{I}} \frac{f\left(r(k),r(k+N)\right)}{f\left(r(k)\right) f\left(r(k+N)\right)} = \prod_{m=0}^{M-1} \left(\prod_{k\in\mathcal{I}_m} \frac{f\left(r(k),r(k+N)\right)}{f\left(r(k)\right) f\left(r(k+N)\right)} \right).$$

Using the statistical properties of $r(k)$ and following the derivation in and [11] and in Appendix A the log-likelihood function given the observation of M symbols now becomes

$$\begin{aligned} \Lambda\left(\theta,\varepsilon\right) &= \sum_{m=0}^{M-1} \sum_{k=\theta}^{\theta+L-1} \mathrm{Re}\left\{ e^{-j2\pi\varepsilon} r^*(k+m\left(N+L\right)) r(k+m\left(N+L\right)+N) \right\} \\ & \quad -\frac{\rho}{2} \sum_{m=0}^{M-1} \sum_{k=\theta}^{\theta+L-1} \left|r(k+m\left(N+L\right))\right|^2 + \left|r(k+m\left(N+L\right)+N)\right|^2. \end{aligned}$$

C Approximate estimators for channel dispersion

To simplify the time offset estimator in a dispersive channel, we first define the matrix

$$\mathbf{A}\left(\theta\right) = \mathbf{C}_r^{-1}\left(\theta\right) - \left(\mathbf{C}_0 + \sigma_n^2\mathbf{I}\right)^{-1}. \tag{29}$$

Then, combining (26) and (29) we get

$$\widehat{\theta}_{\text{dispersion}} = \arg\max_{\theta} \left\{ -\mathbf{r}^H \mathbf{A}\left(\theta\right)\mathbf{r} - \mathbf{r}^H \left(\mathbf{C}_0 + \sigma_n^2\mathbf{I}\right)^{-1}\mathbf{r} \right\} = \arg\max_{\theta} \left\{ -\mathbf{r}^H \mathbf{A}\left(\theta\right)\mathbf{r} \right\},$$

since the maximizing argument does not depend on $\mathbf{r}^H\left(\mathbf{C}_0 + \sigma_n^2\mathbf{I}\right)^{-1}\mathbf{r}$. Variations in θ shift the elements of $\mathbf{A}\left(\theta\right)$ along the diagonals. The addition of $\mathbf{r}^H\left(\mathbf{C}_0 + \sigma_n^2\mathbf{I}\right)^{-1}\mathbf{r}$ to the loglikelihood function is the equivalent of the addition of $\frac{1}{\sigma_n^2}\frac{1}{\mathrm{SNR}+1}\sum_{k=-\infty}^{\infty}\left|r(k)\right|^2$ in the derivation of the estimator for pulse-shaping (14).

The complexity of the ML estimator is now determined by the properties of matrix $\mathbf{A}\left(\theta\right)$ for different communication scenarios. We have observed that information about θ is largely concentrated in a relatively small section of $\mathbf{A}\left(\theta\right)$. Therefore, we will approximate $\mathbf{A}\left(\theta\right)$ by a matrix $\widetilde{\mathbf{A}}\left(\theta\right)$ whose entries are zero outside the submatrix of size $(N+H+L)\times(N+H+L)$. Although the difference between the matrices may often be quite small, this does not necessarily mean that the estimator performance degradation is negligible. Rather, this is a means of getting a more practical estimator.

We can further simplify our time-offset estimator by noting that

$$\begin{aligned}\arg\max_{\theta}\left\{\Lambda\left(\theta\right)\right\} &\approx \arg\max_{\theta}\left\{-\mathbf{r}^{H}\widetilde{\mathbf{A}}\left(\theta\right)\mathbf{r}\right\} \\ &= \arg\max_{\theta}\left\{-\sum_{i}\sum_{l}\mathbf{r}_{l+\theta}^{*}\widetilde{\mathbf{A}}_{l,l+i}\left(0\right)\mathbf{r}_{l+\theta+i}\right\},\end{aligned}$$

where $\widetilde{\mathbf{A}}\left(0\right)$ is the θ-independent matrix $\widetilde{\mathbf{A}}\left(\theta\right)\Big|_{\theta=0}$. Since all non-zero elements of $\widetilde{\mathbf{A}}\left(0\right)$ are concentrated in an $(N+L+H)\times(N+L+H)$ submatrix there are only $2(N+L+H)-1$ diagonals of $\widetilde{\mathbf{A}}\left(0\right)$ that contain non-zero elements. Denoting the negative of the ith diagonal of $\widetilde{\mathbf{A}}\left(0\right)$ by $h_i(k)$, (27) follows directly.

References

[1] T. Pollet, M. van Bladel, and M. Moeneclaey, 'BER sensitivity of OFDM systems to carrier frequency offset and Wiener phase noise', *IEEE Transactions on Communications*, vol. 43, no. 2/3/4, pp. 191–193, February/March/April 1995.

[2] T. Pollet and M. Moeneclaey, 'Synchronizability of OFDM signals', in *Proceedings of the IEEE Global Telecommunications Conference (GLOBECOM'95)*, Singapore, November 13–17, 1995, pp. 2054–2058.

[3] L. Wei and C. Schlegel, 'Synchronization requirements for multi-user OFDM on satellite mobile and two-path Rayleigh-fading channels', *IEEE Transactions on Communications*, vol. 43, no. 2/3/4, pp. 887–895, February/March/April 1995.

[4] M. Gudmundson and P.-O. Anderson, 'Adjacent channel interference in an OFDM system', in *Proceedings of the IEEE Vehicular Technology Conference (VTC'96)*, Atlanta, USA, April 28– May 1, 1996, pp. 918–922.

[5] F. Classen and H. Meyr, 'Frequency synchronization algorithms for OFDM systems suitable for communication over frequency-selective fading channels', in *Proceedings of the IEEE Vehicular Technology Conference (VTC'94)*, Stockholm, Sweden, June 8–10, 1994, pp. 1655–1659.

[6] W.D. Warner and C. Leung, 'OFDM/FM frame synchronization for mobile radio data communication', *IEEE Transactions on Vehicular Technology*, vol. 42, no. 3, pp. 302–313, August 1993.

[7] P.H. Moose, 'A technique for orthogonal frequency-division multiplexing frequency offset correction', *IEEE Transactions on Communications*, vol. 42, no. 10, pp. 2908–2914, October 1994.

[8] F. Daffara and O. Adami, 'A new frequency detector for orthogonal multicarrier transmission techniques', in *Proceedings of the IEEE Vehicular Technology Conference (VTC'95)*, Chicago, USA, July 25–28, 1995, pp. 804–809.

[9] F. Daffara and A. Chouly, 'Maximum-likelihood frequency detectors for orthogonal multicarrier systems', in *Proceedings of the International Conference on Communications (ICC'93)*, Geneva, Switzerland, May 23–26, 1993, pp. 766–771.

[10] P.J. Tourtier, R. Monnier, and P. Lopez, 'Multicarrier modem for digital HDTV terrestrial broadcasting', *Signal Processing: Image Communications*, vol. 5, no. 5–6, pp. 379–403, December 1993.

[11] J.J. van de Beek, M. Sandell, and P.O. Börjesson, 'ML estimation of time and frequency offset in OFDM systems', *IEEE Transactions on Signal Processing*, vol. 45, no. 7, pp. 1800–1805, July 1997.

[12] J.J. van de Beek, M. Sandell, M. Isaksson, and P.O. Börjesson, 'Low-complex frame synchronization in OFDM systems', in *Proceedings of the International Conference Universal Personal Communications (ICUPC'95)*, Tokyo, Japan, November 6–10, 1995, pp. 982–986.

[13] T. Seki, Y. Sugita, and T. Ishikawa, *OFDM Synchronization Demodulation Unit*, United States Patent, no. 5,602,835, February 1997.

[14] A. Peled and A. Ruiz, 'Frequency domain data transmission using reduced computational complexity algorithms', in *Proceedings of the IEEE International Conference on Acoustics, Speech, and Signal Processing (ICASSP'80)*, Denver, USA, 1980, pp. 964–967.

[15] R. Haas. *Application des Transmissions à Porteuses Multiples aux Communications Radio Mobiles*, Phd. thesis, Ecole National Supérieure des Télécommunications, Paris, France, January 1996. In English

[16] B. Le Floch, M. Alard, and C. Berrou, 'Coded orthogonal frequency-division multiplexing', *Proceedings of the IEEE*, vol. 83, no. 6, pp. 982–996, June 1995.

[17] A. Vahlin and N. Holte, 'Optimal finite duration pulses for OFDM', *IEEE Transactions on Communications*, vol. 44, no. 1, pp. 10–14, January 1996.

[18] D. Landström, J. Martinez Arenas, J.J. van de Beek, P.O. Börjesson, M.-L. Boucheret, and P. Ödling. 'Time and frequency offset estimation in OFDM systems employing pulse shaping', in *Proceedings of the International Conference on Universal Personal Communications (ICUPC'97)*, San Diego, USA, October 1997, pp. 279–283.

[19] J. Martinez Arenas, D. Landström, J.J. van de Beek, P.O. Börjesson, M.-L. Boucheret, and P. Ödling, 'Synchronization in OFDM systems – Sensitivity to the choice of pulse shape', in *Proceedings of the 16th GRETSI Symposium on Signal and Image Processing*, Grenoble, France, September 15–19, 1997, pp. 315-319.

[20] European Telecommunications Standards Institute (ETSI), *OFDMA Evaluation Report – The Multiple Access Scheme Proposal for the UMTS Terrestrial Radio Air*

Interface (UTRA), Technical Document Tdoc 896/97, ETSI SMG meeting no. 24, Madrid, December 1997. Available from the ETSI Secreteriat, F-06921 Sophia Antipolis Cedex, France.

[21] W.C. Jakes, *Microwave Mobile Communications*, Classic Reissue, IEEE Press, Piscataway, New Jersey, 1974.

[22] P. Billingsley, *Probability and Measure*, second edition, John Wiley & Sons, New York, 1986.

[23] G. Malmgren, *Single Frequency Broadcasting Networks*, PhD thesis, Royal Institute of Technology, Stockholm, Sweden, April 1997.

[24] J.J. van de Beek, P.O. Börjesson, M.-L. Boucheret, D. Landström, J. Martinez Arenas, P. Ödling, 'On Synchronization in an OFDM based UMTS proposal', in *Proceedings of the COST 254 workshop 'Emerging Techniques for Communication Terminals'*, Toulouse, France, July 7–9, 1997, pp. 315–320.

[25] European Telecommunications Standards Institute (ETSI), *Radio Broadcasting Systems; Digital Audio Broadcasting (DAB) to Mobile, Portable and Fixed Receivers*, European Telecommunication Standard ETS 300 401, 1st edition, reference DE/JTC-DAB, February 1995. Available from the ETSI Secreteriat, F-06921 Sophia Antipolis Cedex, France.

[26] European Telecommunications Standards Institute (ETSI), *Digital Video Broadcasting (DVB); Framing Structure, Channel Coding and Modulation for Digital Terrestrial Television*, European Telecommunications Standard, ETS 300 744 1st edition, reference DE/JTC-DVB-8, March 1997. Available from the ETSI Secreteriat, F-06921 Sophia Antipolis Cedex, France.

Part 4

This part has been published as

J.J. van de Beek, P.O. Börjesson, M.L. Boucheret, D. Landström, J. Martinez Arenas, P. Ödling, C. Östberg, M. Wahlqvist, and S.K. Wilson, 'A Time and Frequency Synchronization Scheme for Multiuser OFDM', Research Report 1998:06, Division of Signal Processing, Luleå University of Technology, August 1998.

A Time and Frequency Synchronization Scheme for Multiuser OFDM

J.J. van de Beek, P.O. Börjesson, M.-L. Boucheret, D. Landström,
J. Martinez Arenas, P. Ödling, C. Östberg, M. Wahlqvist,
and S.K. Wilson

Abstract – We present a multiuser synchronization scheme tracking the mobile's uplink time and frequency offsets. It is based on a recently developed estimation concept which uses the redundancy introduced by the cyclic prefix. We give performance results of an OFDM-based radio interface based on *universal mobile telecommunication system* (UMTS) parameters. For a UMTS-typical mobile channel environment the performance of a coherent system employing the novel scheme is virtually indistinguishable from the performance of a perfectly synchronized system. In a differentially modulated system synchronization errors decrease the system performance by about 0.7 **dB compared to a perfectly synchronized system.**

1 Introduction

Orthogonal frequency-division multiplexing (OFDM) has been proposed for multiuser systems such as the *universal mobile telecommunication system* (UMTS) [1] and *wireless local area networks* (WLANs) [2]. In multiuser OFDM the orthogonality of the subcarriers facilitates a subcarrier-division of different users, where one OFDM symbol contains many users. In the uplink of such systems users must be aligned in time and frequency to maintain the orthogonality of the subcarriers. How to synchronize different users in the uplink of such a multiuser OFDM-based systems has been unclear so far and is a frequently-raised question.

Multiuser OFDM uplink synchronization is more difficult than synchronization in a broadcast or downlink scenario for a couple of reasons. First, because one OFDM symbol contains many users, the corrections of one user's time and frequency offsets can not be accomplished at the base station receiver, as the correction to one user would misalign other, initially aligned, users. Secondly, estimation of time and frequency offsets is more difficult in such a multiuser system. The performance of the estimator in [3], for example, decreases as the number of subcarriers assigned to each user decreases. The receiver signal-to-noise ratios also vary for different users. Proper synchronization is, however, necessary to keep the orthogonality of the users, which is essential for reliable transmission. This paper describes a novel synchronization scheme for tracking in the uplink of multiuser OFDM systems. Acquisition of the symbol clock and carrier frequency is discussed in [4]. Our scheme is generally applicable to OFDM-based systems where

users are separated in bands of adjacent subcarriers. The work presented in this paper was motivated by the UMTS proposal [1]. We evaluate the scheme for a target system similar to this proposal.

Symbol time and carrier frequency offset estimation methods for OFDM transmission systems have been presented in a number of contributions, see, *e.g.*, [3,5,6]. Most of these offset estimators are explicitly evaluated for a broadcast or downlink scenario. Multiuser synchronization provides some extra challenges for the estimators not addressed in these papers. Our synchronization scheme contains an implementable time- and frequency offset estimator structure based on results in [3]. This estimator uses the redundancy in the received signal due to the cyclic prefix. We adapt this estimator to properties of the multiuser system and the fading channel. The estimates of the users' offsets are returned on a downlink control channel to the mobile transmitters which adapt their clocks and oscillators to the free-running reference clocks and oscillators at the base station.

Whereas frequency requirements on the estimator performance are tight (see, *e.g.*, [7]), the time offset requirements are relaxed by an additional extension of the cyclic prefix. If a time offset error is within the range of this extension, a channel estimation algorithm, required for coherent detection, acts as a fine time synchronizer. In differential systems which do not employ channel estimation and equalization this extra extension provides some robustness, too. The absence of a channel equalizer with its fine synchronizing capabilities in these systems, however, causes a small performance degradation compared to coherent systems. We show by simulation that the time and frequency offset estimator satisfies both the tight frequency requirements and the coarse time requirements.

This paper is organized as follows. We first describe the multiuser OFDM scenario in Section 2. In particular we focus on the multiple access schemes OFDM offers. In Section 3 we focus on a multiple access scheme where users are divided across the subcarriers. We discuss the system sensitivity to time and frequency offsets and present the novel synchronization scheme including the offset estimator at the base station. In Section 4 we then present simulation results illustrating the performance of the offset estimation algorithm and the system performance in terms of symbol error-rate and we conclude this paper with Section 5 summarizing the main results.

2 Multiuser OFDM

2.1 OFDM transmission and multiple access

In an OFDM transmission system the available spectrum is accessed by a large number of subcarriers. Data symbols are efficiently modulated on these carriers by means of a *fast Fourier transform* (FFT) [8], both in the uplink and the downlink. We assume a frequency division duplex scheme and concentrate on the uplink frequency band. In a multiuser mobile environment an OFDM scheme has two main advantages. First, the receiver does not require an adaptive time-domain equalizer if a cyclic prefix is properly used and the channel does not change much during one OFDM symbol [9]. Secondly, dynamic channel assignment across the spectrum is straightforward as each user can conveniently access all subcarriers by the FFT-implemented modulation.

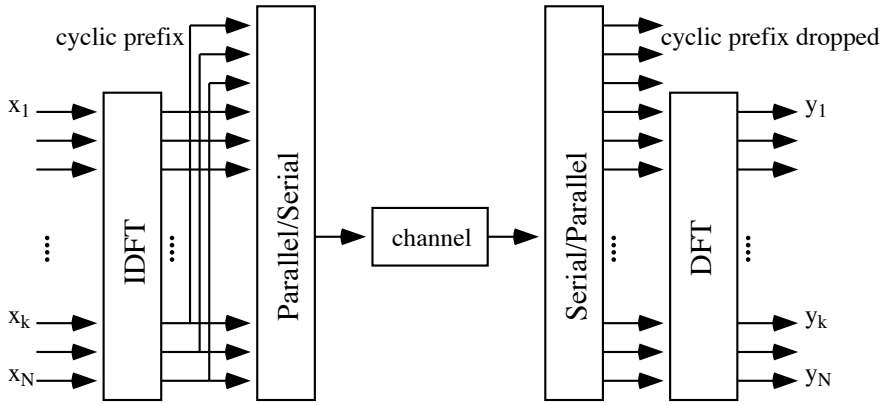

Figure 1: An OFDM system.

Figure 1 illustrates the OFDM transmission technique. The complex data symbols x_k are coherently modulated on N subcarriers by an inverse discrete Fourier transform (IDFT) and the last L samples are copied and put as a preamble (cyclic prefix) to form the OFDM symbol. This data vector is serially transmitted over a discrete-time channel, whose impulse response is shorter than L samples. At the receiver, the cyclic prefix is removed and the signal r_k is demodulated with a discrete Fourier transform (DFT). In OFDM systems employing this cyclic prefix the frequency-selective channel distortion appears as a multiplicative distortion of the transmitted data symbols [8] and the received data symbol during the nth OFDM symbol at the kth subcarrier becomes

$$y_{k,n} = h_{k,n}x_{k,n} + n_{k,n} \qquad k = 0, \ldots, N-1, \qquad n = -\infty, \ldots, \infty, \tag{1}$$

where $h_{k,n}$ is the channel attenuation at the kth subcarrier during the nth OFDM symbol and $n_{k,n}$ is the *additive white Gaussian noise* (AWGN).

Data symbols can modulate the subcarriers coherently or differentially. Proposal [1] suggests a differential scheme across the subcarriers in an OFDM symbol (a coherent extension is suggested for future extensions). In Section 4 we evaluate our synchronization scheme for both such a differential and a coherent modulation scheme. For coherent modulation, the base station receiver must estimate and compensate for the channel attenuations. For this purpose pilot symbols are transmitted. Our simulations confirm that channel equalization can act as a fine-tuning synchronizer [10, 11]. This property makes coherent systems less sensitive to synchronization errors than differential systems.

Because OFDM separates symbols in both time and frequency, it allows for a number of multiple access schemes. First, in a *time-division multiple access* (TDMA) structure users are assigned entire OFDM symbols, and they share the channel by a time-slot structure. Secondly, the large number of subcarriers allows for a *frequency-division multiple access* (FDMA) -like multiple access scheme where different users are assigned different subcarriers. Since OFDM subcarriers spectrally overlap this scheme is not true FDMA. However, for convenience we will use FDMA for OFDM-subcarrier divided access schemes. Finally, in [12] OFDM is combined with a code-division multiple access scheme. A TDMA scheme is proposed for the European WLAN standard and an FDMA scheme combined with a time slot structure and a frequency-hopping scheme was proposed for

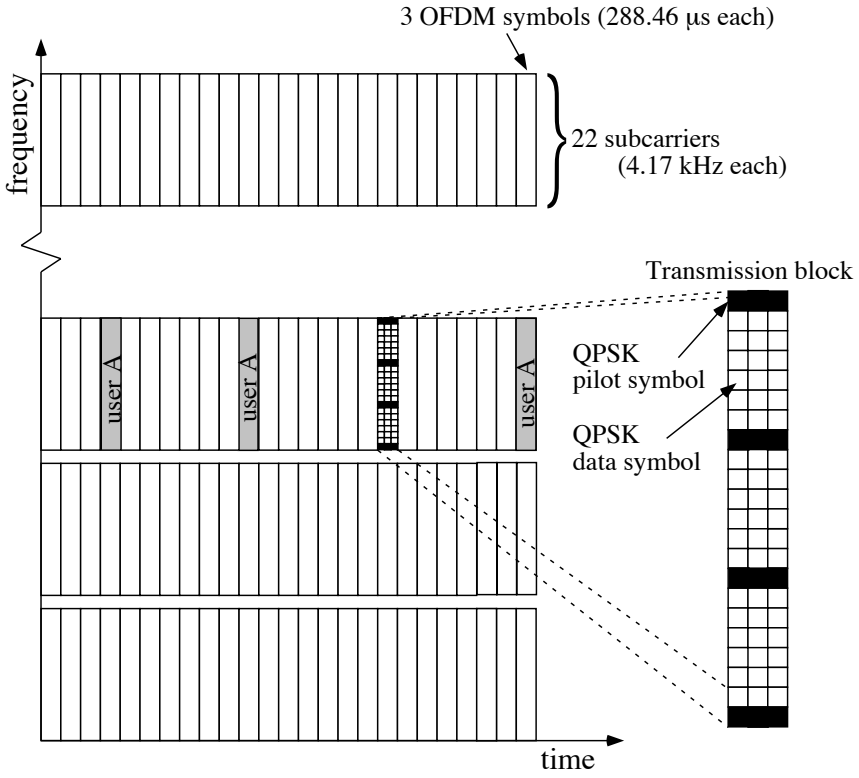

Figure 2: Time-frequency grid for the UMTS scenario. The users are assigned transmission blocks consisting of 22 adjacent subcarriers and 3 adjacent OFDM symbols. Each transmission block contains pilot symbols supporting the channel estimation.

the UMTS radio interface. In Section 4 we evaluate our synchronization scheme for such a hybrid TDMA/FDMA multiple access scheme.

Figure 2 illustrates this access scheme. The available spectrum is subdivided in bands of adjacent subcarriers (FDMA). Within each of these bands a TDMA scheme is applied. Users are thus separated both in frequency (each user is allocated to a particular subband) and in time (each user is to allocated a particular time slot). In our target system the minimum access entity is 22 adjacent subcarriers during 3 consecutive OFDM symbols, see Figure 2, as will be explained in Section 4.

2.2 Synchronization Requirements

Accurate demodulation and detection of an OFDM signal requires subcarrier orthogonality. Variations of the carrier oscillator, the sample clock or the symbol clock affect the orthogonality of the system, see [7, 13, 14]. Whereas sample clock variations below 50 ppm have little effect on the system performance [13], symbol time and frequency offsets may cause *intersymbol interference* (ISI) and *intercarrier interference* (ICI) [7, 14] and must usually be counteracted. Therefore, we assume that the sample clocks of the users and the basestation are identical (no offset effects) and we focus on a frequency offset and a symbol time offset. We separately consider their effects on the system performance.

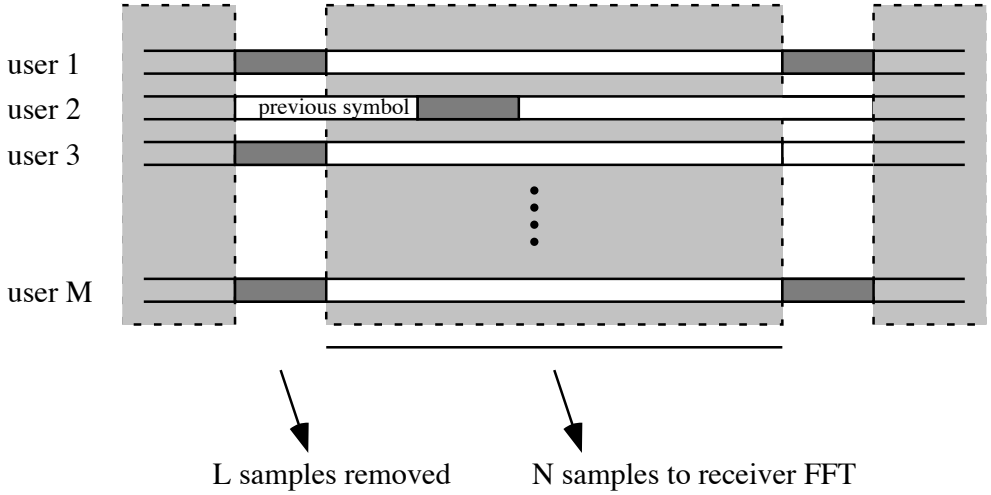

Figure 3: How one user being misaligned in time with the other users affects the receiver demodulation.

The effect of a symbol time offset is the following (assume first perfect carrier frequency synchronization). The demodulator FFT at the base station processes blocks of N samples in the FFT. If different users' transmitted signals are not time-aligned, ISI and ICI (or in a multiuser system: interuser interference) appear at the FFT outputs. Figure 3 illustrates this interference caused by one user being misaligned with the others. Note first that since we assume perfect sample clocks, such an offset is modeled by an integer-valued number of samples. Note also that the receiver at the base station may identify (and as we will see estimate) one user's time offset, but has no simple means to counteract this offset without becoming misaligned with other users. This is the particular synchronization problem distinguishing broadcast and multiuser synchronization. We focus on the unknown integer-valued time offset θ of a user's symbol clock: that is, how much this user is misaligned with the block of N samples the receiver processes in the FFT.

Consider a system in which the cyclic prefix is longer than the length of the channel impulse response. Such extra overhead provides robustness against symbol time offsets: as long as a symbol time offset is shorter than the difference between the length of the cyclic prefix and the length of the channel impulse response, the cyclic appearance of the OFDM symbol is preserved and the offset appears as a linear phase across the subcarrier FFT outputs [15]. In a coherent system this effect is identified by the channel estimator, which does not distinguish between phase shifts introduced by the radio channel and those introduced by symbol timing delays [14]. Therefore, the channel equalizer provides the *fine* synchronization, see also [10]. The requirements on the *coarse* synchronizer in a coherent system are thus determined by the number of samples the cyclic prefix exceeds the length of the channel impulse response. This provides a system designer with a trade-off tool: by sacrificing data rate a longer cyclic prefix relaxes the requirements of the symbol synchronizer.

A carrier frequency offset (assuming perfect symbol synchronization) causes a loss of orthogonality between the subcarriers resulting in ICI [7,16]. Since the system bandwidth

is small compared to the carrier frequency, we assume that each subcarrier is equally affected by a carrier frequency offset. In [16] it is shown that the effect of a frequency offset is threefold. First, the amplitudes of the FFT outputs are reduced. Secondly, as with symbol time offsets, one user's frequency misalignment with the base station causes the subcarriers to loose their orthogonality resulting in ICI. These first two effects cause a loss of the effective SNR and are hard to counteract.

A third effect of a frequency offset is a common rotation of the subcarriers [11]. This effect will be recognized by a channel estimator, which does not distinguish between phase offsets caused by the channel and those caused by a frequency offset. Thus a channel equalizer appears also to have *fine* frequency synchronization capabilities, see also [11]. The analysis of multiuser OFDM systems in [7] shows that a frequency accuracy of 1%–2% of the inter-carrier spacing is necessary to obtain a signal-to-interference ratio of 30 dB or higher. A frequency offset may be estimated at the receiver. However, as for symbol time offsets, an adjustment of the receiver base station oscillator would cause the misalignment in frequency with other users.

3 A multiuser synchronization scheme

Synchronization in broadcast OFDM systems has been investigated in for instance [3, 5] and is in most cases identified with the actual estimation of the offsets. Although synchronization in the downlink yields some difficulties, the uplink in a multiuser system is a more challenging task. In this Section we propose a tracking scheme based on a multiuser time and frequency offset estimator and a downlink control channel on which estimates are fed back to the mobiles.

3.1 Base station receiver structure and control channel

In Figure 4 the receiver structure of the base station is shown. It consists of two parts. In one part the cyclic prefix is removed and the data are demodulated by means of an FFT. In our target system, the demodulated symbols are equalized by a 1-tap channel equalizer and fed the detector. The channel equalizer also compensates for small time offsets and some of the effects of a frequency offset as discussed above. In systems employing convolutional coding the channel estimates may also be used by the decoder for metric calculation. The second part of the base station receiver serves to track the users' time and frequency offsets. The received sampled baseband signal is fed into a bank of filters, each selecting the frequencies of one band of adjacent subcarriers. This filterbank may be efficiently implemented by means of polyphase filters. Depending on the filter characteristics a guardcarrier may be used between adjacent frequency bands. Each filter output roughly represents one user's signal from which time- and frequency offsets can be estimated.

The important difference between the broadcast and multiuser synchronization is how symbol and frequency synchronization is accomplished. In a broadcast or downlink scenario offsets are estimated by the mobile receiver. These offset estimates then control the adjustments of the local symbol clock and demodulation oscillator. Synchronization

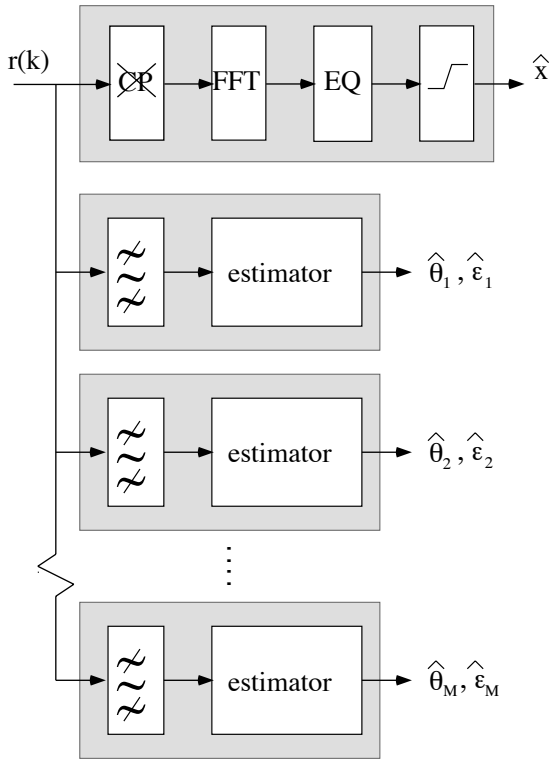

Figure 4: The structure of the receiver at the base station. One path serves the detection of the data, while other paths estimate the time and frequency offsets for each user.

thus takes place at the receiver. In the uplink, on the other hand, time and frequency offset *estimation* is performed in the base station but the clock and oscillator *adjustments* are made in the user's transmitter. Since all users must arrive at the base station aligned in time and frequency in order to maintain the orthogonality between the subcarriers, all users adapt to the base station's receiver clock and oscillator.

Therefore, in our scheme for every connected user a control channel is embedded in the downlink on which control information based on the offset estimates is transmitted back to the user. With the aid of these control parameters the user aligns its transmitted signal to the receiver reference symbol clock and to the receiver oscillator. The control channel is embedded in the downlink frequency band, which may have a similar multiuser structure as the uplink band and is set up during the initial phase of the connection. Apart from offset estimates other control parameters for one user include, for instance, which time slots and subband must be used for the uplink transmission, and which transmission power must be applied. Successful tracking synchronization of the user thus relies on the control channel.

3.2 Time and frequency offset estimation

The estimation of time and frequency offsets is addressed in a number of contributions, *e.g.*, [3, 5, 6, 16]. As a key part of our synchronization scheme, we propose an estimator based on the concept in [3] which works without the aid of pilot symbols and which is

independent of the modulation of the carriers. In this concept statistical redundancy in the received signal, introduced by the cyclic prefix, provides the information about the offsets. Our estimator modifies this concept to suit the multiuser and fading channel environment.

Consider one OFDM symbol received by the base station. Assume that the N subcarriers constituting this symbol are subdivided in M bands of subcarriers, the indexes of which we collect in the set $\mathcal{M}_m$. One transmitted OFDM symbol in the mth band of subcarriers is

$$s_m(t) = \sum_{k \in \mathcal{M}_m} x_k e^{j2\pi kt/NT}, \qquad -T_g < t < NT, \tag{2}$$

where NT is the duration of the OFDM symbol without the cyclic prefix and T_g is the length of the cyclic prefix. We associate with the mth transmitted signal a time offset θ_m relative to the receiver symbol clock and a frequency offset ε_m relative to the receiver demodulation frequency. We consider at the base station the sampled received OFDM signal and model the received signal as

$$r_m(k) = \sum_{m=0}^{M-1} s_m(k - \theta_m) e^{j2\pi\varepsilon_m k/N} + n(k), \tag{3}$$

where the $s_m(k)$ is the transmitted signal (2). The above model focuses on the frequency- or subband division property of the multiple-access scheme as this property significantly affects the offset estimation. The receiver offset estimator addresses the time-division property of our target system by applying one estimator to every time slot.

The bank of bandpass filters in the receiver, discussed in Section 3.1 separates the users' signals. Note that the signals $r_m(k)$ spectrally overlap and that even the use of ideal brickwall filters in the filterbank does not perfectly separate these bands. Perfect separation of the users typically is accomplished by the removal of the cyclic prefix and the demodulation by the FFT. Such separation, however, removes the redundancy which is needed by the offset estimation in our synchronization scheme. Therefore, we use bandpass filters to separate the subcarriers groupings. We will see that the filters separate different users' signals sufficiently for our estimation purpose.

We apply the following estimator to the outputs of the mth filter (dropping the subscript m) [3]:

$$\begin{aligned} \widehat{\theta} &= \arg\max_{\theta} \left\{ |\gamma(\theta)| - \rho\Phi(\theta) \right\}, \\ \widehat{\varepsilon} &= \frac{-1}{2\pi} \angle\gamma(\widehat{\theta}), \end{aligned} \tag{4}$$

where

$$\gamma(\theta) = \sum_{k=\theta}^{\theta+L-1} r^*(k) r(k+N), \tag{5}$$

$$\Phi(\theta) = \frac{1}{2} \sum_{k=\theta}^{\theta+L-1} |r(k)|^2 + |r(k+N)|^2, \tag{6}$$

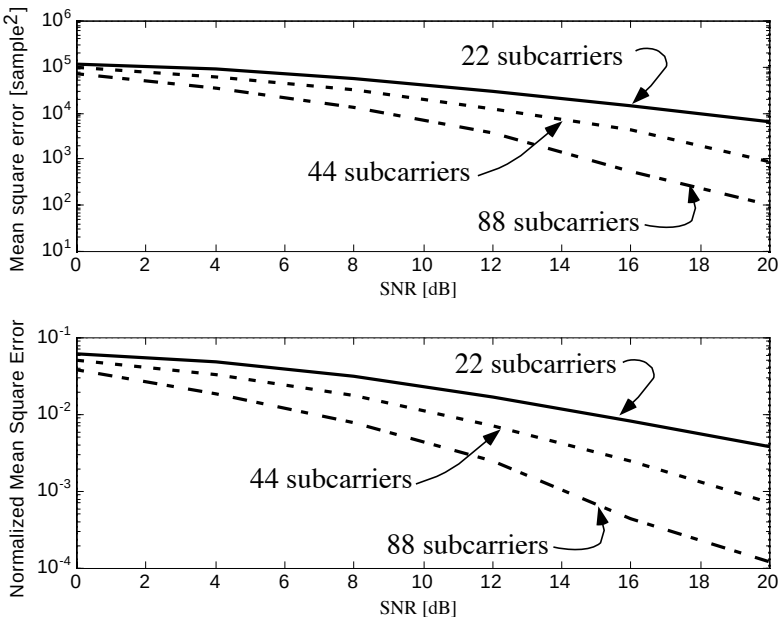

Figure 5: The effect the number of the number of subcarriers in one subband on the mean-squared error of the time offset estimator (top) and the frequency offset estimator (bottom). The target system consists of 1024 subcarriers and the subbands consist of 22 subcarriers (solid), 44 subcarriers (dashed), and 88 subcarriers (dash-dotted).

and where $\rho = \frac{\mathrm{SNR}}{\mathrm{SNR}+1}$. Estimator (4) exploits the correlation introduced by the cyclic prefix to estimate the offsets, see [3]. Its strength is that it is independent of the modulation and that it does not need pilot symbols. It is a one-shot estimator in the sense that the estimates are based on the observation of one OFDM symbol.

This estimator is shown to be the joint *Maximum Likelihood* (ML) estimate of θ and ε [3] if the output of each filter can be written as

$$r(k) = \tilde{s}(k-\theta)e^{j2\pi\varepsilon k/N} + n(k), \tag{7}$$

where the samples $\tilde{s}(k)$ are Gaussian distributed and uncorrelated except for the pairs of identical samples contained in the cyclic prefix. In our multiuser scenario the mth transmitted signal is, however, a narrowband signal and thus does not have this simple correlation property. Moreover, the filters do not perfectly separate the various users, and the filter outputs contain contributions from other subbands with other time and frequency offsets. The performance of estimator (4) in our scenario is shown in Figure 5. This figure shows the mean-squared error of the estimates (4) for our target system with three different sizes of the subbands: 22, 44, an 88 adjacent subcarriers per subband. Note that the estimator's performance is very sensitive to the number of subcarriers in one subband. Typically in a pure time-division multiple access scenario (only one subband consisting of all subcarriers) the estimator (4) can be applied directly. However, in a system with many narrow subbands the performance of the estimator does not meet the requirements.

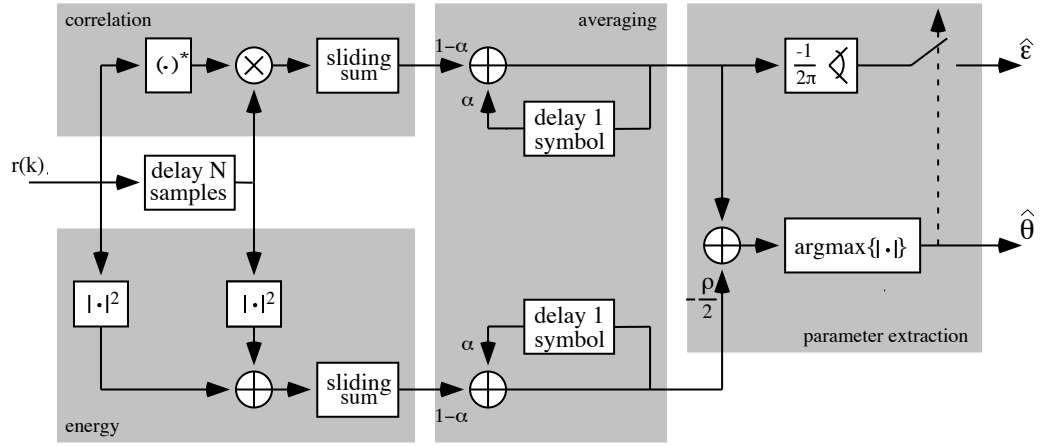

Figure 6: The structure of the time and frequency offset estimator

We now assume that time and frequency offsets do not change very much between two clock or oscillator updates. The characteristics of the clocks and oscillators may affect the choice of the update frequency in a system. We generalize estimator (4) and consider the statistics

$$\begin{aligned} \overline{\gamma}_t(\theta) &= \alpha\overline{\gamma}_{t-1}(\theta) + (1-\alpha)\gamma_t(\theta), \\ \overline{\Phi}_t(\theta) &= \alpha\overline{\Phi}_{t-1}(\theta) + (1-\alpha)\Phi_t(\theta), \end{aligned} \tag{8}$$

where $0 \leq \alpha \leq 1$ is a forgetting factor and $\gamma_t(\theta)$ and $\Phi_t(\theta)$ are the one-shot statistics (5). For $\alpha = 0$ this estimator is identical to (5), but for other α it exploits information about the offsets carried by past redundancies. In the rest of this paper we show results for $\alpha = 0.75$. Based on this statistic and following estimator structure (4) we use the estimator

$$\begin{aligned} \widehat{\theta}_t &= \arg\max\left\{|\overline{\gamma}_t(\theta)| + \rho\overline{\Phi}_t(\theta)\right\}, \\ \widehat{\varepsilon}_t &= \frac{-1}{2\pi}\angle\overline{\gamma}(\widehat{\theta}_t). \end{aligned} \tag{9}$$

The exponential weighting is suitable in environments where θ and ε vary slowly. Figure 6 shows the structure of the estimator. Estimator (10) weights the one-symbol statistics $\overline{\gamma}_t(\theta)$ and $\overline{\Phi}_t(\theta)$ exponentially. Such an IIR implementation of the averaging requires the receiver to store only the joint statistic $\gamma_t(\theta)$ and $\Phi_t(\theta)$.

4 Simulation results

4.1 Multiuser scenario

Table 1 specifies the transmission parameters of our target multiuser system based on [1], which we will use to evaluate our synchronization scheme. UMTS has been assigned frequencies in the 2.2 GHz band. The uplink and downlink use different frequency bands, each 4.27 MHz wide, containing 1024 subcarriers. The intercarrier spacing is thus 4.17

Center frequency	2.2 GHz
Uplink / Downlink bandwidth	4.27 MHz / 4.27 MHz
Intercarrier spacing	4.17 kHz
Symbol length	240 μsec (1024 samples)
Cyclic prefix	48 μsec (205 samples)

Table 1: Transmission characteristics of the system [1]

Transmission block	22 subcarriers $\times$ 3 symbols
Data rate	multiples of 5.7 kbits/second
Minimum data rate (Speech service)	17.1 kbits/second
Maximum data rate	5 Mbits/second

Table 2: Multiple access characteristics of the system [1]

kHz and the symbol length (without cyclic prefix) is 240 μsec. In this system the requirement of a maximum frequency offset of 1-2% of the intercarrier spacing becomes about 50 Hz. Each symbol is cyclically extended by 48 μsec (205 samples), such that the total symbol length becomes 288 μsec. The length of the cyclic prefix is sufficiently long to provide immunity against channel dispersion.

The prefix accommodates both delay spread of the channel and offsets of the symbol clock. As long as the accumulated effect of a symbol clock offset and a far echo in the channel impulse response does not exceed 48 μsec, the system performance is equal to a system with a perfect symbol clock. As discussed in Section 2.2 the cyclic prefix thus provides robustness to small symbol time offsets. For example, if the channel impulse response contains echoes up to 34 μsec, the symbol synchronizer must provide synchronization to within the remaining 14 μsec (60 samples). In Section 4 we will see that our synchronization scheme rarely exceeds these 14 μsec (60 samples). Therefore, the system accommodates channel impulse responses with echoes up to 34 μsec.

Table 2 specifies and Figure 2 illustrates the multiple access characteristics of our target system [1], already briefly discussed in Section 2. As a minimal access entity, every user is assigned 22 adjacent subcarriers during 3 consecutive OFDM symbols. We will refer to such an entity as a *transmission block*. In between two subbands are two guard carriers which are not modulated.

For a typical low-rate circuit service, such as a speech service, 3 such transmission blocks are transmitted every 18.47 msec. For higher data rates, users would typically request more transmission blocks. The proposal [1] provides more frequency diversity via a slow frequency-hopping system which we in our simulations do not regard. The proposed synchronization scheme would benefit from this hopping scheme.

We evaluate the synchronization scheme for two types of modulation. First, a differential QPSK system modulates the data symbols differentially across the subcarriers. Therefore 21 information symbols are transmitted in each OFDM symbol in a transmission block. Secondly, a coherent QPSK system is simulated, in which the base station uses a channel estimator and a channel equalizer to correct for the multiplicative channel distortion of the data symbols. The pilot positions for channel estimation are shown in

tap	relative delay (nsec)	average power (dB)
1	0	0
2	310	−1.0
3	710	−9.0
4	1090	−10.0
5	1730	−15.0
6	2510	−20.0

Table 3: Characteristics of the ETSI 'Vehicular A' channel environment

Figure 2. Each OFDM symbol in a transmission block contains 22 QPSK symbols, 4 of which are known pilot symbols. This modulation system differs from the proposal [1] which employs DQPSK.

For the coherent system simulations the base station channel estimator $\widehat{h}_k$ is the following. We base our estimator on the 4 received data symbols at the pilot positions which we collect in the 4×1 vector $\mathbf{y}_P$. The base station then estimates the channel attenuations with the linear estimator

$$\widehat{\mathbf{h}} = \mathbf{R}_{hy_P}\mathbf{R}^{-1}_{y_Py_P}\mathbf{y}_P \tag{10}$$

where $\mathbf{R}_{hy_P}$ is the cross-correlation matrix between the channel $\mathbf{h}$ and the received data $\mathbf{y}_P$, and $\mathbf{R}_{y_Py_P}$ is the auto-correlation matrix of the received pilot data. Since we do not know these channel correlations, we design generic matrices based on the following correlation properties: The assumed channel delay spread is exponentially decaying with an rms-value of 10 samples. The channel correlation matrices for this channel are given in [17]. The correlation matrix is designed for an assumed SNR of 20 dB, see [17].

4.2 Channel model

We have evaluated the synchronization scheme in one of the channel environments defined by ETSI for the evaluation of radio interface proposals. The time-varying channel impulse response for these models can be described by

$$h(\tau, t) = \sum_i \alpha_i(t)\delta(\tau - \tau_i). \tag{11}$$

This equation defines the channel impulse response at time t as a function of the lag τ. In this paper we will evaluate our synchronization algorithm for the choices of α_i and τ_i associated with the Vehicular–A channel environment [18]. The channel taps $\alpha_i(t)$ are complex independent stochastic variables, fading with a Jakes' Doppler spectrum [19], with a maximum Doppler frequency of 240 Hz, reflecting a mobile speed of approximately 120 km/h (and scatterers uniformly distributed around the mobile). The real-valued τ_i and the variance of the complex-valued α_i are given in [18] and repeated in Table 3.

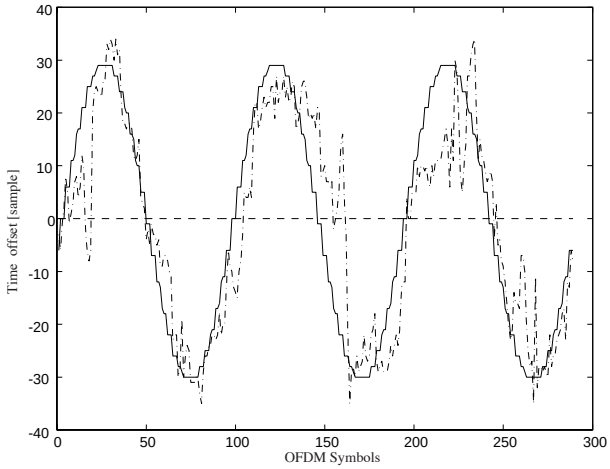

Figure 7: Timing offsets versus time. The true timing offset (solid) and the estimated timing offset (dashed).

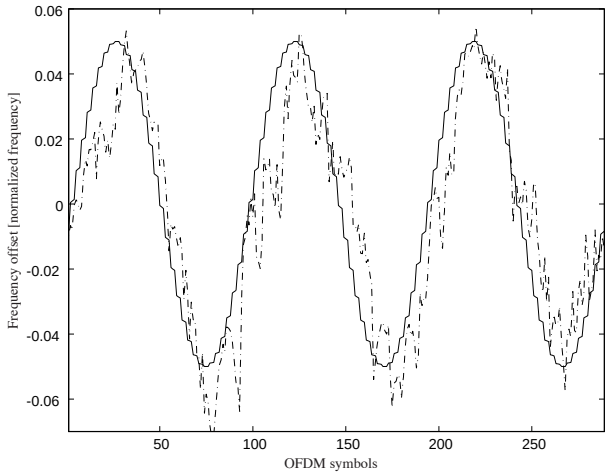

Figure 8: Frequency offsets versus time. The true frequency offset (solid) and the estimated frequency offset (dashed).

4.3 Estimator performance

In our synchronization scheme we assume that the users' signals arrive at the base station with equal power, that is, we assume ideal power control. The characteristics of the filters determine the sensitivity of our estimator in systems with large power variations between users. The estimates $\widehat{\theta}_t$ and $\widehat{\varepsilon}_t$ are fed back to the transmitter 10 times per second. The system performance is determined by both the performance of the estimator and the characteristics of the feedback scheme. We first investigate the performance of the joint time and frequency offset estimator (10) employed in the base station and then we present simulation results for the system performance in Section 4. We consider the low-rate service with 3 transmission blocks each 18.47 ms.

We evaluate the tracking performance of the estimators. Figures 7 and 8 show the estimates versus time. The time axis in the figures shows the index of the transmitted

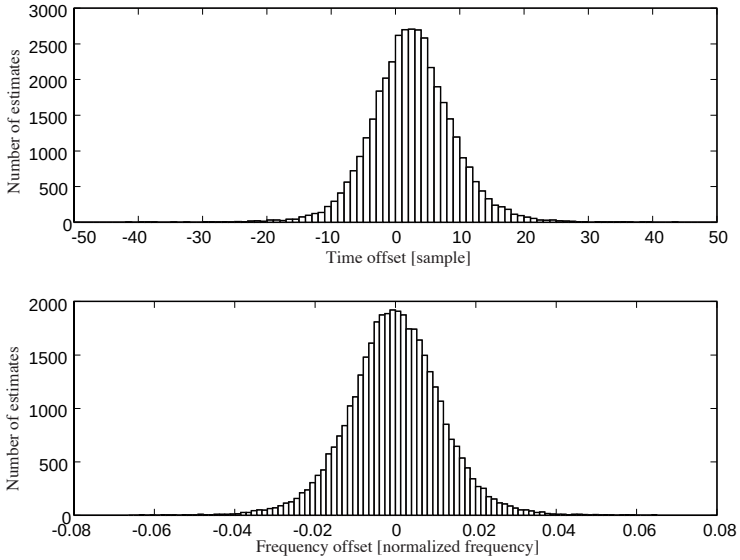

Figure 9: The distribution of the time and frequency offset estimates.

SNR = 10 dB	
$\sqrt{E\left\{\left\|\theta-\widehat{\theta}\right\|^2\right\}}$	6.41
$\left\|\theta-\widehat{\theta}\right\| > 20$ samples	0.98 %
$\left\|\theta-\widehat{\theta}\right\| > 30$ samples	0.08 %
$\left\|\theta-\widehat{\theta}\right\| > 40$ samples	0.01 %
$\sqrt{E\left\{\left\|\varepsilon-\widehat{\varepsilon}\right\|^2\right\}}$	1.17 %
$\left\|\varepsilon-\widehat{\varepsilon}\right\| > 1$ %	35.22 %
$\left\|\varepsilon-\widehat{\varepsilon}\right\| > 2$ %	8.32 %
$\left\|\varepsilon-\widehat{\varepsilon}\right\| > 3$ %	1.96 %

Table 4: Performance of the time and frequency offset estimates

OFDM symbol for one user. The true time offset follows a sinusoid with 30 samples amplitude and a period of 96 OFDM symbols. Such time offset variations exceed practical offset variations a base station in our UMTS scenario would experience. The purpose of these curves is to show the tracking ability of the estimator. The true frequency offsets also follow a sinusoid with an amplitude of 5% of the intercarrier spacing. As for the time offsets, such frequency drifts exceed practical drifts and show here the frequency estimator's tracking ability.

The distribution of the estimation error for this run is shown in Figure 9 while Table 4, shows the estimator standard deviations. Of special interest is the percentage of the time offset estimates which fall outside a particular interval. This percentage together with the length of the channel dispersion shows how often ISI will occur.

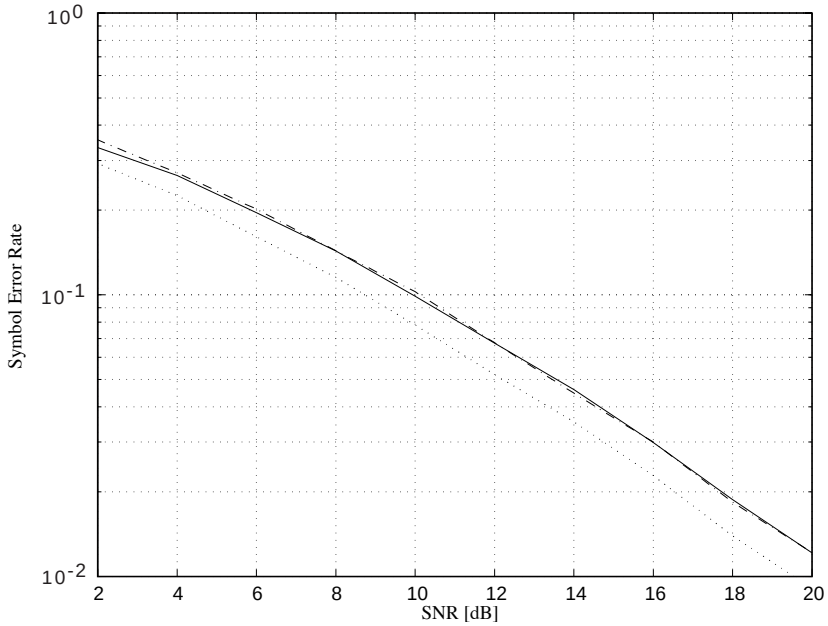

Figure 10: The uncoded symbol error rate of the UMTS scenario with QPSK modulated subcarriers and channel estimation/equalization. System performance without synchronization errors and known channel (dotted); system performance without synchronization errors but with channel estimation (solid); system performance for the proposed synchronization scheme (dash-dotted). In the simulations none of the time offset estimates that were fed back to the mobile caused ISI.

4.4 System performance

In Section 3 we have proposed a synchronization scheme and in Section 3 we have proposed an estimator of the user's time and frequency offset to the base station. Here we evaluate the uplink synchronization performance of the UMTS proposal employing the proposed synchronization scheme in the UMTS scenario.

Figure 10 shows the uncoded symbol error rate (SER) of the system (employing QPSK on each subcarrier) for a system with perfect synchronization and ideal channel knowledge in the receiver equalizer as well as the SER for a system employing the channel estimator (10) in the base station receiver and fed back estimates of the time and frequency offsets (using (10)) in the transmitter. In the latter case we have assumed a clock drift of 10 ppm and estimates are fed back to the mobile 10 times per second. A loss with respect to the perfectly synchronized system with channel estimation is indistinguishable because the channel estimator compensates for parts of the time and frequency offsets. In the simulations none of the time offset estimates that were fed back to the mobile caused ISI. For long runs there may be instances when the time offset and the length of the channel impulse response exceed the cyclic prefix and ISI will occur.

Figure 11 shows the same curves for a system employing differential PSK across the tones. In this scenario no channel estimation is performed. Besides the 3 dB loss in SNR compared to the coherent QPSK modulation with perfect channel knowledge, the tracking loop now results in a performance decrease because of time offsets. In this case

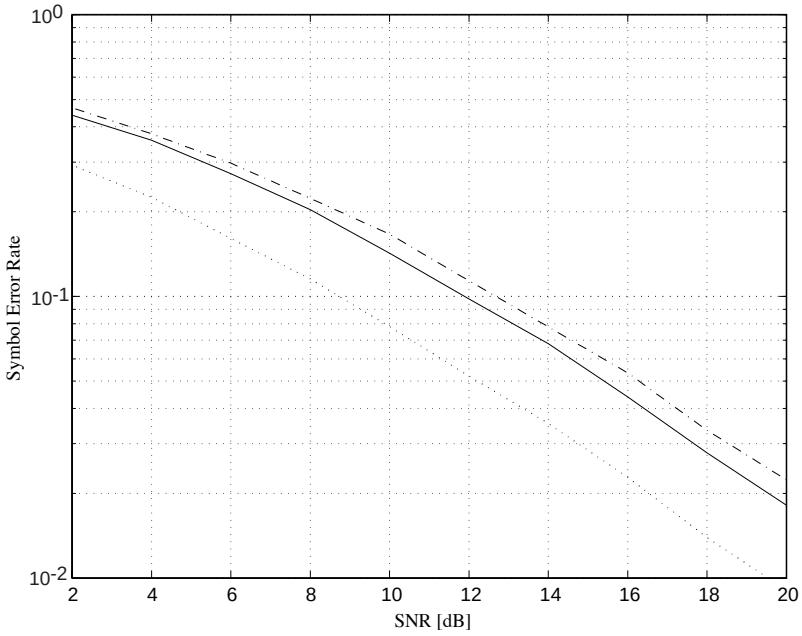

Figure 11: The uncoded symbol error rate of the UMTS scenario with DPSK modulated subcarriers. System performance without synchronization errors (solid); system performance for the proposed synchronization scheme (dash-dotted); system performance for the system with QPSK modulated subcarriers without synchronization errors and known channel (dotted). In the simulations none of the time offset estimates that were fed back to the mobile caused ISI.

the effects of a time offset, which appears as a linear phase distortion across the tones, are not compensated for by a channel estimator.

5 Summary and conclusions

We have shown a way to track different users in the multiuser uplink of an OFDM-based system. Time and frequency offsets are estimated at the base station. Control information, based on these estimates, is returned on a downlink control channel to the user, who adjusts its symbol clock and its local oscillator accordingly. The estimation is done by exploiting statistical redundancy due to the presence of the cyclic prefix.

We have illustrated the synchronization scheme with parameter choices and simulation results for the proposal [1] and show that the synchronization requirements are satisfied. Simulations show that the performance of a coherently modulated system employing our synchronization scheme is not visibly decreased compared to the performance of a system without time and frequency offsets. In a differentially modulated system the effect of the time errors on the system performance decreases the performance by about 0.7 dB compared to a system without time and frequency offsets.

References

[1] Concept group Beta, 'OFDMA Evaluation Report – The multiple access proposal for the UMTS Terrestrial Radio Air Interface (UTRA)', Tdoc/SMG 896/97, ETSI SMG meeting no. 24, Madrid, Spain, December 1997.

[2] 'Broadband Radio Access Networks (BRAN); 'Inventory of broadband radio technologies and techniques', ETSI Technical Report, DTR/BRAN-030001, 1998.

[3] J.J. van de Beek, M. Sandell, and P.O. Börjesson, 'ML estimation of timing and frequency offset in OFDM systems', *IEEE Transactions on Signal Processing*, vol. 45, no. 7, pp. 1800–1805, July 1997.

[4] T.M. Schmidl, '*Synchronization algorithms for wireless data transmission using orthogonal frequency division multiplexing (OFDM)*', PhD thesis, Stanford University, CA, June 1997.

[5] W.D. Warner and C. Leung, 'OFDM/FM frame synchronization for mobile radio data communication', *IEEE Transactions on Vehicular Technology*, vol. 42, no. 3, pp. 302–313, August 1993.

[6] P.J. Tourtier, R. Monnier, and P. Lopez, 'Multicarrier modem for digital HDTV terrestrial broadcasting', *Signal Processing: Image Communications*, vol. 5, no. 5–6, pp. 379–403, December 1993.

[7] L. Wei and C. Schlegel, 'Synchronization requirements for multi-user OFDM on satellite mobile and two-path Rayleigh-fading channels', *IEEE Transactions on Communications*, vol. 43, np. 2/3/4, pp. 887–895, February/March/April 1995.

[8] J.A.C. Bingham, 'Multicarrier modulation for data transmission: An idea whose time has come', *IEEE Communications Magazine*, vol. 28, no. 5, pp. 5–14, May 1990.

[9] A. Peled and A. Ruiz, 'Frequency domain data transmission using reduced computational complexity algorithms', in *Proceedings of the IEEE International Conference on Acoustics, Speech, and Signal Processing (ICASSP'80)*, Denver, USA, 1980, pp. 964–967.

[10] L. Hazy and M. El-Tanany, 'Synchronization of OFDM systems over frequency selective fading channels', in *Proceedings of the Vehicular Technology Conference (VTC'97)*, Phoenix, USA, May 1997, pp. 2094–2098.

[11] A. Garcia Armada and M. Calvo, 'Phase Noise and Sub-Carrier Spacing Effects on the Performance of an OFDM Communication System', *IEEE Communications Letters*, vol. 2, no. 1, pp. 11-13, January 1998.

[12] S. Hara and R. Prasad, 'Overview of multicarrier CDMA', *IEEE Communications Magazine*, vol. 35, no. 12, pp. 126–133, December 1997.

[13] T. Pollet, P. Spruyt, and M. Moeneclaey, 'The BER performance of OFDM systems using non-synchronized sampling', in *Proceedings of the IEEE Global Telecommunications Conference (GLOBECOM'94)*, San Francisco, USA, November 1994, pp. 253–257.

[14] T. Pollet and M. Moeneclaey, 'Synchronizability of OFDM signals', in *Proceedings of the IEEE Global Telecommunications Conference (GLOBECOM'95)*, Singapore, November 1995, pp. 2054–2058.

[15] M. Speth, F. Classen, and H. Meyr, 'Frame synchronization of OFDM systems in frequency selective fading channels', in *Proceedings of the Vehicular Technology Conference* (VTC'97), Phoenix, May 1997.

[16] P.H. Moose, 'A technique for orthogonal frequency-division multiplexing frequency offset correction', *IEEE Transactions on Communications*, vol. 42, no. 10, pp. 2908–2914, October 1994.

[17] O. Edfors, M. Sandell, J.J. van de Beek, S.K. Wilson, and P.O. Börjesson, 'OFDM channel estimation by singular value decomposition', *IEEE Transactions on Communications*, July 1998.

[18] ETSI SMG, 'Overall requirements on the radio interface(s) of the UMTS', Technical Report ETR/SMG-21.02, v.3.0.0., ETSI, Valbonne, France, 1997.

[19] W.C. Jakes, '*Microwave mobile communications*', Classic Reissue. IEEE Press, Piscataway, New Jersey, 1974.

Part 5

This part will be published as

O. Edfors, M. Sandell, J.J. van de Beek, S.K. Wilson, and P.O. Börjesson, 'Analysis of DFT-Based Channel Estimators for OFDM', *Wireless Personal Communications*, Kluwer Academic Publishers, in press.

Analysis of DFT-Based Channel Estimators for OFDM

O. Edfors, M. Sandell, J.J. van de Beek, S.K. Wilson,
and P.O. Börjesson

Abstract – In this paper we analyze the performance of three low-complexity channel estimators, based on the *discrete Fourier-transform* (DFT), for *orthogonal frequency-division multiplexing* (OFDM) systems. Estimators of this type have been analyzed for discrete-time channels, and we extend this analysis to continuous-time channels. We present analytical expressions for their *mean-squared error* (MSE) and evaluate their complexity versus *symbol-error rate* (SER) for 16-QAM. The analysis shows that this type of estimators may experience an irreducible error floor at high SNRs. However, in one of the three estimators the error floor can be eliminated while the complexity stays low and the performance is maximized.

1 Introduction

Wireless digital communication systems using coherent signaling schemes, such as a *quadrature amplitude modulation* (QAM), require estimation and tracking of the fading channel. In general, this means a more complex receiver than for differential modulation schemes, such as *differential phase-shift keying* (DPSK), where the receivers operate without a channel estimate [1]. In *orthogonal frequency-division multiplexing* (OFDM) systems [2,3], DPSK is appropriate for relatively low data rates, such as in the European *digital-audio broadcast* (DAB) system [4]. However, for more spectrally-efficient OFDM systems, coherent modulation is more appropriate.

We address linear estimators for OFDM where all channel attenuations in a received symbol are estimated simultaneously. Using the *linear minimum mean-squared error* (LMMSE) estimator, which takes advantage of the correlation between all N subcarriers, requires an $N \times N$ matrix multiplication. This complexity can be large depending on the number of subcarriers in the system. This paper presents and analyzes three low-complexity, suboptimal, approximations of the LMMSE channel estimator. These estimators all share the property that they use the *discrete Fourier transform* (DFT) to estimate the channel in the time domain, where the channel energy is more concentrated. Estimators of this type have been proposed [5–8], but only analyzed for discrete-time channels [6]. We focus on a DFT's suitability as part of an efficient channel attenuation estimator for OFDM systems. We compare the performance and complexity for different estimator designs using DFT's, assuming perfect knowledge of channel statistics. This is to see what is the best possible performance of each of these estimators. The techniques

described in this paper could use either decision-directed data [9] or pilot symbols [10]. Furthermore, time correlation can be used for channel estimation and in some slow fading cases, see, *e.g.*, [11], estimation in only the time direction provides sufficient performance. Both the choice of decision-directed versus pilot symbols and the use of time correlation are beyond the scope of this paper.

The addressed estimators take the N noisy frequency-domain observations and transform them to the time domain by an inverse DFT (IDFT). The linear estimation is then performed in the time-domain, and the result transformed back to the frequency domain by a DFT. The transforms can be implemented with fast algorithms requiring only a few multiplications per estimated attenuation, but there are still N coefficients to estimate simultaneously in the time-domain. However, an OFDM symbol time is, by design, much larger than the length of the channel. The time-domain estimation takes advantage of the fact that this concentrates the channel power to a relatively small number of time-domain samples. Three of the strategies for doing time-domain approximations are: approximating time-domain samples with low channel power as zero, ignoring cross correlations and ignoring differences in variance. The three estimators analyzed here use these three strategies cumulatively.

After presenting the OFDM system model in Section 2, we introduce the three DFT-based estimators in Section 3. In Section 4 we present an analysis of the average mean-squared error (MSE) and show that there is an irreducible MSE-floor inherent in DFT-based low-complexity estimators. We also illustrate their performance by presenting the uncoded 16-QAM symbol error rate for a 64 tone OFDM system. A complexity versus performance comparison is done, which singles out the second of the three estimators as a good trade-off. A summary and concluding remarks appear in Section 5.

2 System model

Figure 1 displays the OFDM base-band system used in this paper. We assume that the use of a *cyclic prefix* (CP) both preserves the orthogonality of the subcarriers and eliminates *intersymbol interference* (ISI) between consecutive OFDM symbols [12]. Further, the channel $g(\tau;t)$ is assumed to be slowly Rayleigh-fading and considered constant during one OFDM symbol. The number of tones in the system is N, and the length of the cyclic prefix is L samples.

Under these assumptions we can describe the system as a set of parallel Gaussian channels [2], shown in Figure 2, with correlated attenuations

$$h_k = h\left(\frac{k}{NT_s}\right), k = 0 \ldots N-1, \tag{1}$$

where $h(\cdot)$ is the frequency response[1] of the channel $g(\tau;t)$ during the OFDM symbol, and T_s is the sampling period of the system. In matrix notation we describe the OFDM

[1]To obtain a clear linear algebra notation we represent matrices with bold upper-case and vectors with bold lower-case. Consequently, the time and frequency representations of the channel are chosen as g and h, respectively.

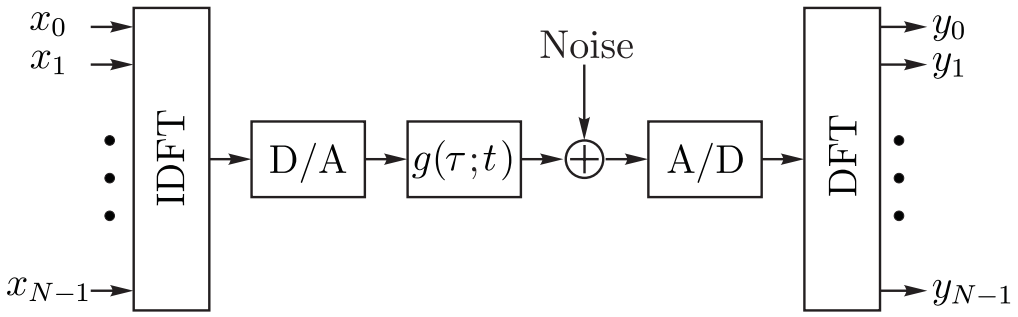

Figure 1: Base band OFDM system. The cyclic prefix is not shown in this figure.

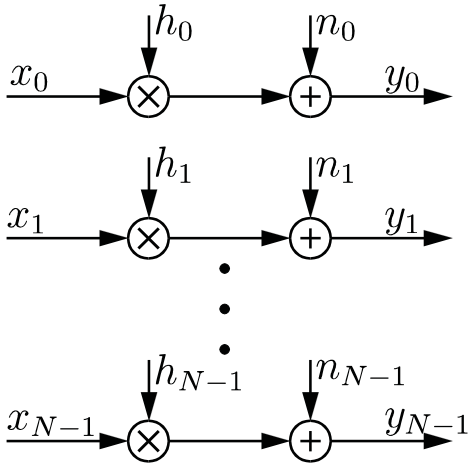

Figure 2: The OFDM system, described as a set of parallel Gaussian channels with correlated attenuations.

system as

$$\mathbf{y} = \mathbf{X}\mathbf{h} + \mathbf{n}, \tag{2}$$

where $\mathbf{y}$ is the received vector, $\mathbf{X}$ is a diagonal matrix containing the transmitted signal points, $\mathbf{h}$ is a channel attenuation vector, and $\mathbf{n}$ is a vector of independent and identically distributed complex, zero-mean, Gaussian noise variables with variance σ_n^2. Without loss of generality, we assume that $E\left\{|h_k|^2\right\} = 1$.

3 DFT-based estimators

The task of the channel estimator is to estimate the channel attenuations $\mathbf{h}$ from the observations $\mathbf{y}$, given the transmitted symbols $\mathbf{X}$. For the sake of a tractable analysis we assume the x_ks to be known at the receiver.

Since OFDM systems are designed such that the symbol time is significantly longer than the duration of the channel impulse response, the inverse DFT of the channel attenuation vector $\mathbf{h}$ has most of its power concentrated to relatively few samples. As an illustration of this power concentration, Figure 3 shows the channel power in the

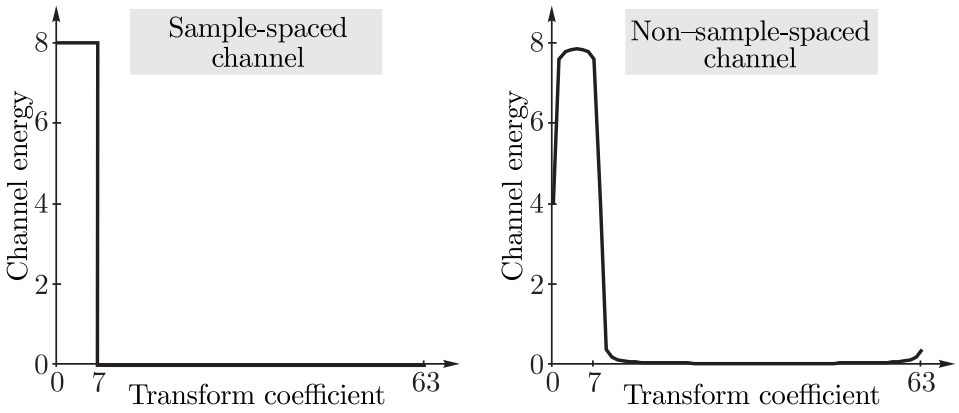

Figure 3: Schematic pictures of the energy distribution of the channel after the transform IDFT (**h**). A 64 tone system with an 8 sample cyclic prefix is used in this example.

time domain (IDFT (**h**)) for two channel types, sample-spaced and non-sample-spaced. Sample-spaced channels are channels that have all fading impulses at integer multiples of the system sampling rate, and for which the DFT gives optimal power concentration [6]. Given a non-sampled spaced continuous-time channel, the IDFT of **h** is no longer confined to the cyclic prefix. This is because **h** is the sampled version of the continuous Fourier transform of the channel $g(\tau; t)$. In general, the IDFT of a sampled continuous-time Fourier transform is not equal to the sampled original time signal. This, however does not mean that the system orthogonality is compromised when the channel is non-sample-spaced. The only requirement for orthogonality is that the continuous time channel has a length that is less than the cyclic prefix [12].

DFT-based estimation of sample-spaced channels is addressed in [6], and the three estimators we present and analyze are generalizations thereof for non-sample-spaced channels. For clarity, we first calculate the *linear minimum mean-squared error* (LMMSE) estimate of **h**.

We base our estimates on the *least squares* (LS) estimate (the backrotated observations)

$$\widehat{\mathbf{h}}_{ls} = \mathbf{X}^{-1}\mathbf{y} = \mathbf{h} + \widetilde{\mathbf{n}}, \tag{3}$$

where $\widetilde{\mathbf{n}} = \mathbf{X}^{-1}\mathbf{n}$ is a vector of independent Gaussian noise variables with covariance matrix $\mathbf{R}_{\widetilde{n}\widetilde{n}} = \sigma_n^2 \left(\mathbf{X}\mathbf{X}^H\right)^{-1}$. The LS estimate $\widehat{\mathbf{h}}_{ls}$ constitutes a sufficient statistic since $\mathbf{X}$ is non-singular. The LS estimate is a noisy observation of the channel attenuations and can be smoothed using correlation properties of the channel. The optimal linear estimator in terms of mean-squared error (MSE) is [8, 13]

$$\widehat{\mathbf{h}} = \mathbf{W}_{\mathbf{X}}\widehat{\mathbf{h}}_{ls}, \tag{4}$$

where

$$\mathbf{W}_{\mathbf{X}} \triangleq \mathbf{R}_{hh}\left(\mathbf{R}_{hh} + \sigma_n^2\left(\mathbf{X}\mathbf{X}^H\right)^{-1}\right)^{-1}, \tag{5}$$

and $\mathbf{R}_{hh} = E\left\{\mathbf{h}\mathbf{h}^H\right\}$ is the auto-covariance matrix of the channel vector **h**.

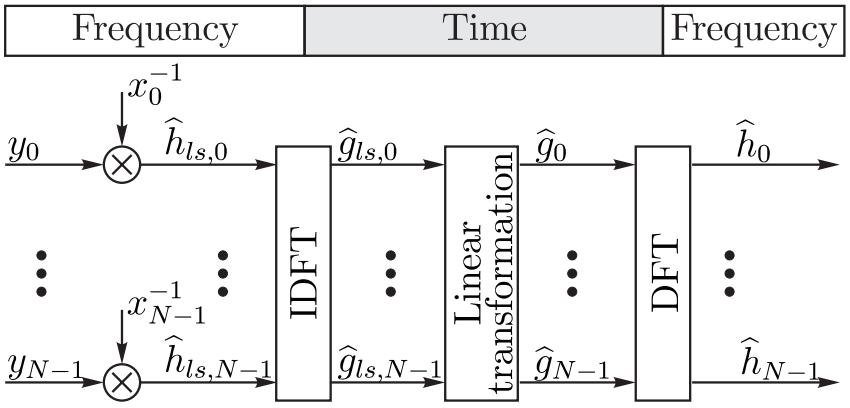

Figure 4: Structure of DFT-based channel estimators, where the linear transformation consists of a matrix multiplication $\widehat{\mathbf{g}} = \mathbf{Q}\widehat{\mathbf{g}}_{ls}$.

At this point we recognize that the weighting matrix $\mathbf{W}_{\mathbf{X}}$ is of size $N \times N$ and depends on the transmitted data $\mathbf{X}$. As a first step towards low-complexity estimators we want to find a weighting matrix that is independent of the transmitted data. This can be obtained by considering $\widehat{\mathbf{h}}_{ls}$ to be our observation and derive an LMMSE estimator that considers $\mathbf{X}$ to be stochastic with independent and uniformly distributed constellation points. In that case, the auto-covariance matrix of the noise becomes $\mathbf{R}_{\widetilde{nn}} = \frac{\beta}{\mathrm{SNR}}\mathbf{I}$, where $\beta \triangleq E\left\{|x_k|^2\right\} E\left\{|x_k|^{-2}\right\}$ is a constellation factor ($\beta = 17/9$ for 16-QAM) and $\mathrm{SNR} \triangleq E\left\{|x_k|^2\right\}/\sigma_n^2$ is the per-symbol signal-to-noise ratio.

The LMMSE estimate of $\mathbf{h}$ from $\widehat{\mathbf{h}}_{ls}$ now becomes

$$\widehat{\mathbf{h}}_{lmmse} = \mathbf{W}\widehat{\mathbf{h}}_{ls}, \tag{6}$$

where the fixed weighting matrix is given by

$$\mathbf{W} \triangleq \mathbf{R}_{hh}\left(\mathbf{R}_{hh} + \frac{\beta}{\mathrm{SNR}}\mathbf{I}\right)^{-1}. \tag{7}$$

This LMMSE estimator still requires N multiplications per estimated attenuation and we use it both as a reference and as a starting point in the derivation of the DFT-based low-complexity estimators.

We now use the property of OFDM systems identified above and in [6–8]: $\mathbf{h}$ is the sampled frequency response of a channel with short time duration compared to the OFDM symbol length and, hence, its associated cyclic impulse response $\mathbf{g} = \mathrm{IDFT}(\mathbf{h})$ has only a few taps with significant power. If we perform the estimation in the time-domain, we can reduce the complexity of the estimation by using this power concentration.

This prompts the estimator structure in Figure 4, where the LS estimate is transformed into its time-domain equivalent $\widehat{\mathbf{g}}_{ls} = \mathrm{IDFT}\left(\widehat{\mathbf{h}}_{ls}\right)$. The smoothing is then performed by a linear transformation

$$\widehat{\mathbf{g}} = \mathbf{Q}\widehat{\mathbf{g}}_{ls} \tag{8}$$

and the result is transformed back to the frequency-domain, $\widehat{\mathbf{h}} = \mathrm{DFT}\,(\widehat{\mathbf{g}}_{ls})$. The important benefit of this estimator structure in terms of complexity is the low complexity of the DFT/IDFT (implemented as fast transforms) and the time-domain power concentration. This offers a simplification of (8) without sacrificing too much in performance.

Our approach is to find sparse approximations of the LMMSE estimator's equivalent time-domain smoothing matrix

$$\mathbf{Q} = \mathbf{F}^H \mathbf{W} \mathbf{F}, \tag{9}$$

where $\mathbf{F}$ is the $N \times N$ unitary DFT matrix and $\mathbf{W}$ is defined in (7). This will reduce the number of required multiplications, and thus the estimator complexity. A straightforward way is to simply ignore the coefficients in $\widehat{\mathbf{g}}_{ls}$ that contain more noise than channel power and only transform the remaining elements back to the frequency domain. For sample-spaced channels, this is a fruitful approach [5, 6] since the major part of the coefficients only contain noise and no channel power. If the channel is not sample-spaced, however, the channel power is still concentrated but distributed over all coefficients. Due to the lost channel power in the ignored coefficients the simplification causes an irreducible error floor [8].

We now move through three simplification steps and obtain three different low-complexity estimators, of which the last is the straightforward approach described above. The general concept is based on reducing the number of non-zero elements in the time-domain matrix multiplication (8), with the aim of reducing the computational complexity and preserving the performance. The three estimators are selected as follows: (See Appendix A for a detailed derivation.)

- **Estimator A**

  By choosing the M coefficients in $\widehat{\mathbf{g}}_{ls}$ that have the highest channel power, we restrict the linear transform in the time-domain to a fixed matrix of size $M \times M$. If M is chosen much smaller than N, the complexity reduction compared to the LMMSE is considerable. The complexity of the time-domain processing in this case is M^2/N multiplications per estimated attenuation. This estimator converges to the LMMSE when $M \to N$. We have presented a related estimator previously in [8].

- **Estimator B**

  Further reductions in complexity can be done by ignoring cross-correlation between the M chosen taps in $\widehat{\mathbf{g}}_{ls}$ and only weighting them individually. This essentially means that we restrict the time-domain processing to be a diagonal $M \times M$ matrix multiplication. Since this matrix only has M non-zero elements, the complexity of this processing is M/N multiplications per estimated attenuation. To the authors' knowledge, this estimator has not been presented before.

- **Estimator C**

  In this last estimator, we further restrict the time-domain processing to only use the M chosen coefficients directly as input to the DFT. This means restricting the

Table 1: Analyzed DFT-based estimators. See Appendix A for details.

Estimator	**Restriction (cumulative)**	**Linear transformation**	**Effective matrix size**	**Required mult. / attenuation**
LMMSE	N.A.	N.A.	$N \times N$	$N+1$
A	Use M coefficients	$\mathbf{Q}_A = \begin{bmatrix} \mathbf{Q}_{M\times M} & \mathbf{0} \\ \mathbf{0} & \mathbf{0} \end{bmatrix}$	$M \times M$	$\log_2 N + \frac{M^2}{N} + 1$
B	Diagonal matrix	$\mathbf{Q}_B = \begin{bmatrix} \mathbf{D}_{M\times M} & \mathbf{0} \\ \mathbf{0} & \mathbf{0} \end{bmatrix}$	$M \times M$ (diag.)	$\log_2 N + \frac{M}{N} + 1$
C	Identity matrix	$\mathbf{Q}_C = \begin{bmatrix} \mathbf{I}_{M\times M} & \mathbf{0} \\ \mathbf{0} & \mathbf{0} \end{bmatrix}$	$M \times M$ (ident.)	$\log_2 N + 1$
LS	N.A.	N.A.	N.A.	1

matrix to an $M \times M$ identity matrix, which does not require any multiplications at all. When $M \to N$ this estimator converges to the LS estimator. This estimator is similar to the estimator designed for sample-spaced channels in [5, 6].

The outlined estimators (A-C) are summarized in Table 1, where we have also included the LMMSE and LS estimators as references. The table shows the total computational complexity, including the IDFT and DFT [2] for estimators A–C. In general, unless M is close to N, the complexity decreases in Table 1 from the LMMSE to the LS.

4 Performance analysis

The estimators presented in the previous section all have different computational complexities, and the design variations give them different performances as well. To illustrate the performance of these estimators, we calculate the MSE and use formulae from [15] to obtain the uncoded 16-QAM *symbol-error rate* (SER).

The parameters we have chosen for the OFDM system are $N = 64$ subcarriers and a cyclic prefix of length $L = 8$ samples. The impulse response of the physical channel

$$g(\tau; t) = \sum_m \alpha_m(t)\delta(\tau - \tau_m)$$

consists of independent Rayleigh-fading (α_m) impulses, uniformly distributed (τ_m) over the length of the cyclic prefix and with a constant power delay profile. From this channel model we calculate the auto-covariance matrix $\mathbf{R}_{hh}$ of the channel attenuations $\mathbf{h}$ [16]. The cyclic impulse response $\mathbf{g} = \mathbf{F}^H\mathbf{h}$ has a corresponding auto-covariance matrix $\mathbf{R}_{gg} = \mathbf{F}^H\mathbf{R}_{hh}\mathbf{F}$. In the analysis, we reorder the time-domain indices so that the variances, $\gamma_k = E\left\{|g_k|^2\right\}$, are in decreasing order, *i.e.* $\gamma_0 \geq \gamma_1 \ldots \geq \gamma_{N-1}$. This simplifies the indexing in the analysis. In a more practical system, the designer could reorder the indices based on a generic channel model. Though this may result in a mismatch, this consideration

[2] To obtain a complexity measure we have assumed that N is a power of two and that the DFT and the IDFT requires $\frac{1}{2}N\log_2 N$ complex multiplications each [14].

Estimator	Average MSE
LMMSE	$\frac{1}{N}\frac{\beta}{\mathrm{SNR}}\sum_{k=0}^{N-1}\frac{\lambda_{k,N}}{\lambda_{k,N}+\frac{\beta}{\mathrm{SNR}}}$
A	$\frac{1}{N}\frac{\beta}{\mathrm{SNR}}\sum_{k=0}^{M-1}\frac{\lambda_{k,M}}{\lambda_{k,M}+\frac{\beta}{\mathrm{SNR}}}+\underline{\mathrm{MSE}}$
B	$\frac{1}{N}\frac{\beta}{\mathrm{SNR}}\sum_{k=0}^{M-1}\frac{\gamma_{k}}{\gamma_{k}+\frac{\beta}{\mathrm{SNR}}}+\underline{\mathrm{MSE}}$
C	$\frac{M}{N}\frac{\beta}{\mathrm{SNR}}+\underline{\mathrm{MSE}}$
LS	$\frac{\beta}{\mathrm{SNR}}$

$\lambda_{k,M}$ – eigenvalues of $\mathbf{R}_{gg,M}$.

γ_k – diagonal elements of $\mathbf{R}_{gg}$ in decreasing order.

$\underline{\mathrm{MSE}} = \frac{1}{N}\sum_{k=M}^{N-1}\gamma_k$ (MSE floor)

Table 2: Average MSE for the investigated estimators. $\mathbf{R}_{gg,M}$ denotes the covariance matrix of the M dominating taps in $\mathbf{g}$. Note that the $\lambda_{k,N}$s are eigenvalues of $\mathbf{R}_{gg}$.

is beyond the scope of this paper. After index reordering, the auto-covariance matrix of the M used transform coefficients, $\mathbf{R}_{gg,M}$, is the upper left $M \times M$ corner of $\mathbf{R}_{gg}$.

Through direct calculation of the auto-covariance matrix of the estimation error

$$\mathbf{R}_{e_Q e_Q} = E\left\{\left(\widehat{\mathbf{h}}-\mathbf{h}\right)\left(\widehat{\mathbf{h}}-\mathbf{h}\right)^H\right\} \tag{10}$$

for all estimators, we obtain their respective average MSEs

$$\mathrm{MSE} = \frac{1}{N}\mathrm{Trace}\left(\mathbf{R}_{e_Q e_Q}\right). \tag{11}$$

Note that the diagonal elements of $\mathbf{R}_{e_Q e_Q}$ are the individual error variances for each channel attenuation. The calculations are derived in Appendix A. The final MSE expressions for the LMMSE estimator, the low-complexity estimators (A–C) and the LS estimator are displayed in Table 2. Appendix A also contains a note on sample-spaced channels that is of interest when comparing this analysis with the analysis in [6]. As displayed in the table, estimators A, B, and C experience an error floor ($\underline{\mathrm{MSE}}$) due to the channel power in the $N-M$ excluded channel taps. This error floor is the same for all DFT-based low-complexity estimators. The individual ranking of the low-complexity estimators in terms of MSE, for a fixed M, is $\mathrm{MSE}_A \leq \mathrm{MSE}_B \leq \mathrm{MSE}_C$.

Using the formulae from [15], we display 16-QAM SER curves for two different numbers of included transform coefficients ($M = 10$ and $M = 40$) in Figure 5. The 16-QAM SER of the full LMMSE estimator and the LS estimator are also included in the figure, as references. The LMMSE, which is the best estimator, is about 1 dB away from known channel at all SNRs.Note that for $M = 10$ there is no visible difference in SER between

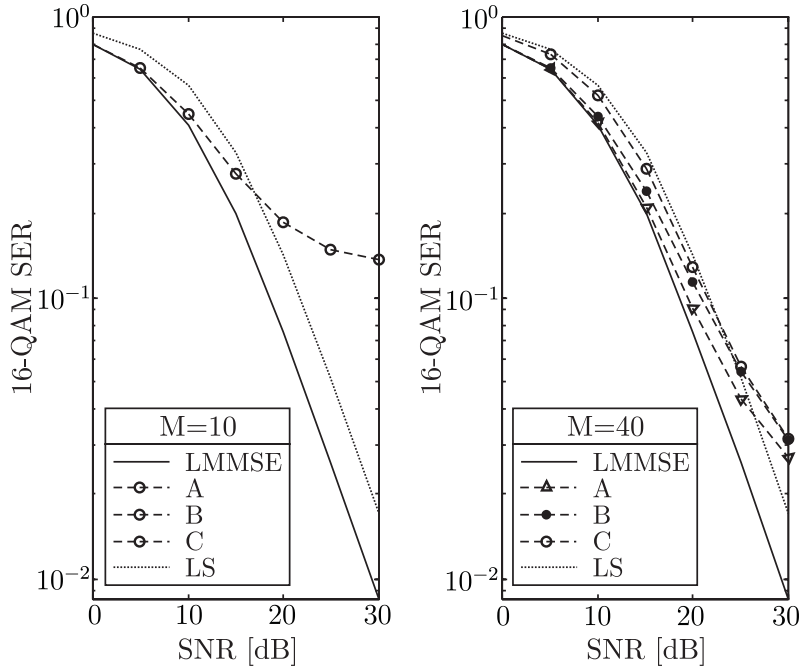

Figure 5: Uncoded 16-QAM SER for three systems using the low-complexity estimators A, B, and C, respectively. (Note: Estimators A, B and C have the same SER for $M = 10$.)

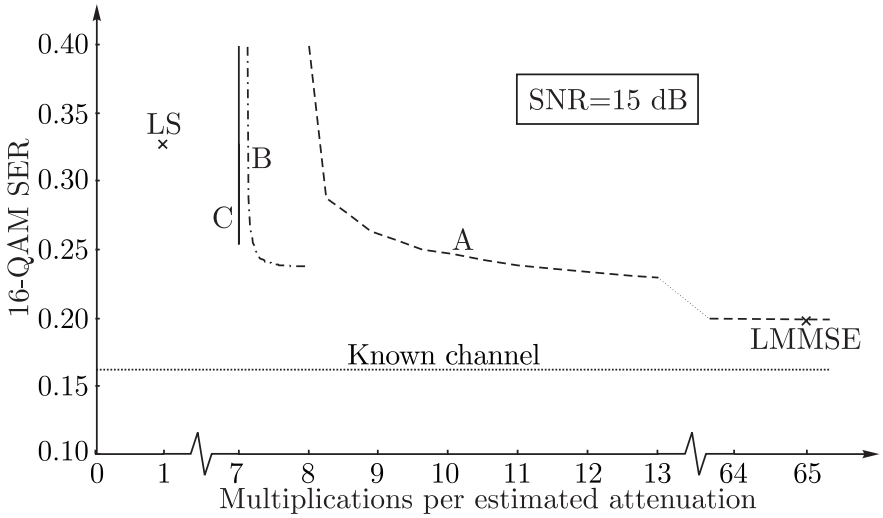

Figure 6: SER versus estimator complexity at SNR = 15 dB. Note the discontinuities of the abscissa.

the three low-complexity estimators and that the SER levels off at high SNRs, due to the error floor. It is only for higher values of M that a difference in SER is noticeable between the low-complexity estimators. It is also noteworthy that even at $M = 40$ (out of a possible $N = 64$) the error floor is visible, and the low-complexity estimators perform worse than the LS estimator above a certain SNR. For $M = 40$, the figure also shows that the performance of the estimators is decreasing from A to C.

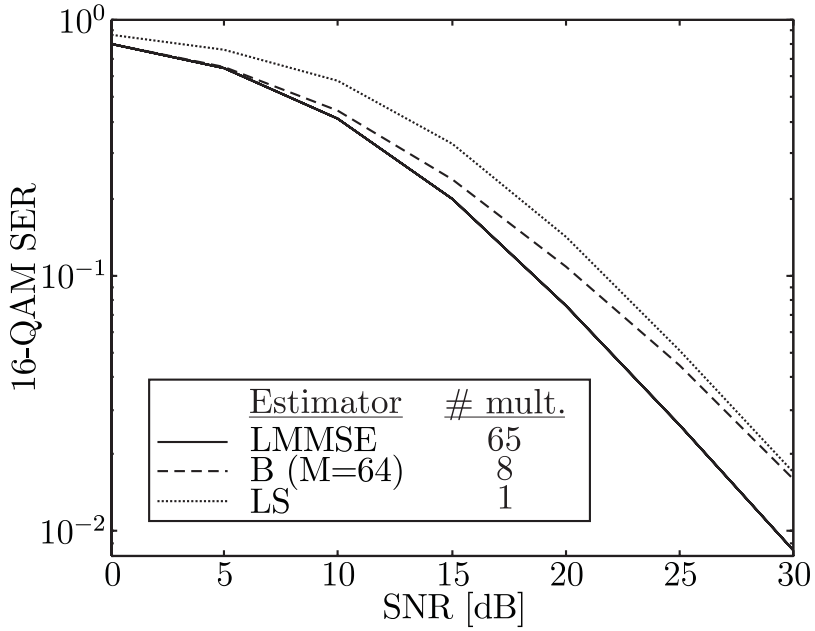

Figure 7: Uncoded 16-QAM SER for estimator B where all 64 taps are used ($M = N$). Curves for the LMMSE and LS estimators are included as references.

The performance of the low-complexity estimators, especially for high SNRs, depends strongly on the number of included taps. An analysis of this behavior shows that the three low-complexity estimators are quite different in terms of complexity versus performance. This is illustrated in Figure 6, which shows that the complexity needs to be high to make estimator A the best in terms of SER. In general, estimators B and C are more efficient per required multiplication. For a 64 subcarrier system, the complexity of estimator C is always 7 multiplications per attenuation while estimator B has a complexity of between 7 and 8 multiplications per attenuation, depending on the number of taps used.

If we want to eliminate the error floor entirely, we have to use all taps ($M = N$) in estimators A–C. Effectively, this turns estimator A into the high-complexity LMMSE estimator and estimator C into the low-performance LS estimator. However, estimator B which has lower complexity than estimator A and better performance than estimator C is a good compromise between the two. Estimator A does not have a complexity low enough to compete with the other two and the approximations in estimator C seem to be too crude to provide a good estimate. This enables us to single out estimator B as the best trade-off between complexity and performance among the three estimators analyzed.

As a final comparison, we present the 16-QAM SER performance of estimator B (with all taps included), the LMMSE estimator, and the LS estimator in Figure 7. The SER performance of estimator B is good for low SNRs where it resembles that of the LMMSE estimator, and this at less than 1/8 of the complexity (number of multiplications) of the LMMSE. At high SNRs it converges to the SER of the LS estimator, but there is no error floor and the performance never becomes worse than that of the LS estimator. Estimator B has more than a 2 dB gain over the LS estimate for SNRs less than 15 dB and a 3 dB gain for SNRs below 5 dB.

5 Conclusions

In this paper we have presented the MSE and SER performances of three low-complexity DFT-based estimators (A–C). Using M of the N time-domain coefficients yields estimators with complexity (excluding the DFT/IDFT) of M^2/N, M/N and 0 multiplications per estimated channel attenuation, respectively. Only the first of these estimators is potentially of high complexity since $M \leq N$. We have provided analytical expressions for the mean-squared error of all three estimators and shown that, if the number of included taps is less than N, they suffer from an irreducible error floor.

The error-floor can be removed if all taps are used in the linear transform, but only estimator B maintains both its performance and its low complexity in this case. The other two designs either experience a drastically increased complexity (estimator A) or converge to the poor performance of the LS estimator (estimator C). Estimator B maintains good performance with low complexity by ignoring the relatively small cross-correlation between the time-domain channel coefficients. So, we consider estimator B using all N coefficients to be the most suitable of the DFT-based channel estimators. At low SNRs in the investigated system it has almost the same performance as the LMMSE estimator, which in turn is only about 1 dB away from known channel, and this at less than 1/8 of the complexity.Further, in terms of symbol-error rate, this estimator has more than a 2 dB gain over the LS estimator for SNRs less than 15 dB.

A Estimator expressions

In this appendix we provide expressions for the linear transformations of the three low-complexity estimators and the MSE for each estimator. At the end we have also included a note on sample-spaced channels, which is of interest when comparing our analysis to the one in [6].

To simplify the matrix notation we assume that the coefficients in the cyclic impulse response $\widehat{\mathbf{g}}_{ls}$ are ordered according to decreasing channel power. This is justified since permutations of the DFT/IDFT coefficients do not change the estimators – it only changes the order in which the coefficients are indexed. The channel power in coefficient $\widehat{g}_{ls,k}$ is denoted $\gamma_k = E\left\{|g_k|^2\right\}$, which are the diagonal elements of $\mathbf{R}_{gg}$.

Before we start the derivation, we write the estimator structure, Figure 4, in matrix notation

$$\widehat{\mathbf{h}}_Q = \mathbf{F}\mathbf{Q}\mathbf{F}^H\mathbf{X}^{-1}\mathbf{y} = \mathbf{F}\mathbf{Q}\mathbf{F}^H\widehat{\mathbf{h}}_{ls}, \tag{12}$$

where $\mathbf{Q}$ is the matrix representing the linear transformation in the time domain and $\mathbf{F}$ is the $N \times N$ unitary DFT matrix (Note: $\mathbf{F}^{-1} = \mathbf{F}^H$). Further, we need the auto-covariance matrix of $\mathbf{g}$ which is

$$\mathbf{R}_{gg} = E\left(\mathbf{g}\mathbf{g}^H\right) = \mathbf{F}^H\mathbf{R}_{hh}\mathbf{F}. \tag{13}$$

We are minimizing the MSE, and thus need an explicit expression for the auto-covariance matrix of the estimation error (10)

$$\mathbf{R}_{e_Q e_Q} = E\left\{\left(\widehat{\mathbf{h}}_\mathbf{Q} - \mathbf{h}\right)\left(\widehat{\mathbf{h}}_\mathbf{Q} - \mathbf{h}\right)^H\right\} \tag{14}$$

$$
\begin{aligned}
&= \mathbf{F}\mathbf{Q}\mathbf{F}^H \left(\mathbf{R}_{hh} + \frac{\beta}{\mathrm{SNR}}\mathbf{I}\right) \mathbf{F}\mathbf{Q}^H\mathbf{F}^H - \\
&\quad \mathbf{R}_{hh}\mathbf{F}\mathbf{Q}^H\mathbf{F}^H - \mathbf{F}\mathbf{Q}\mathbf{F}^H\mathbf{R}_{hh}^H + \mathbf{R}_{hh},
\end{aligned}
$$

which gives the MSE according to (11).

To save space, the calculations below are not presented in detail. However, the respective $\mathbf{Q}$ matrices of the estimators are substituted in (14) and the following equalities are applied:

- $\mathrm{Trace}\left(\mathbf{U}\mathbf{R}\mathbf{U}^H\right) = \mathrm{Trace}\left(\mathbf{R}\right)$, when $\mathbf{U}$ is a unitary matrix.
- $\mathrm{Trace}\left(\mathbf{D}_1\mathbf{R}\mathbf{D}_2\right) = \mathrm{Trace}\left(\mathbf{D}_1\mathbf{D}_2\mathbf{R}\right)$, when $\mathbf{D}_1$ and $\mathbf{D}_2$ are diagonal matrices.
- $\mathbf{R}_{gg,M} = \mathbf{U}_M^H\mathbf{R}_{hh}\mathbf{U}_M$, where $\mathbf{F} = \left[\begin{array}{cc} \mathbf{U}_M & \mathbf{V}_{N-M} \end{array}\right]$ and $\mathbf{U}_M$ contains the first M columns of $\mathbf{F}$.
- $\mathbf{U}_M^H\mathbf{V}_M = \mathbf{0}$, where $\mathbf{U}_M$ and $\mathbf{V}_{N-M}$ are defined above.

To simplify the MSE expressions we also use that the trace of a matrix is equivalent to the sum of its eigenvalues [17]. Further, relation (13) implies that $\mathbf{R}_{hh}$ and $\mathbf{R}_{gg}$ share the same eigenvalues [17], which is used to avoid separate notations.

- **LS estimator**

  The LS estimate (3) is used as input to the IDFT in Figure 4, and its MSE is

  $$\mathrm{MSE} = \frac{\beta}{\mathrm{SNR}}.$$

  This estimate only requires one multiplication per estimated attenuation. Since it is the input to the rest of the estimators, this one multiplication will show up in the following complexity expressions.

- **LMMSE estimator**

  The LMMSE estimator is given in (6) and (7) and its MSE becomes

  $$
  \begin{aligned}
  \mathrm{MSE} &= \frac{1}{N}\mathrm{Trace}\left(\mathbf{R}_{hh}\left(\mathbf{I} - \left(\mathbf{R}_{hh} + \frac{\beta}{\mathrm{SNR}}\mathbf{I}\right)^{-1}\mathbf{R}_{hh}\right)\right) \\
  &= \frac{1}{N}\frac{\beta}{\mathrm{SNR}}\sum_{k=0}^{N-1}\frac{\lambda_{k,N}}{\lambda_{k,N} + \frac{\beta}{\mathrm{SNR}}},
  \end{aligned}
  $$

  where the $\lambda_{k,N}$s are eigenvalues of $\mathbf{R}_{hh}$ (and $\mathbf{R}_{gg}$).

  Implementing this estimator as a matrix multiplication as in (6) requires $N + 1$ multiplications per estimated attenuation.

- **Estimator A**

  Imposing the first restriction on the linear transformation,

  $$\mathbf{Q}_A = \begin{bmatrix} \mathbf{Q}_{M\times M} & \mathbf{0} \\ \mathbf{0} & \mathbf{0} \end{bmatrix},$$

  the minimal MSE is obtained if

  $$\mathbf{Q}_{M\times M} = \mathbf{R}_{gg,M}\left(\mathbf{R}_{gg,M} + \frac{\beta}{\mathrm{SNR}}\mathbf{I}\right)^{-1},$$

  where $\mathbf{R}_{gg,M}$ is the upper left $M \times M$ corner of $\mathbf{R}_{gg}$.

  The MSE of this estimator is

  $$\begin{aligned} \mathrm{MSE} &= \frac{1}{N}\mathrm{Trace}\left(\mathbf{R}_{gg,M}\left(\mathbf{I} - \left(\mathbf{R}_{gg,M} + \frac{\beta}{\mathrm{SNR}}\mathbf{I}\right)^{-1}\mathbf{R}_{gg,M}\right)\right) + \underline{\mathrm{MSE}} \\ &= \frac{1}{N}\frac{\beta}{\mathrm{SNR}}\sum_{k=0}^{M-1}\frac{\lambda_{k,M}}{\lambda_{k,M} + \frac{\beta}{\mathrm{SNR}}} + \underline{\mathrm{MSE}} \end{aligned}$$

  where the $\lambda_{k,M}$s are eigenvalues of $\mathbf{R}_{gg,M}$ and

  $$\underline{\mathrm{MSE}} = \mathrm{Trace}\left(\mathbf{V}_{N-M}^H \mathbf{R}_{hh}\mathbf{V}_{N-M}\right) = \frac{1}{N}\sum_{k=M}^{N-1}\gamma_k, \tag{15}$$

  where $\mathbf{V}_{N-M}$ contains the last $N-M$ columns of $\mathbf{F}$. We call $\underline{\mathrm{MSE}}$ the *MSE floor*, since it only depends on the number of excluded taps $(N-M)$ and lower bounds the MSE.

  Implementing this estimator according to Figure 4 requires $\log_2 N + \frac{M^2}{N} + 1$ multiplications per estimated attenuation.

- **Estimator B**

  Applying the second restriction on the linear transformation,

  $$\mathbf{Q}_B = \begin{bmatrix} \mathbf{D}_{M\times M} & \mathbf{0} \\ \mathbf{0} & \mathbf{0} \end{bmatrix}$$

  where $\mathbf{D}_M = \mathrm{diag}\left(\delta_0, \delta_1, \ldots, \delta_{M-1}\right)$, we obtain a minimal MSE if

  $$\delta_k = \frac{\gamma_k}{\gamma_k + \frac{\beta}{\mathrm{SNR}}}.$$

  The MSE of this estimator is

  $$\mathrm{MSE} = \frac{1}{N}\frac{\beta}{\mathrm{SNR}}\sum_{k=0}^{M-1}\frac{\gamma_k}{\gamma_k + \frac{\beta}{\mathrm{SNR}}} + \underline{\mathrm{MSE}},$$

where $\underline{\text{MSE}}$ is given by (15).

Implementing this estimator according to Figure 4 requires $\log_2 N + \frac{M}{N} + 1$ multiplications per estimated attenuation.

- **Estimator C**

  Applying the last restriction on the linear transformation,

$$\mathbf{Q}_C = \begin{bmatrix} \mathbf{I}_{M\times M} & \mathbf{0} \\ \mathbf{0} & \mathbf{0} \end{bmatrix},$$

  we do not have any choice in the design, except for M, and the MSE becomes

$$\text{MSE} = \frac{M}{N}\frac{\beta}{\text{SNR}} + \underline{\text{MSE}}$$

  where, again, $\underline{\text{MSE}}$ is given by (15).

  Implementing this estimator according to Figure 4 requires $\log_2 N + 1$ multiplications per estimated attenuation.

A note on sample-spaced channels

The above expressions are derived for a general case, but they have some interesting properties for sample-spaced channels that are worth noting. Consider a channel impulse response

$$g(\tau; t) = \sum_{m=0}^{L} \alpha_m(t)\,\delta(\tau - mT_s),$$

where the fading amplitudes $\alpha_m(t)$, of the sample-spaced impulses, are independent. Then $\mathbf{F}$ diagonalizes $\mathbf{R}_{hh}$, and $\mathbf{R}_{gg}$ becomes diagonal with only L non-zero elements. The channel power in the kth coefficient of $\widehat{\mathbf{g}}_{ls}$ is therefore equivalent to the kth largest eigenvalue $\lambda_{k,N}$ of $\mathbf{R}_{hh}$ (and $\mathbf{R}_{gg}$), and the eigenvalues of $\mathbf{R}_{gg,M}$ becomes $\lambda_{k,M} = \lambda_{k,N} = \gamma_k$, of which only the first L are non-zero. Hence, the MSEs for the estimators become:

Estimator	**Average MSE**
LMMSE	$\frac{1}{N}\frac{\beta}{\text{SNR}}\sum_{k=0}^{N-1}\frac{\gamma_k}{\gamma_k+\frac{\beta}{\text{SNR}}}$
A	$\frac{1}{N}\frac{\beta}{\text{SNR}}\sum_{k=0}^{M-1}\frac{\gamma_k}{\gamma_k+\frac{\beta}{\text{SNR}}} + \underline{\text{MSE}}$
B	$\frac{1}{N}\frac{\beta}{\text{SNR}}\sum_{k=0}^{M-1}\frac{\gamma_k}{\gamma_k+\frac{\beta}{\text{SNR}}} + \underline{\text{MSE}}$
C	$\frac{M}{N}\frac{\beta}{\text{SNR}} + \underline{\text{MSE}}$
LS	$\frac{\beta}{\text{SNR}}$

First of all, estimator A is now equivalent to estimator B and, since $\gamma_k = 0$ for $k \geq L$, both estimator A and B are equivalent to the LMMSE estimator for $M \geq L$. Further, since $\underline{\text{MSE}} = 0$ for $M \geq L$, we can choose $M = L$ in estimator C which reduces the noise, compared to the LS estimator, to a fraction L/N. This last observation was also done in [6], where the use of a standard (non-unitary) DFT results in a different notation for γ_k.

References

[1] J.G. Proakis, *Digital Communications*, 3rd edition, McGraw-Hill, New York, 1995.

[2] J.A.C. Bingham, 'Multicarrier modulation for data transmission: An idea whose time has come', *IEEE Communications Magazine*, vol. 28, no. 5, pp. 5–14, May 1990.

[3] L.J. Cimini, 'Analysis and simulation of a digital mobile channel using orthogonal frequency-division multiplexing', *IEEE Transactions on Communications*, vol. 33, no. 7, pp. 665–675, July 1985.

[4] European Telecommunications Standards Institute (ETSI), *Radio Broadcasting Systems; Digital Audio Broadcasting (DAB) to Mobile, Portable and Fixed Receivers*, European Telecommunication Standard ETS 300 401, 1st edition, reference DE/JTC-DAB, February 1995. Available from the ETSI Secreteriat, F-06921 Sophia Antipolis Cedex, France.

[5] A. Chini, M.S. El-Tanany, and S.A. Mahmoud, 'Transmission of high rate ATM packets over indoor radio channels', *IEEE Journal on Selected Areas in Communications*, vol. 14, no. 3, pp. 469–476, April 1996.

[6] A. Chini, *Multicarrier Modulation in Frequency Selective Fading Channels*, PhD thesis, Carleton University, Ottawa, Canada, 1994.

[7] J.M. Cioffi, Personal communication, 1994.

[8] J.J. van de Beek, O. Edfors, M. Sandell, S.K. Wilson, and P.O. Börjesson, 'On channel estimation in OFDM systems', in *Proceedings of the IEEE Vehicular Technology Conference (VTC'95)*, Chicago, USA, July 25–28, 1995, pp. 815–819.

[9] V. Mignone and A. Morello, 'CD3-OFDM: A novel demodulation scheme for fixed and mobile receivers', *IEEE Transactions on Communications*, vol. 44, no. 9, pp. 1144–1151, September 1996.

[10] P. Höher, 'TCM on frequency-selective land-mobile fading channels', in E. Biglieri and M. Luise (editors), *Proceedings of the Tirrenia International Workshop on Digital Communications, 'Coded Modulation and Bandwidth-Efficient Transmission'*, Tirrenia, Italy, September 8–12, 1991, Elsevier, 1992, pp. 317-328.

[11] K. Fazel, S. Kaiser, P. Robertson, and M.J. Ruf, 'A concept of digital terrestrial television broadcasting', Wireless Personal Communications, vol. 2, no. 13, pp. 9–27, 1995.

[12] A. Peled and A. Ruiz, 'Frequency domain data transmission using reduced computational complexity algorithms', in *Proceedings of the IEEE International Conference on Acoustics, Speech, and Signal Processing* (ICCASP'80), Denver, USA, 1980, pp. 964–967.

[13] L.L. Scharf, *Statistical Signal Processing: Detection, Estimation, and Time Series Analysis*, Addison-Wesley, 1991.

[14] A.V. Oppenheim and R.V. Schafer, *Discrete-Time Signal Processing*, Prentice-Hall, 1989.

[15] S.K. Wilson, *Digital Audio broadcasting in a Fading and Dispersive Channel*, PhD thesis, Stanford University, CA, August 1994.

[16] O. Edfors, M. Sandell, J.J. van de Beek, S.K. Wilson, and P.O. Börjesson, 'OFDM channel estimation by singular value decomposition', Research Report TULEA 1996:18, Division of Signal Processing, Luleå University of Technology, September 1996.

[17] G. Strang, *Linear Algebra and its Applications*, Academic Press, 2nd edition, 1980.

Part 6

This part has been published as

O. Edfors, M. Sandell, J.J. van de Beek, S.K. Wilson, and P.O. Börjesson, 'OFDM Channel Estimation by Singular Value Decomposition', *IEEE Transactions on Communications*, vol. 46, no. 7, pp. 931–939, July 1998.

OFDM Channel Estimation by Singular Value Decomposition

O. Edfors, M. Sandell, J.J. van de Beek, S.K. Wilson,
and P.O. Börjesson

Abstract – In this paper we present and analyze low-rank channel estimators for *orthogonal frequency-division multiplexing* (OFDM) systems using the frequency correlation of the channel. Low-rank approximations based on the *discrete Fourier transform* (DFT) have been proposed but these suffer from poor performance when the channel is not sample-spaced. We apply the theory of optimal rank-reduction to *linear minimum mean-squared error* (LMMSE) estimators and show that these estimators, when using a fixed design, are robust to changes in channel correlation and *signal-to-noise ratio* (SNR). The performance is presented in terms of uncoded *symbol-error rate* (SER) for a system using 16-*quadrature amplitude modulation* (QAM).

1 Introduction

Wireless digital communication systems using multiamplitude modulation schemes, such as *quadrature amplitude modulation* (QAM), generally require estimation and tracking of the fading channel. In general, this means a more complex receiver than for differential modulation schemes, such as *differential phase-shift keying* (DPSK), where the receivers operate without a channel estimate [1].

In *orthogonal frequency-division multiplexing* (OFDM) systems, DPSK is appropriate for relatively low data rates, such as in the European *digital-audio broadcast* (DAB) system [2]. However, for more spectrally-efficient OFDM systems, coherent modulation is more appropriate.

The structure of OFDM signalling allows a channel estimator to use both time and frequency correlation. Such a two-dimensional estimator structure is generally too complex for a practical implementation. To reduce the complexity, separating the use of time and frequency correlation has been proposed [3]. This combined scheme uses two separate *finite-impulse response* (FIR) Wiener filters, one in the frequency direction and the other in the time direction.

In this paper we present and analyze a class of block-oriented channel estimators for OFDM, where only the frequency correlation of the channel is used in the estimation. Whatever their level of performance, they may be improved with the addition of a second filter using the time correlation [3, 4].

Though the *linear minimum mean-squared error* (LMMSE) estimator using only frequency correlation has lower complexity than one using both time and frequency cor-

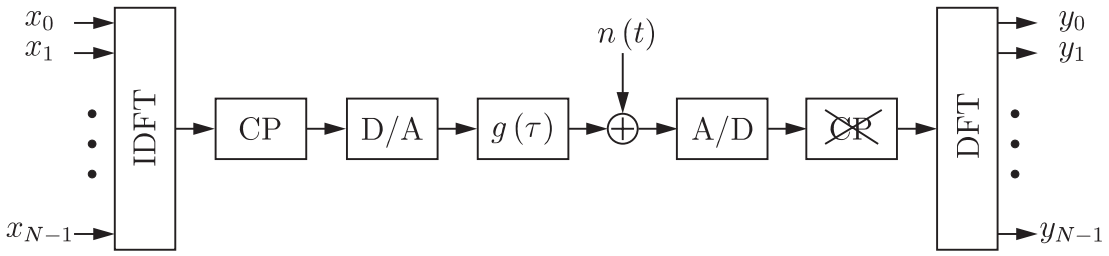

Figure 1: Base-band model of an OFDM system. CP denotes the cyclic prefix.

relation, it still requires a large number of operations. We introduce a low-complexity approximation to the frequency-based LMMSE estimator that uses the theory of optimal rank reduction [5]. Other types of low-rank approximations, based on the *discrete-time Fourier transform* (DFT), have been proposed for OFDM systems before [6–8]. The work presented in this paper was inspired by the observations in [8], where it is shown that DFT-based low-rank channel estimators have limited performance for nonsample-spaced channels and high *signal-to-noise ratios* (SNR's).

After presenting the OFDM system model and our scenario in Section 2, we introduce the estimators and derive their complexities in Section 3. We analyze the *symbol-error rate* (SER) performance in Section 4, where we also discuss design considerations. The proposed low-rank estimator is compared to other estimators in Section 5 and a summary and concluding remarks appear in Section 6.

2 System description

2.1 System model

Figure 1 displays the OFDM baseband model used in this paper. We assume that the use of a *cyclic prefix* (CP) [9] both preserves the orthogonality of the tones and eliminates *intersymbol interference* (ISI) between consecutive OFDM symbols. Further, the channel is assumed to be slowly fading, so it is considered to be constant during one OFDM symbol. The number of tones in the system is N, and the length of the cyclic prefix is L samples.

Under these assumptions we can describe the system as a set of parallel Gaussian channels, shown in Figure 2, with correlated attenuations h_k. The attenuations on each tone are given by

$$h_k = G\left(\frac{k}{NT_s}\right),\ k = 0 \ldots N-1,$$

where $G(\cdot)$ is the frequency response of the channel $g(\tau)$ during the OFDM symbol, and T_s is the sampling period of the system. In matrix notation we describe the OFDM system as

$$\mathbf{y} = \mathbf{X}\mathbf{h} + \mathbf{n}, \tag{1}$$

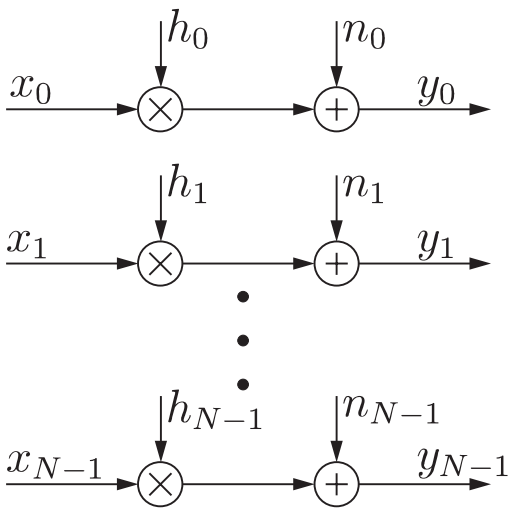

Figure 2: The OFDM system, described as a set of parallel Gaussian channels with correlated attenuations.

where $\mathbf{y}$ is the received vector, $\mathbf{X}$ is a diagonal matrix containing the transmitted signalling points, $\mathbf{h}$ is a channel attenuation vector, and $\mathbf{n}$ is a vector of i.i.d. complex, zero-mean, Gaussian noise with variance σ_n^2. The noise $\mathbf{n}$ is assumed to be uncorrelated with the channel $\mathbf{h}$.

2.2 Channel model

We consider a fading multipath channel model [1], consisting of M impulses

$$g(\tau) = \sum_{k=0}^{M-1} \alpha_k \delta(\tau - \tau_k T_s), \tag{2}$$

where α_k are zero-mean, complex Gaussian, random variables with a power-delay profile $\theta(\tau_k)$. In this paper we use $M = 5$ impulses, an exponentially decaying power-delay profile $\theta(\tau_k) = Ce^{-\tau_k/\tau_{rms}}$ and delays τ_k that are uniformly and independently distributed over the length of the CP. For correlation properties of this channel model, see Appendix A.

2.3 Scenario

Our scenario consists of a wireless 16-QAM OFDM system, designed for an outdoor environment, that is capable of carrying digital video. The system operates with a 500 kHz bandwidth and is divided into 64 tones with a total symbol period of 136 μs, of which 8 μs constitute the CP. One OFDM symbol thus consists of 68 samples ($N + L = 68$), four of which constitute the cyclic prefix ($L = 4$). The uncoded data rate of the system is 1.9 Mbit/sec. We assume that the root-mean square (rms) width is $\tau_{rms} = 1$ sample (2 μs) for the power-delay profile.

3 Linear estimation across tones

In the following section we present a reduced-complexity LMMSE estimate of the channel attenuations $\mathbf{h}$ from the received vector $\mathbf{y}$ and the transmitted data $\mathbf{X}$. We assume that the received OFDM symbol contains data known to the estimator – either training data or receiver decisions [10]. The proposed estimator can also be used in *pilot-symbol assisted modulation* (PSAM) [3], where known symbols (pilots) are multiplexed into the transmitted data stream and channel estimation is performed by interpolation, see Section 5.2. However, to analyze the properties of the estimator, it is more enlightening to assume that the receiver knows the transmitted data $\mathbf{X}$.

The complexity reduction of the LMMSE estimator consists of two separate steps. In the first step we modify the LMMSE by averaging over the transmitted data, obtaining a simplified estimator. In the second step we reduce the number of multiplications required by applying the theory of optimal rank reduction [5].

3.1 LMMSE estimation

The LMMSE estimate of the channel attenuations $\mathbf{h}$ in (1), given the received data $\mathbf{y}$ and the transmitted symbols $\mathbf{X}$ is [8]

$$\widehat{\mathbf{h}}_{lmmse} = \mathbf{R}_{hh}\left(\mathbf{R}_{hh} + \sigma_n^2\left(\mathbf{X}\mathbf{X}^H\right)^{-1}\right)^{-1}\widehat{\mathbf{h}}_{ls}, \tag{3}$$

where

$$\widehat{\mathbf{h}}_{ls} = \mathbf{X}^{-1}\mathbf{y} = \left[\begin{array}{cccc} \frac{y_0}{x_0} & \frac{y_1}{x_1} & \cdots & \frac{y_{N-1}}{x_{N-1}} \end{array}\right]^T \tag{4}$$

is the *least-squares* (LS) estimate of $\mathbf{h}$, σ_n^2 is the variance of the additive channel noise and $\mathbf{R}_{hh} = E\left\{\mathbf{h}\mathbf{h}^H\right\}$ is the channel autocorrelation matrix. The superscript $(\cdot)^H$ denotes Hermitian transpose. In the following we assume, without loss of generality, that the variances of the channel attenuations in $\mathbf{h}$ are normalized to unity, *i.e.*, $E\left\{|h_k|^2\right\} = 1$.

The LMMSE estimator (3) is of considerable complexity since a matrix inversion is needed every time the data in $\mathbf{X}$ changes. We reduce the complexity of this estimator by averaging over the transmitted data [1], *i.e.*, we replace the term $(\mathbf{X}\mathbf{X}^H)^{-1}$ in (3) with its expectation $E\left\{(\mathbf{X}\mathbf{X}^H)^{-1}\right\}$. Simulations indicate that the performance degradation is negligible. Assuming the same signal constellation on all tones and equal probability on all constellation points, we have $E\left\{(\mathbf{X}\mathbf{X}^H)^{-1}\right\} = E\left\{|1/x_k|^2\right\}\mathbf{I}$, where $\mathbf{I}$ is the identity matrix. Defining the average SNR as $E\left\{|x_k|^2\right\}/\sigma_n^2$, we obtain the simplified estimator

$$\widehat{\mathbf{h}} = \mathbf{R}_{hh}\left(\mathbf{R}_{hh} + \frac{\beta}{\mathrm{SNR}}\mathbf{I}\right)^{-1}\widehat{\mathbf{h}}_{ls}, \tag{5}$$

where

$$\beta = E\left\{|x_k|^2\right\}E\left\{|1/x_k|^2\right\}$$

is a constant depending on the signal constellation. In the case of 16-QAM transmission, $\beta = 17/9$. Because $\mathbf{X}$ is no longer a factor in the matrix calculation, the inversion of

$\mathbf{R}_{hh}+\frac{\beta}{\mathrm{SNR}}\mathbf{I}$ does not need to be calculated each time the transmitted data in $\mathbf{X}$ changes. Furthermore, if $\mathbf{R}_{hh}$ and SNR are known beforehand or are set to fixed nominal values, the matrix $\mathbf{R}_{hh}(\mathbf{R}_{hh}+\frac{\beta}{\mathrm{SNR}}\mathbf{I})^{-1}$ needs to be calculated only once. Under these conditions the estimation requires N multiplications per tone. To further reduce the complexity of the estimator, we proceed with the low-rank approximations below.

3.2 Optimal low-rank approximations

Optimal rank reduction is achieved by using the *singular value decomposition* (SVD) [5]. The SVD of the channel autocovariance matrix is

$$\mathbf{R}_{hh} = \mathbf{U}\mathbf{\Lambda}\mathbf{U}^H, \tag{6}$$

where $\mathbf{U}$ is a unitary matrix containing the singular vectors and $\mathbf{\Lambda}$ is a diagonal matrix, containing the singular values $\lambda_1 \geq \lambda_2 \geq \ldots \geq \lambda_N$ on its diagonal[1]. In Appendix B it is shown that the optimal rank-p estimator is

$$\widehat{\mathbf{h}}_p = \mathbf{U}\mathbf{\Delta}_\mathbf{p}\mathbf{U}^H\widehat{\mathbf{h}}_{ls}, \tag{7}$$

where $\mathbf{\Delta}_p$ is a diagonal matrix with entries

$$\delta_k = \begin{cases} \frac{\lambda_k}{\lambda_k+\frac{\beta}{\mathrm{SNR}}} & k = 1, 2, \ldots, p \\ 0 & k = p+1, \ldots, N \end{cases}. \tag{8}$$

Interpreting the matrix $\mathbf{U}^H$ as a transform[2], the singular value λ_k of $\mathbf{R}_{hh}$ is the channel power (variance) contained in the k^{th} transform coefficient after transforming the LS estimate $\widehat{\mathbf{h}}_{ls}$. Since $\mathbf{U}$ is unitary, this transformation can be viewed as rotating the vector $\widehat{\mathbf{h}}_{ls}$ so that all of its components are uncorrelated [5]. The dimension of the space of essentially time- and band-limited signals leads us to the rank needed in the low-rank estimator. In [11] it is shown that this dimension is about $2BT+1$, where B is the one-sided bandwidth and T is the time interval of the signal. Accordingly, the magnitude of the singular values of $\mathbf{R}_{hh}$ should become small after about $L+1$ values, where L is the length of the CP ($2B = 1/T_s$, $T = LT_s$ and $2BT+1 = L+1$). This is illustrated in Figure 3, where the singular values of the channel are shown. The system and channel parameters are chosen according to Section 2.3. A block diagram of the rank$-p$ estimator in (7) is shown in Figure 4, where the LS estimate is calculated from $\mathbf{y}$ by multiplying by $\mathbf{X}^{-1}$. The low-rank estimator can be interpreted as first projecting the LS-estimates onto a subspace and then performing the estimation. If the subspace has a small dimension and can describe the channel well, the complexity of the estimator will be low while showing a good performance.

[1]Since we are dealing with Hermitian matrices the λ_ks are also eigenvalues. However, we use the terminology of the SVD since it is more general and can be used in optimal rank reduction of nonsquare matrices.

[2]The transform in this special case of low-rank approximation is the Karhunen-Loeve (a.k.a. Hotelling) transform of $\mathbf{h}$.

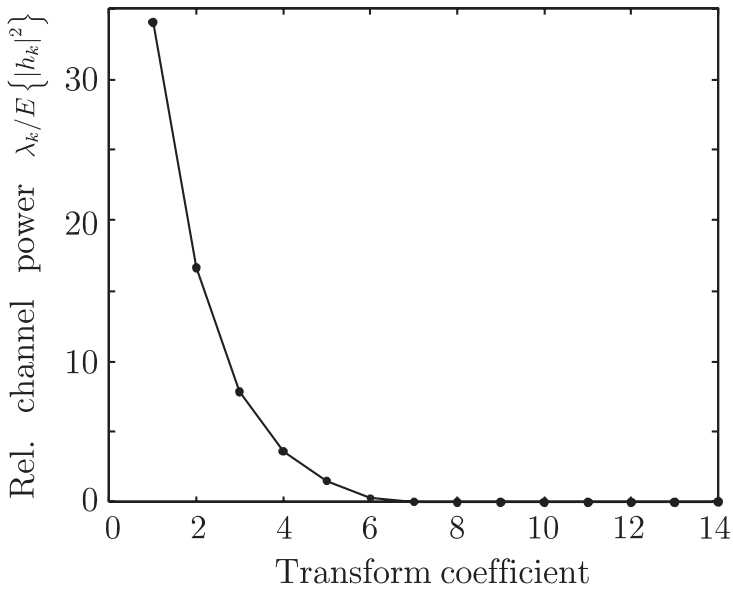

Figure 3: Relative channel power $\lambda_k/E\left\{|h_k|^2\right\}$, of the transform coefficients. The system uses 64 tones and the channel parameters are $L = 4$ and $\tau_{rms} = 1$; see Sections 2.2 and 2.3

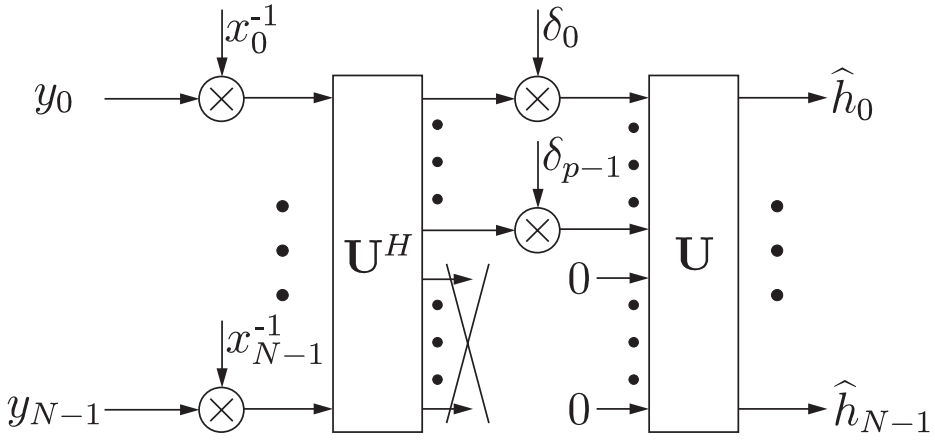

Figure 4: Block diagram of the rank-p channel estimator.

3.3 Estimator complexity

The low-rank estimators will have an irreducible error floor due to the part of the channel that does not belong to the subspace. To eliminate this error floor up to a given SNR we need to make sure our estimator rank is sufficiently large. This prompts an analysis of the computational complexity of the rank$-p$ estimator. In Appendix C the low-rank estimator is shown to require $2p$ multiplications per tone. In comparison with the estimator (5), we have managed to reduce the number of multiplications from N to $2p$ per tone. The smaller p is, the lower the computational complexity, but the larger the approximation error becomes. Following the analysis in Section 3.2, we can expect a

good approximation when p is in the range of the number of samples in the CP, which is usually much smaller than the number of tones, N.

3.4 Partitioning into subsystems

A legitimate question at this point is: what happens for a system with many tones and many samples in the CP. The number of calculations per tone can be considerable if a rank$-p$ estimator is used directly on all tones in the system. One solution to this problem is to partition the tones into reasonably sized blocks and, at a certain performance loss, perform the estimation independently in these blocks. By dividing the channel attenuations into K equally sized blocks, the bandwidth in each block is reduced by a factor K. Referring again to the dimension of the space of essentially time- and band-limited signals [11], the expected number of essential base vectors is reduced from $L+1$ to $L/K+1$. Hence the complexity of the estimator decreases accordingly.

To illustrate the idea, let us assume a system with $N = 1024$ tones and an $L = 64$ sample CP. The uniform channel correlation between the attenuations h_m and h_n in this system is, see Appendix A,

$$r_{m,n} = \begin{cases} 1 & \text{if} \quad m = n \\ \frac{1-e^{-j2\pi L\frac{m-n}{N}}}{j2\pi L\frac{m-n}{N}} & \text{if} \quad m \neq n \end{cases} .$$

This only depends on the distance between the tones $m - n$ and the ratio between the length of the cyclic prefix and the number of tones, L/N. The 1024 tone system can be described by

$$\begin{bmatrix} \mathbf{y}^{(1)} \\ \vdots \\ \mathbf{y}^{(16)} \end{bmatrix} = \begin{bmatrix} \mathbf{X}^{(1)} & & \\ & \ddots & \\ & & \mathbf{X}^{(16)} \end{bmatrix} \begin{bmatrix} \mathbf{h}^{(1)} \\ \vdots \\ \mathbf{h}^{(16)} \end{bmatrix} + \begin{bmatrix} \mathbf{n}^{(1)} \\ \vdots \\ \mathbf{n}^{(16)} \end{bmatrix},$$

that is, as 16 parallel 64-tone systems,

$$\mathbf{y}^{(k)} = \mathbf{X}^{(k)}\mathbf{h}^{(k)} + \mathbf{n}^{(k)}, \ k = 1, 2, \ldots 16.$$

We have the same channel correlation in each subsystem as we have in the 64-tone scenario in this paper ($L/N = 4/64 = 64/1024$). By estimating the channel attenuations $\mathbf{h}^{(k)}$ in each subsystem independently, we neglect the correlation between tones in different subsystems, but obtain the same mean-squared error (MSE) performance as in our 64-tone scenario. The advantage is a significant reduction of complexity.

4 Estimator performance and design

To further simplify this estimator, we propose a generic low-rank frequency-based channel estimator, *i.e.*, an estimator which is designed for fixed, nominal values of SNR and channel correlation. Hence, we need to study the choice of the rank, channel correlation and SNR for this estimator so that it is robust to variations in the channel statistics. As a performance measure, we use uncoded SER for 16-QAM signaling. The SER in this case can be calculated from the mean-squared error with the formulas in [12].

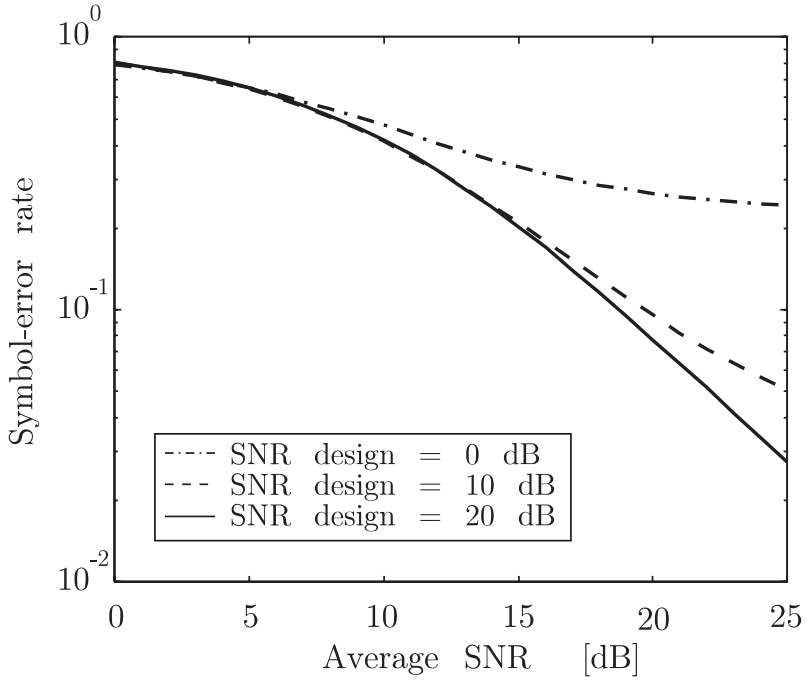

Figure 5: Effects of SNR design mismatch. The channel estimator is designed for a uniform power-delay profile and evaluated for an exponentially decaying power-delay profile.

4.1 SER performance under mismatch

In practice, the true channel correlation and SNR are not known. To get a general expression for the estimator SER, we derive it under the assumption that the estimator is designed for correlation $\mathbf{R}_{hh}$ and SNR, while the true values are $\mathbf{R}_{\widetilde{hh}}$ and $\widetilde{\text{SNR}}$, respectively, where $\widetilde{\mathbf{h}}$ denotes a channel with different statistics than $\mathbf{h}$. This allows us to analyze this estimator's sensitivity to design errors. Under these assumptions, the MSE (relative to the channel power) of the rank$-p$ estimate (7) becomes, see Appendix D,

$$\text{mse}\,(p) = \frac{1}{N}\sum_{k=1}^{p}\left[\mu_k\left(1-\delta_k\right)^2 + \frac{\beta}{\widetilde{\text{SNR}}}\delta_k^2\right] + \frac{1}{N}\sum_{k=p+1}^{N}\mu_k, \tag{9}$$

where δ_k is defined in (8) and μ_k is the k^{th} diagonal element of $\mathbf{U}^H\mathbf{R}_{\widetilde{hh}}\mathbf{U}$, cf. (6). Since

$$E\left\{\left(\mathbf{U}^H\widetilde{\mathbf{h}}\right)\left(\mathbf{U}^H\widetilde{\mathbf{h}}\right)^H\right\} = \mathbf{U}^H\mathbf{R}_{\widetilde{hh}}\mathbf{U},$$

μ_k can be interpreted as the variance of the transformed channel, $\mathbf{U}^H\widetilde{\mathbf{h}}$, under correlation mismatch. It should be noted that the elements of $\mathbf{U}^H\widetilde{\mathbf{h}}$ are no longer uncorrelated. However, due to the fact that the power-delay profile is short compared to the OFDM symbol, the first p elements can be expected to contain most of the power. This property will ensure only a small performance loss when the estimator is designed for wrong channel statistics.

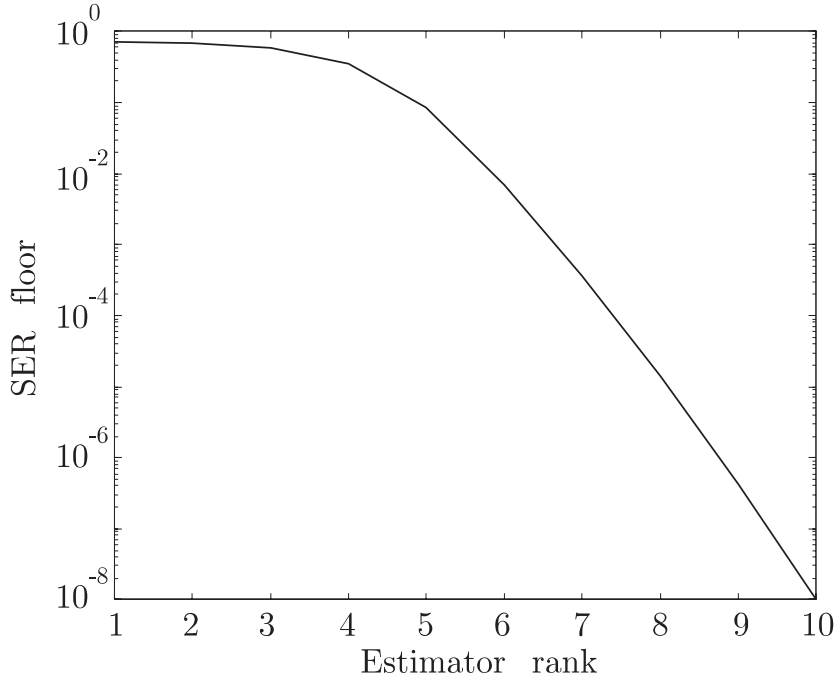

Figure 6: SER floor as a function of estimator rank.

Fixed FIR estimators have been investigated in [3] and [13] where it is shown that a design for the worst correlation is robust to mismatch. This design rule turns out to hold for low-rank estimators as well. Hence we will design the estimator for a uniform power-delay profile [3]. As for mismatch in SNR, a design for a high SNR is preferable. This can intuitively be explained by the fact that a channel estimation error is concealed in noise for low SNR, whereas it tends to dominate for high SNR where the noise is low. Hence, it is important to keep the channel estimation error low at high SNR, which justifies a design for high SNR. This interpretation is confirmed in Figure 5 where the SER curves for a design SNR of 0, 10 and 20 dB are shown.

4.2 Rank reduction

The MSE of the rank$-p$ estimator is mainly determined by the channel power contained in the transform coefficients and can be expressed as (9). The MSE is a monotonically decreasing function of SNR and can be bounded from below by the last term,

$$\underline{\mathrm{mse}}(p) = \frac{1}{N} \sum_{m=p+1}^{N} \mu_m \leq \mathrm{mse}\,(p)\,, \tag{10}$$

which is the sum of the channel power in the transform coefficients not used in the estimate. This MSE-floor $\underline{\mathrm{mse}}(p)$ will cause an irreducible error floor in the SER's.

The irreducible error floor is the main limitation on the complexity reduction achieved by optimal rank reduction. The SER floors are shown as a function of the rank in Figure 6. If the rank is too low, the irreducible error floor will become visible for the SNR of

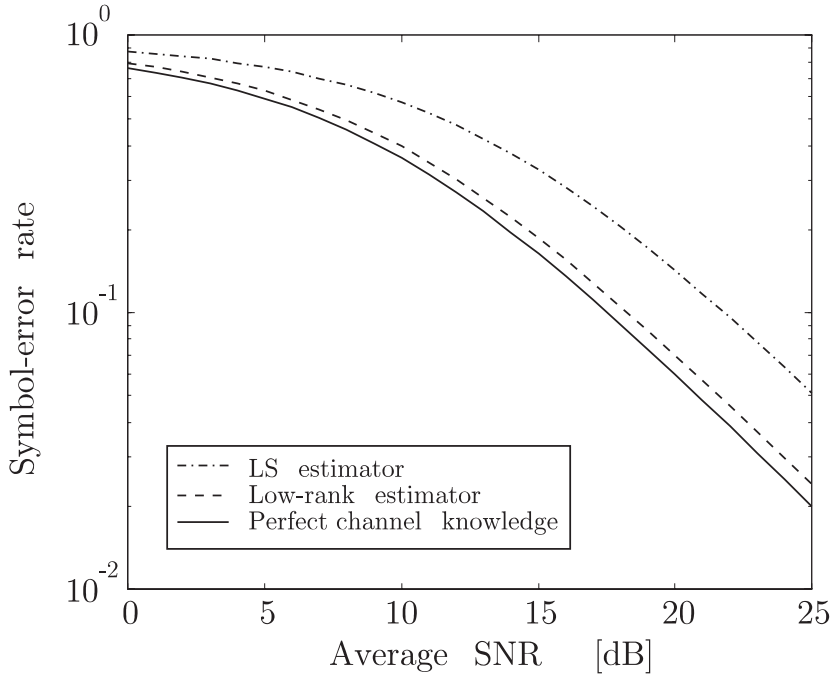

Figure 7: SER for the low-rank estimator, the LS estimator and perfect channel knowledge.

interest. By choosing the appropriate rank on the estimator, we can essentially avoid the impact from the SER floor up to a given SNR. For a full rank estimator $p = N$, no SER floor exists. From Figure 6, it can be seen that the irreducible error floor decreases rapidly for rank $p > L + 1 = 5$. We are therefore able to obtain a good estimator approximation with a relatively low rank.

5 Generic low-rank estimator

If we want a robust generic channel estimator design for OFDM systems, of the low-rank type, the analysis in the previous section suggests the use of the uniform channel correlation and a relatively high SNR as nominal design parameters. The design of such an estimator only requires knowledge about the length of the CP, the number of tones in the system and the target range of SNR's for the application. If the receiver cannot afford an estimator that includes tracking of channel correlation and SNR, this channel estimator works reasonably well for fixed SNR and channel correlation.

5.1 Performance evaluation

For the scenario used in this paper we choose a rank-8 estimator and a design for a uniform power-delay profile and SNR = 20 dB. The performance of this estimator is presented in Figure 7, where the SER for the LS estimate (4) and perfect channel knowledge are also

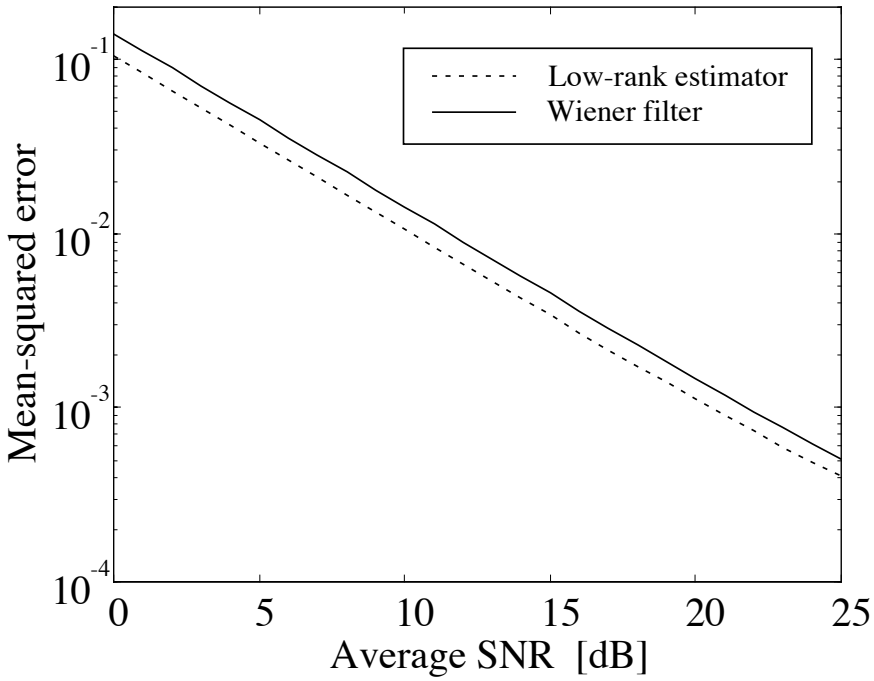

Figure 8: The MSE of the low-rank estimator (rank $p = 8$) and the FIR Wiener filter estimator (16 taps). The two estimators have the same computational complexity.

shown. The low-rank estimator is 3.5 dB better than the LS-estimator and about 0.8 dB from perfect channel knowledge.

An alternative to using low-rank estimators is to use FIR Wiener filters. Their use in OFDM has been investigated in [3]. To make a comparison, we design the FIR Wiener filters for the same channel correlation and SNR as for the low-rank estimator and use the same complexity. For a rank 8 estimator we have 16 multiplications per tone and hence we can use 16 taps in the FIR Wiener filter. In Figure 8, the mean-squared estimation error is shown for both estimators. As can be seen, the MSE of the low-rank estimator is about 1.5 times smaller than the MSE of the FIR Wiener filter estimator for all evaluated SNR values.

5.2 PSAM

A proposed scheme for coherent OFDM is PSAM [3, 14]. In this case known symbols (pilots) are multiplexed into the transmitted data stream and channel estimation is performed by interpolation between these pilots. This interpolation can be performed by FIR Wiener filters [3], but our proposed low-rank estimator is also applicable. In this case, our proposed channel estimator is similar to the all-pilots case. The difference is that only those tones on which pilots are transmitted are used for channel estimation, not all tones. The optimal rank reduction is shown in Appendix B and the structure of the estimator is depicted in Figure 9 , (*cf* Figure 4).

The expression for the MSE for this low-rank interpolator will consist of matrix expressions, and, so, is more complex than (9). However, the interpolator has similar

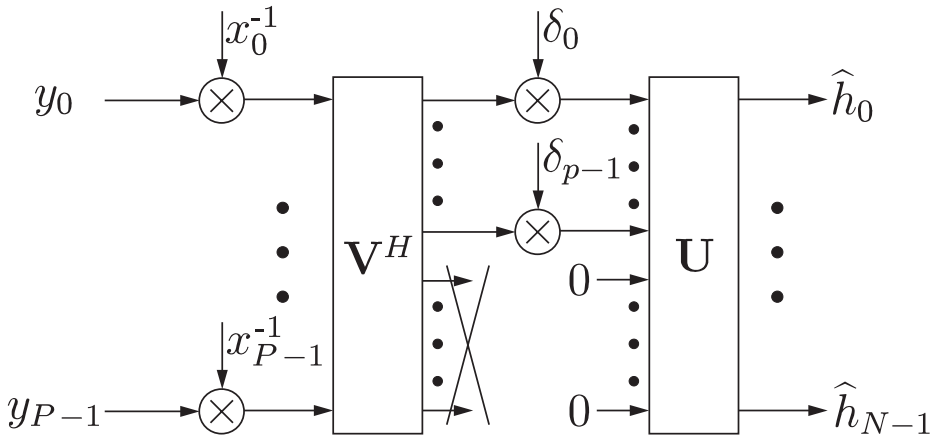

Figure 9: Low-rank estimator for the PSAM case. For each OFDM symbol, P pilots are used to estimate N tones.

properties as the estimator (7) and the same design considerations hold. The irreducible error floor is mainly determined by the power of the unused transform coefficients as in (10).

To compare the low-rank estimator with an FIR Wiener filter, we consider a scenario similar to *digital video broadcast* (DVB) [14]. The system has a bandwidth of 8 MHz and uses 8192 subcarriers with pilot symbols on every twelfth subcarrier. Every OFDM symbol is partitioned into subsymbols consisting of 384 subcarriers, each containing $384/12 = 32$ pilots. The power delay profile is exponentially decaying with $\tau_{\text{rms}} = 2.5\,\mu s$ (20 samples) and a maximum delay spread of 10 μs ($L = 80$ samples). The number of coefficients used for the low-rank estimator is seven, resulting in an average complexity of 7.6 multiplications per tone, see Appendix C, and the number of taps for the FIR estimator is eight. As can be seen from the curves in Figure 10, the MSE of the low-rank estimator is about 1.3 times smaller than the MSE of the FIR estimator for all evaluated SNR values.

5.3 The use of time correlation

The low-rank estimator presented in this paper is based on frequency correlation only, but the time correlation of the channel can also be used. The two-dimensional LMMSE estimator can be simplified using the same technique with rank reduction as described here. However, in [15] it is shown that such an estimator gives an inferior performance for a fixed complexity. Hence, it seems that separating the use of frequency correlation and time correlation is the most efficient way of estimating the channel, as was pointed out in [3].

Other approaches to exploit the time correlation is, *e.g.*, to use a decision-directed scheme [12] or FIR filters [3, 13]. The former can be used in a slow-fading environment, where it offers good performance for a small complexity, whereas the latter is preferred in a fast-fading environment.

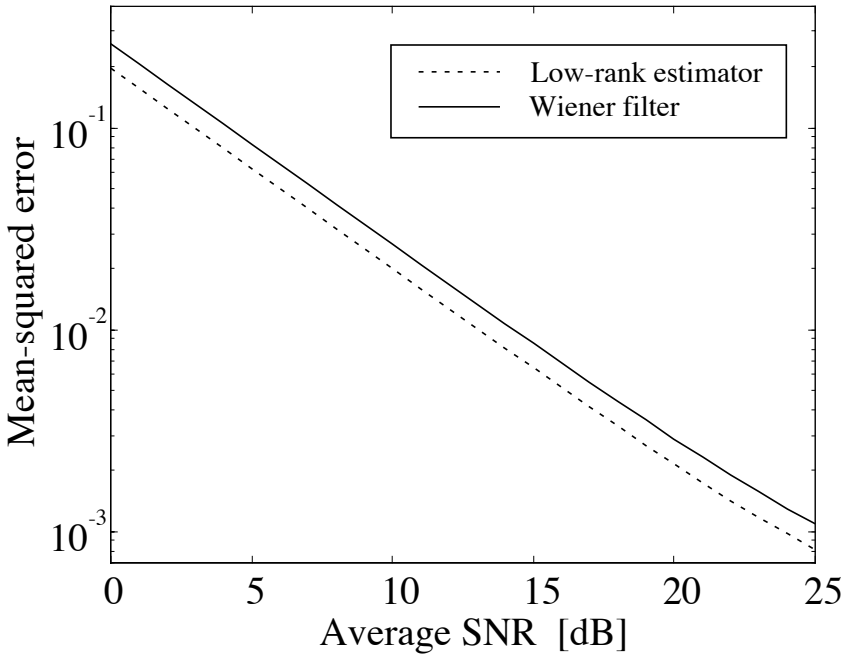

Figure 10: The MSE of the low-rank estimator and the FIR Wiener filter estimator for the PSAM case. The two estimators have the same computational complexity (8 multiplications per tone)

6 Conclusions

We have investigated low-complexity low-rank approximations of the LMMSE channel estimator for nonsample-spaced channels. The investigation shows that an estimator error-floor, inherent in the low-rank approximation, is the significant limitation to the achieved complexity reduction. Its performance degradation can be limited by choosing a sufficient rank. We showed that a generic low-rank estimator design, based on the uniform channel correlation and a nominal SNR, can be used in our 64-tone scenario. Compared with the full LMMSE (5) there is only a small loss in performance, up to an SNR of 25 dB, but a reduction in complexity with a factor $N/2p = 4$. For systems with more subchannels, this gain is even larger. The generic estimator design only requires knowledge of the length of the CP, the number of tones in the system and the target range of SNR's for the application.

We compared a low-rank estimator to FIR filters across the tones. It was shown that the MSE of the low-rank estimator is about 1.5 times smaller than that of the FIR Wiener filter estimator of equal complexity. Since low-rank estimators are based on subspace projection, it is an advantage if the dimension of the subspace is small. This means that they will improve their performance as the channel length becomes smaller.

The proposed estimator can also be used in PSAM. The principle is the same – the observed channel attenuations are projected onto a (much smaller) subspace where estimation is performed. The final channel estimates are then found by linear combinations of the basis vectors of the subspace. Here the MSE of the low-rank estimator is about 1.3 times smaller than the FIR Wiener filter estimator of equal complexity.

A Channel-correlation matrices

Using the channel model in (2), the attenuation on tone k becomes

$$h_k = \sum_{i=0}^{M-1} \alpha_i e^{-j2\pi \frac{k}{N}\tau_i}.$$

The correlation matrix for the attenuation vector $\mathbf{h}$

$$\mathbf{R}_{hh} = E\left\{\mathbf{h}\mathbf{h}^H\right\} = [r_{m,n}]$$

can be expressed as (τ_k's independent)

$$\begin{aligned} r_{m,n} &= \int \cdots \int \prod_{k=0}^{M-1} f_{\tau_k}(\tau_k) \left[\sum_{i=0}^{M-1} \theta(\tau_i)\, e^{-j2\pi\tau_i \frac{m-n}{N}}\right] d\tau_0 \ldots d\tau_{M-1} \\ &= \sum_{i=0}^{M-1} \int f_{\tau_i}(\tau_i)\, \theta(\tau_i)\, e^{-j2\pi\tau_i \frac{m-n}{N}} d\tau_i, \end{aligned} \tag{11}$$

where $\theta(\tau)$ is the multipath intensity profile and $f_{\tau_k}(\tau_k)$ is the probability density function of τ_k.

The probability distributions for the delays are

$$f_{\tau_i}(\tau_i) = \begin{cases} 1/L & \text{if } \tau_i \in [0, L] \\ 0 & \text{otherwise} \end{cases}, \; i = 0, 1, \ldots, M-1,$$

and the power-delay profile is $\theta(\tau) = Ce^{-\tau/\tau_{rms}}$. Substituting in (11), and normalizing $r_{k,k}$ to unity, gives us

$$r_{m,n} = \frac{1 - e^{-L\left(\frac{1}{\tau_{rms}} + 2\pi j \frac{m-n}{N}\right)}}{\tau_{rms}\left(1 - e^{-\frac{L}{\tau_{rms}}}\right)\left(\frac{1}{\tau_{rms}} + j2\pi\frac{m-n}{N}\right)}.$$

A uniform power-delay profile can be obtained by letting $\tau_{rms} \to \infty$, resulting in

$$r_{m,n} = \frac{1 - e^{-2\pi j L \frac{m-n}{N}}}{2\pi j L \frac{m-n}{N}}.$$

B Optimal rank reduction

The optimal rank reduction is found from the correlation matrices

$$\begin{aligned} \mathbf{R}_{h\widehat{h}_{ls}} &= E\left\{\mathbf{h}\widehat{\mathbf{h}}_{ls}^H\right\} \\ \mathbf{R}_{\widehat{h}_{ls}\widehat{h}_{ls}} &= E\left\{\widehat{\mathbf{h}}_{ls}\widehat{\mathbf{h}}_{ls}^H\right\} \end{aligned}$$

and the SVD

$$\mathbf{R}_{h\widehat{h}_{ls}} \mathbf{R}_{\widehat{h}_{ls}\widehat{h}_{ls}}^{-1/2} = \mathbf{Q}_1 \mathbf{D} \mathbf{Q}_2^H, \tag{12}$$

where $\mathbf{Q}_1$ and $\mathbf{Q}_2$ are unitary matrices and $\mathbf{D}$ is a diagonal matrix with the singular values $d_1 \geq d_2 \geq \cdots \geq d_N$ on its diagonal. The best rank-p estimator [5] is then

$$\widehat{\mathbf{h}}_p = \mathbf{Q}_1 \begin{bmatrix} \mathbf{D}_p & \mathbf{0} \\ \mathbf{0} & \mathbf{0} \end{bmatrix} \mathbf{Q}_2^H \mathbf{R}_{h_{\text{ls}} h_{\text{ls}}}^{-1/2} \widehat{\mathbf{h}}_{ls}, \tag{13}$$

where $\mathbf{D}_p$ is the $p \times p$ upper left corner of $\mathbf{D}$, *i.e.,* we exclude all but the p largest singular vectors. For the PSAM case we have $\mathbf{Q}_1 \neq \mathbf{Q}_2$, so it is difficult to further reduce (13). However, in the case of all pilots we have $\mathbf{R}_{h\widehat{h}_{ls}} = \mathbf{R}_{hh}$ and $\mathbf{R}_{\widehat{h}_{ls}\widehat{h}_{ls}} = \mathbf{R}_{hh} + \frac{\beta}{\text{SNR}}\mathbf{I}$. We note that they share the same singular vectors, *i.e.,* the ones of $\mathbf{R}_{hh} = \mathbf{U}\mathbf{\Lambda}\mathbf{U}^H$. Thus, we may express (12) as

$$\mathbf{R}_{h\widehat{h}_{ls}} \mathbf{R}_{\widehat{h}_{ls}\widehat{h}_{ls}}^{-1/2} = \mathbf{U}\mathbf{\Lambda}\mathbf{U}^H \left(\mathbf{U} \left(\mathbf{\Lambda} + \frac{\beta}{\text{SNR}}\mathbf{I} \right) \mathbf{U}^H \right)^{-1/2} =$$
$$\mathbf{U}\mathbf{\Lambda} \left(\mathbf{\Lambda} + \frac{\beta}{\text{SNR}}\mathbf{I} \right)^{-1/2} \mathbf{U}^H = \mathbf{Q}_1 \mathbf{D} \mathbf{Q}_2^H,$$

where

$$\begin{aligned} \mathbf{Q}_1 &= \mathbf{Q}_2 = \mathbf{U} \\ \mathbf{D} &= \mathbf{\Lambda} \left(\mathbf{\Lambda} + \frac{\beta}{\text{SNR}}\mathbf{I} \right)^{-1/2}. \end{aligned}$$

The rank-p estimator (13) now becomes

$$\begin{aligned} \widehat{\mathbf{h}}_p &= \mathbf{U} \begin{bmatrix} \mathbf{D}_p & \mathbf{0} \\ \mathbf{0} & \mathbf{0} \end{bmatrix} \mathbf{U}^H \left(\mathbf{U} \left(\mathbf{\Lambda} + \frac{\beta}{\text{SNR}}\mathbf{I} \right) \mathbf{U}^H \right)^{-1/2} \widehat{\mathbf{h}}_{ls} = \\ &= \mathbf{U} \begin{bmatrix} \mathbf{D}_p & \mathbf{0} \\ \mathbf{0} & \mathbf{0} \end{bmatrix} \left(\mathbf{\Lambda} + \frac{\beta}{\text{SNR}}\mathbf{I} \right)^{-1/2} \mathbf{U}^H \widehat{\mathbf{h}}_{ls} = \mathbf{U} \begin{bmatrix} \mathbf{\Delta}_p & \mathbf{0} \\ \mathbf{0} & \mathbf{0} \end{bmatrix} \mathbf{U}^H \widehat{\mathbf{h}}_{ls}, \end{aligned}$$

where $\mathbf{\Delta}_p$ is the $p \times p$ upper left corner of

$$\mathbf{\Delta} = \mathbf{\Lambda} \left(\mathbf{\Lambda} + \frac{\beta}{\text{SNR}}\mathbf{I} \right)^{-1} = \text{diag} \left(\frac{\lambda_1}{\lambda_1 + \frac{\beta}{\text{SNR}}}, \cdots, \frac{\lambda_N}{\lambda_N + \frac{\beta}{\text{SNR}}} \right).$$

C Estimator complexity

For the all-pilot case, the implementation we have chosen is based on writing (7) as a sum of rank-1 matrices,

$$\widehat{\mathbf{h}}_p = \left(\sum_{k=1}^{p} \delta_k \mathbf{u}_k \mathbf{u}_k^H \right) \widehat{\mathbf{h}}_{ls} = \sum_{k=1}^{p} \mathbf{q}_k \left\langle \mathbf{u}_k, \widehat{\mathbf{h}}_{ls} \right\rangle, \tag{14}$$

where $\mathbf{q}_k = \delta_k \mathbf{u}_k$ and $\left\langle \mathbf{u}_k, \widehat{\mathbf{h}}_{ls} \right\rangle = \mathbf{u}_k^H \widehat{\mathbf{h}}_{ls}$ are the Euclidian inner products, requiring pN multiplications. The linear combination of p vectors of length N also requires pN

multiplications. The estimation thus requires $2pN$ multiplications and the total number of multiplications per tone becomes $2p$.

Similarly, the rank-p PSAM estimator can be formulated as

$$\widehat{\mathbf{h}}_p = \left(\sum_{k=1}^{p} \mathbf{g}_k \widetilde{\mathbf{g}}_k^H \right) \widehat{\mathbf{h}}_{ls,\text{pilots}} = \sum_{k=1}^{p} \mathbf{g}_k \left\langle \widetilde{\mathbf{g}}_k, \widehat{\mathbf{h}}_{ls,\text{pilots}} \right\rangle,$$

where $\widehat{\mathbf{h}}_{ls,\text{pilots}}$ contains the least-squares channel estimates of the N_{pilots} pilot positions and $\mathbf{g}_k$ and $\widetilde{\mathbf{g}}_k$ are vectors of length N and N_{pilots}, respectively. The inner products $\left\langle \widetilde{\mathbf{g}}_k, \widehat{\mathbf{h}}_{ls,\text{pilots}} \right\rangle$ require N_{pilots} multiplications each, *i.e.*, a total of pN_{pilots} multiplications. The linear combination is over p vectors of length N, *i.e.*, requires pN multiplications. Since N attenuations are simultaneously estimated, the number of multiplications per attenuation becomes

$$\frac{pN_{\text{pilots}} + pN}{N} = p\left(1 + \frac{N_{\text{pilots}}}{N}\right).$$

D Estimator mean-squared error

In this appendix we derive the MSE of the rank$-p$ estimator in (7) for the case of all pilots (the data is known to the receiver). We also present the MSE floor, which bounds the achievable MSE from below in low-rank approximations of the LMMSE estimator. To get a general expression for the MSE for the rank$-p$ approximation of the LMMSE estimator, we assume that the estimator has been designed for channel correlation $\mathbf{R}_{hh}$ and SNR, but the real channel $\widetilde{\mathbf{h}}$ has the correlation $\mathbf{R}_{\widetilde{hh}}$ and the real SNR is $\widetilde{\text{SNR}}$. From (1) and (4), we have $\widehat{\mathbf{h}}_{ls} = \widetilde{\mathbf{h}} + \widetilde{\mathbf{n}}$, where the noise term $\widetilde{\mathbf{n}} = \mathbf{X}^{-1}\mathbf{n}$ has the autocovariance matrix $\mathbf{R}_{\widetilde{nn}} = \frac{\beta}{\widetilde{\text{SNR}}}\mathbf{I}$. The estimation error $\mathbf{e}_p = \widetilde{\mathbf{h}} - \widehat{\mathbf{h}}_p$ of the rank$-p$ estimator (7) is

$$\mathbf{e}_p = \mathbf{U}\left(\mathbf{I} - \begin{bmatrix} \mathbf{\Delta}_p & \mathbf{0} \\ \mathbf{0} & \mathbf{0} \end{bmatrix}\right)\mathbf{U}^{\mathbf{H}}\widetilde{\mathbf{h}} - \mathbf{U}\begin{bmatrix} \mathbf{\Delta}_p & 0 \\ 0 & 0 \end{bmatrix}\mathbf{U}^{\mathbf{H}}\widetilde{\mathbf{n}}, \tag{15}$$

and the average MSE is

$$\text{mse}(p) = \frac{1}{N}\text{Trace}E\left\{\mathbf{e}_p\mathbf{e}_p^H\right\}. \tag{16}$$

To simplify the expression we use the facts that:

- $\widetilde{\mathbf{h}}$ and $\widetilde{\mathbf{n}}$ are uncorrelated, hence the cross terms are canceled in the expectation.
- $\text{Trace}\left(\mathbf{U}\mathbf{A}\mathbf{U}^H\right) = \text{Trace}\mathbf{A}$ if $\mathbf{U}$ is a unitary matrix.
- $\text{Trace}\left(\mathbf{A} + \mathbf{B}\right) = \text{Trace}\mathbf{A} + \text{Trace}\mathbf{B}$.
- $\text{Trace}\left(\mathbf{D}\mathbf{A}\mathbf{D}\right) = \sum_k a_{k,k}d_k^2$ when $\mathbf{D}$ is a diagonal matrix with the elements d_k on its diagonal and $\mathbf{A}$ (not necessarily a diagonal matrix) has diagonal elements $a_{k,k}$.

Using (15) in (16), the mean-squared error becomes

$$\begin{aligned}
\mathrm{mse}\,(p) &= \frac{1}{N}\mathrm{Trace}\left[\mathbf{U}\left(\mathbf{I}-\begin{bmatrix}\mathbf{\Delta}_p & \mathbf{0}\\ \mathbf{0} & \mathbf{0}\end{bmatrix}\right)\mathbf{U^H}\mathbf{R}_{\widetilde{\mathbf{hh}}}\,\mathbf{U}\left(\mathbf{I}-\begin{bmatrix}\mathbf{\Delta}_p & \mathbf{0}\\ \mathbf{0} & \mathbf{0}\end{bmatrix}\right)^H\mathbf{U}^H+\right.\\
&\quad\left.\mathbf{U}\begin{bmatrix}\mathbf{\Delta}_p & 0\\ 0 & 0\end{bmatrix}\mathbf{U^H}\mathbf{R}_{\widetilde{\mathbf{nn}}}\mathbf{U}\begin{bmatrix}\mathbf{\Delta}_p & 0\\ 0 & 0\end{bmatrix}^H\mathbf{U^H}\right]\\
&= \frac{1}{N}\left(\sum_{k=1}^{p}\mu_k\left(1-\delta_k\right)^2+\sum_{k=p+1}^{N}\mu_k\right)+\frac{1}{N}\sum_{k=1}^{p}\frac{\beta}{\widetilde{\mathrm{SNR}}}\delta_k^2\\
&= \frac{1}{N}\sum_{k=1}^{p}\left(\mu_k\left(1-\delta_k\right)^2+\frac{\beta}{\widetilde{\mathrm{SNR}}}\delta_k^2\right)+\frac{1}{N}\sum_{k=p+1}^{N}\mu_k, \qquad (17)
\end{aligned}$$

where μ_k is the channel power in the k^{th} transform coefficient, *i.e.*, the k^{th} diagonal element of the matrix $\mathbf{U}^H\mathbf{R}_{\widetilde{hh}}\mathbf{U}$. The MSE can be lower-bounded, $\mathrm{mse}(p) \geq \underline{\mathrm{mse}}(p)$, by what we call the MSE-floor

$$\underline{\mathrm{mse}}(p) = \frac{1}{N}\sum_{k=p+1}^{N}\mu_k.$$

If there is no mismatch in SNR or channel correlation, we have $\mu_k =$ diagonal elements of $\mathbf{U}^H\mathbf{R}_{hh}\mathbf{U} = \lambda_k$ and $\widetilde{\mathrm{SNR}} = \mathrm{SNR}$, and the MSE becomes

$$\mathrm{mse}\,(p) = \frac{1}{N}\sum_{k=1}^{p}\left(\lambda_k\left(1-\delta_k\right)^2+\frac{\beta}{\mathrm{SNR}}\delta_k^2\right)+\frac{1}{N}\sum_{k=p+1}^{N}\lambda_k.$$

References

[1] J.G. Proakis, *Digital communications*, 3rd edition, McGraw-Hill, New York, 1995.

[2] Radio broadcasting systems; Digital Audio Broadcasting (DAB) to mobile, portable and fixed receivers, ETS 300 401, ETSI – European Telecommunications Standards Institute, Valbonne, France, February 1995.

[3] P. Höher, 'TCM on frequency-selective land-mobile fading channels' in *Proceedings of the Tirrenia International Workshop on Digital Communications*, Tirrenia, Italy, September 1991, pp. 317-328.

[4] S.K. Wilson, R.E. Khayata, and J.M. Cioffi, '16-QAM modulation with orthogonal frequency-division multiplexing in a Rayleigh-fading environment', in *Proceedings of the IEEE Vehicular Technology Conference (VTC'94)*, Stockholm, Sweden, June 1994, pp. 1660–1664.

[5] L.L. Scharf, *Statistical signal processing: Detection, estimation, and time series analysis*, Addison-Wesley, 1991.

[6] A. Chini, *Multicarrier modulation in frequency selective fading channels*, PhD thesis, Carleton University, Ottawa, Canada, 1994.

[7] J.M. Cioffi, Personal communication, 1994.

[8] J.J. van de Beek, O. Edfors, M. Sandell, S.K. Wilson, and P.O. Börjesson, 'On channel estimation in OFDM systems', in *Proceedings of the IEEE Vehicular Technology Conference (VTC'95*, Chicago, USA, July 1995, pp. 815–819.

[9] A. Peled and A. Ruiz, 'Frequency domain data transmission using reduced computational complexity algorithms', in *Proceedings of the IEEE International Conference on Acoustics, Speech, and Signal Processing (ICASSP'80)*, Denver, USA, 1980, pp. 964–967.

[10] V. Mignone and A. Morello, 'CD3-OFDM: A novel demodulation scheme for fixed and mobile receivers', *IEEE Transactions on Communications*, vol. 44, no. 9, pp. 1144–1151, September 1996.

[11] H.J. Landau and H.O. Pollak, 'Prolate spheriodal wave functions, Fourier analysis and uncertainty – III: The dimension of the space of essentially time- and band-limited signals', *Bell System Technical Journal*, vol. 41, pp. 1295, 1962.

[12] S.K. Wilson, *Digital audio broadcasting in a fading and dispersive channel*, PhD thesis, Stanford University, CA, August 1994.

[13] J.K. Cavers, 'An analysis of pilot-symbol assisted modulation for Rayleigh-fading channels', *IEEE Transactions on Vehicular Technology*, vol. 40, no. 4, pp. 686–693, November 1991.

[14] Digital broadcasting systems for television, sound and data services, European Telecommunications Standard, prETS 300 744, September 1996.

[15] M. Sandell and O. Edfors, 'A comparative study of pilot-based channel estimators for wireless OFDM', Research Report TULEA 1996:19, Division of Signal Processing, Luleå University of Technology, September 1996.